# Interface Formation between Hydrocarbon Ring Molecules and III-V Semiconductor Surfaces

vorgelegt von
Diplom-Physikerin Regina Paßmann
aus Rheinberg

Von der Fakultät II -Mathematik und Naturwissenschaften
der Technischen Universität Berlin

zur Erlangung des akademischen Grades
Doktor der Naturwissenschaften
(Dr. rer. nat.)
genehmigte Dissertation

Promotionsausschuss:
Vorsitzender: Prof. Dr. M. Lehmann
Berichter: Prof. Dr. rer. nat. N. Esser
Berichter: Prof. Dr. rer. nat. W. Richter
Berichter: Prof. Dr. rer. nat. M. Kneissl

Tag der wissenschaftlichen Aussprache: 15.08.08

Berlin 2008
-D83-

## Parts of this work have already been published in:

R. Passmann, M. Kropp, T. Bruhn, B. O. Fimland, F. L. Bloom, A. C. Gossard, W. Richter, N. Esser, P. Vogt, Appl. Phys. A 87, 469 (2007), *Optical anisotropy of cyclopentene terminated GaAs(001) surfaces*

R. Passmann, P. Favero, W. G. Schmidt, W. Braun, W. Richter, M. Kneissl, N. Esser, P. Vogt, Phys. Rev. B, submitted (2008), *Bonding configuration of cyclopentene on the InP*$(001)(2\times4)$ *surface*

R. Passmann, T. Bruhn, B.O. Fimland, M. Kneissl, W. Richter, N. Esser, P. Vogt, World Scientific Proceedings, submitted (2008), *Adsorption of cyclopentene on GaAs and InP (001), a comparative study by synchrotron-based core-level spectroscopy*

**Grenzflächenbildung zwischen ringförmigen Kohlenwasserstoff-Molekülen und III-V Halbleiteroberflächen**

Regina Paßmann

In dieser Arbeit wurde eine systematische Untersuchung der Adsorptionsstruktur von kleinen organischen Ringmolekülen auf III-V Halbleitern mittels Photoelektronen-Spektroskopie (PES), Reflexions-Anisotropie-Spektroskopie (RAS), Rastertunnelmikroskopie (STM), sowie niederenergetische Elektronenbeugung (LEED) durchgeführt. Durch diese Untersuchungen wurde die Grenzflächenbildung zwischen den organischen Molekülen und den III-V Halbleitern aufgeklärt. Vor dieser Arbeit existierten zwar zahlreiche Untersuchungen zur Adsorptionskonfiguration, sowie den zugrundeliegenden Bindungsmechanismen von organischen Molekülen auf $Si(001)$ Oberflächen, systematische Untersuchungen der Adsorption auf III-V Halbleitern gab es aber keine. Auf $Si(001)$ Oberflächen erfolgt die Adsorption oft mittels einer Cycloadditionsreaktion. Allerdings sind nicht nur Systeme basierend auf Silizium für Anwendungen interessant, sondern auch jene basierend auf
III-V Halbleitern. Kohlenwasserstoff-Moleküle und III-V Halbleiter bieten insbesondere die Möglichkeit systematisch zwei wesentliche Einflüsse zu analysieren:
zum Einen den Einfluss der atomaren Oberflächenstruktur der Halbleitermaterialien und zum Anderen den Einfluss der intra-molekularen Strukturelemente.
Um den Einfluss der Oberflächenstruktur, insbesondere des Dimers, auf den Adsorptionsprozess von organischen Molekülen zu untersuchen, wurden in dieser Arbeit, vergleichend zu Silizium, die ersten Bindungsplätze auf den $GaAs(001)$ Oberflächen, der $c(4\times4)$, $(2\times4)$ und $(4\times2)$, untersucht, sowie die Adsorption von Cyclopenten auf der $InP(001)(2\times4)$ Oberfläche. Im Vergleich zeigte sich, dass Cyclopenten auf $InP(001)(2\times4)$ in einer der Cycloadditionsreaktion ähnlichen Adsorptionsstruktur bindet. Dies ist mit dem Aufspalten der Doppelbindung einhergehend, im Gegensatz zu der Adsorption auf $GaAs(001)$. Somit zeigt sich hier, dass die Oberflächengeometrie einen Einfluss auf die resultierende Adsorptionsstruktur hat.
Zum Zweiten wurde der Einfluss der intra-molekularen Bindungen in dieser Arbeit mittels Cyclopenten (eine Doppelbindung), 1,4-Cyclohexadien (zwei Doppelbindungen), sowie Benzol (drei Doppelbindungen) charakterisiert. Anhand der Untersuchungen auf rekonstruierten $GaAs(001)$ Oberflächen hat sich gezeigt, dass es eine Abhängigkeit der Bindungskonfiguration von der Anzahl der intra-molekularen Doppelbindung gibt. Bei der Adsorption von Cyclopenten wurde nur eine Einfachbindung zur Oberfläche ausgebildet, während für 1,4-Cyclohexadien und Benzol pro Molekül eine Bindung zu vier Atomen der Oberfläche festgestellt werden konnte. Bei der Adsorption von Cyclopenten gab es keinen eindeutigen Nachweis dafür, dass die Doppelbindung in die Bindung zur Oberfläche involviert sein muss, wohingegen die Adsorption von 1,4-Cyclohexadien und Benzol über die Doppelbindungen stattfindet. Weiterhin zeigte sich eine häufigere Ausbildung von Bindungen zu As-Atomen als zu Ga-Atomen der Oberfläche.
Diese systematischen Untersuchungen belegen, dass sowohl die Oberflächengeometrie, als auch die Molekülstruktur einen Einfluss auf die resultierende Adsorptionsstruktur haben und sich daraus eine Systematik bezüglich der Ausbildung der Molekül-Halbleiter-Grenzflächen ergibt.

# Contents

# Chapter 1: Introduction

Hybrid systems consisting of thin organic layers and inorganic semiconductor surfaces are considered a key issue for future developments in the field of advanced electronic devices and sensors with a possible impact in many different research areas such as biotechnology, nanoelectronics, high density data storage and medical diagnostics. Applications like light emitting diodes, field effect transistors, small flexible monitors or biosensors already exist. But to improve for example the biocompatibility, the life time or the performance of the electronic devices more investigations and characterizations of the interfaces between the organic molecules and the semiconductor surfaces are necessary [1].
During the formation of the interface it is not only important to know the semiconductor surface structure, the structure of the organic molecules and their functionality is also a crucial parameter [1–4]. Therefore the final bonding sites and bonding configurations of the organic molecules will influence the functionality of such a modified surface for example the translation of a surface reaction into a measurable signal and the stability [5].
A detailed knowledge of the atomic structure and the bonding sites of the organic molecules on the semiconductor surface is required to improve their applicability. So far, most of the results on hybrid interfaces are reported for the adsorption of organic molecules on Si(001) surfaces (for example [2,3,6–10]). A well understood surface in this case is the $\mathrm{Si}(001)(2\times 1)$ reconstruction, which is described by asymmetric buckled $Si-Si$ surface dimers [11–13]. It was shown that the asymmetry of the dimer results in an adsorption of small organic ring molecules via a cycloaddition reaction where the asymmetric dimer configuration is a basic prerequisite for [3]. Concerning the adsorption of organic molecules on surfaces of the technologically important III-V semiconductor surfaces, on the other hand, only little is known [14–18]. However, the combination of organic molecules and III-V semiconductor materials offers an ideal platform for applications in the field of electronic and optoelectronic devices.
In order to improve the understanding of the interface formation between organic molecules and III-V surfaces it is important to know the first bonding sites of the organic molecules in specific for example if the molecules are flat lying on the surface or upright standing. This knowledge will give the possibility to understand for example in which direction a charge injection or a charge transport through the molecular layer would be possible. This is only one crucial parameter for the improvement of the performance of electronic devices. Hence a systematical study of the adsorption of organic molecules is necessary to find out the parameters which have an influence on the final adsorption structure. For such a study it would be not useful to chose complex molecules because such molecules would provide a

huge number of possible adsorption structures. Hence, in this work a first systematical study of the adsorption of small hydrocarbons ring shaped molecules is performed.

Molecules like hydrocarbons consists only of hydrogen and carbon atoms, but exhibits the possibility to investigate the influence of the different amount of intra-molecular double bonds to the adsorption process. A double bond within an organic molecule is the simplest form of a so called 'functional group'. Thus cyclopentene, 1,4-cyclohexadiene and benzene were chosen for the first investigations. These molecules have in common, that they are hydrocarbons which have a ring shaped structure, but they consist of one, two and three double bonds, respectively. If the intra-molecular double bonds play a role during the adsorption process, or for the choice of the first adsorption sites of the molecules, the adsorption structures of all three molecules should be different. Another possibility is that the influence of this functional group is not strong enough or even can be neglected. Thus the adsorption structures of these molecules could be similar.
The influence of the intra-molecular double bonds is not the only important parameter for the formation of a hybrid system. The dependency of the resulting adsorption structure on the surface dimer configuration and surface stoichiometry is not yet clarified. The III-V surfaces exhibit the possibility to investigate systematically the adsorption of the small organic molecules on different surface stoichiometries and thus different dimer configurations. In this work the three 'main' GaAs$(001)$, the c$(4\times4)$, the $(2\times4)$ and the $(4\times2)$ as well as the InP$(001)(2\times4)$ surface reconstruction exhibit such different surface stoichiometries and dimer configurations. Therefore they are predestinated to investigate the influence of the surface properties to the adsorption process of cyclopentene, 1,4-cyclohexadiene and benzene in a first systematical study. The resulting adsorption structures can be compared and the differences and similarities can be identified.
With the investigation of the influence of both parameters, the amount of intra-molecular double bonds as well as the dimer configuration, it can be ruled out if an influence of these parameters on the adsorption structure exists. This would be important for the development of novel electronic devices because if a surface exhibits no ordered adsorption structure no improvement of the performance can be expected. As it was mentioned before the orientation of the molecules can have an important influence on the increase or decrease of the electron mobilities through the molecular layer or through a charge injection at the interface.

So the main focus of this work is to characterize and understand systematically the interface formation between the three 'main' surface reconstructions of GaAs(001) as well as the InP$(001)(2\times4)$ reconstructed surface with hydrocarbon ring shaped molecules: cyclopentene, 1,4-cyclohexadiene and benzene. Additionally the adsorption structures which results after the adsorption of cyclopentene, 1,4-cyclohexadiene and benzene on the Si$(001)(2\times1)$ reconstructed surface, respectively, will be discussed briefly for a comparison of the resulting adsorption structures of these molecules on the III-V surface reconstructions used in this work.

In detail in the first part of this work the basics, the (001) surface reconstructions, the molecule properties and the experimental methods will be discussed briefly. In chapter 2 the formation rules and surface properties of (001) surfaces in general will be introduced. The

properties and characteristics of the three molecules, cyclopentene, 1,4-cyclohexadiene and benzene will be discussed in chapter 3 and in chapter 4 some details about the experimental methods used in this work will be given. In the last chapter of the first part the clean surface reconstructions of the GaAs$(001)$ and InP$(001)(2\times4)$ will be introduced.

In the second part the interaction of cyclopentene on the InP$(001)(2\times4)$ reconstructed surface is investigated with RAS and SXPS. Additionally a comparison to results derived from DFT calculations is done in chapter 6.1. A final adsorption structure of cyclopentene on the InP$(001)(2\times4)$ reconstructed surface is given.

In the third part the results of the adsorption structure formation of the three 'main' GaAs(001) surfaces, the $c(4\times4)$, the $(2\times4)$ and the $(4\times2)$ surfaces and cyclopentene will be discussed in detail in chapter 7. In chapter 8 and chapter 9 the suggestion of the first adsorption sites and changes in the optical and electronical properties of 1,4-cyclohexadiene and benzene adsorbed on these surface reconstructions will be shown, respectively.

# Part I.

# Basics

# Chapter 2: Reactions between Organic Molecules and Semiconductor Surfaces

The general properties of the (001) surfaces will be introduced in this chapter in order to discuss the resulting adsorption structures of organic molecules depending on the surface stoichiometry and atomic structure. The common characteristics and structural as well as electronic properties will be shown. In the last section of this chapter the results found in literature so far for the adsorption of cyclopentene, 1,4-cyclohexadiene and benzene will be summarized.

## 2.1. The (001) surface reconstructions

The most important compound group-III and group-V element semiconductors crystallize in the zincblende(ZnS)-type structure, for example GaAs, InP, GaP, InSb and InAs. In this structure the (001) planes in the bulk are variantly occupied by cations and anions see Fig. 2.1.

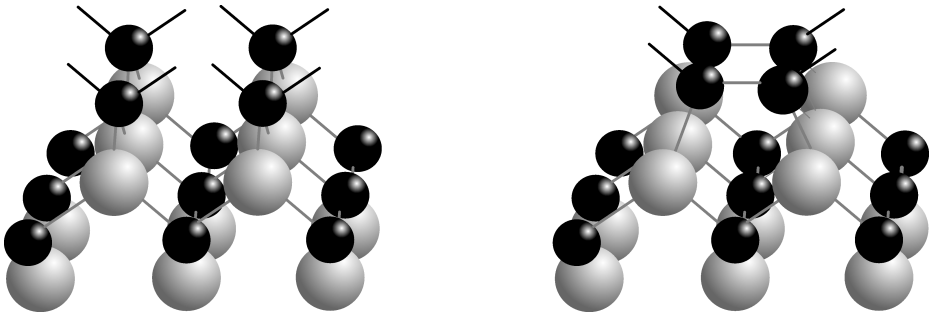

**Figure 2.1:** The (001) plane of a zincblende-type III-V semiconductor. On the left the bulk like surface is shown and on the right the formation of a reconstruction because of missing bonding partners. At the surface the alternating occupied cations (gray) and anions (black) of the (001) plane form bonds to the neighboring atoms. This reduces the amount of dangling bonds (black lines) and thus the surface energy.

In the case that the crystal is cut, the resulting surface differs from the bulk structure in such a way that dangling bonds (black lines in Fig. 2.1) are created. In order to minimize the

surface energy the surface tends to form new bonds to reduce the amount of dangling bonds. Accordingly dimerization of the surface occurs where neighboring atoms create new bonds to each other. Another point which occurs along with the dimerization is the strain energy which changes during the bond formation on the surface. This strain depends on the bond length of the dimer and the nearest neighbor distance in the bulk.

As a result of this, the electronic energies of the surface will be lowest, if the remaining dangling bonds are filled at the surface anions and empty at the surface cations, which is the so-called 'electron-counting-rule' (proposed by Pashley in 1989 [19]). This rule is important for the stability and the geometry for the surface and also for the adsorption structure of molecules.

A fundamental condition for the use of the electron counting rule is the existence of covalent bonds between atoms which are occupied with two electrons, respectively. Additionally the rule is based on the fact that binding energies for surface cations are smaller than for surface anions. Here the electronegativity value is important because it is different for the respective elements. The values for the electronegativities of the elements which are important for this work are given in table 2.1.

| ELEMENT | ELECTRONEGATIVITY |
|---|---|
| *C* | 2.6 |
| *P* | 2.2 |
| *Ga* | 1.8 |
| *As* | 2.2 |
| *In* | 1.8 |

**Table 2.1:** Values for the electronegativities (Pauling) for the elements which are relevant for the investigations in this work taken from [20].

Another point which plays a role for the adsorption of organic molecules later on is the arrangement of the dimer atoms. The dimer configuration and thus the strain on a surface induced by the dimer bond length is not equal for each semiconductor surface. For example the GaAs$(001)(2\times4)$ reconstructed surface consists of a symmetric dimer configuration while the topmost layer of the InP$(001)(2\times4)$ surface is dominated by an asymmetric dimer as shown in Fig. 2.2. The reason for this different dimer configuration on these two surfaces are the rearrangement of the charge at the surface during the dimer bond formation to minimize the surface energy and the rehybridization of the topmost atoms. Thus the buckled up atom on the InP$(001)(2\times4)$ surface is more $sp^3$ hybridized while the buckled down atoms is more $sp^2$ hybridized. In the contrast to this on the GaAs$(001)(2\times4)$ reconstructed surface both topmost As atoms are $sp^3$ hybridized whereas the Ga atoms of the second layer display a $sp^2$ hybridization.

The differences in the surface reconstructions are crucial parameters for the interface reactions. It can be varied by changing the stoichiometry for example on a III-V semiconductor

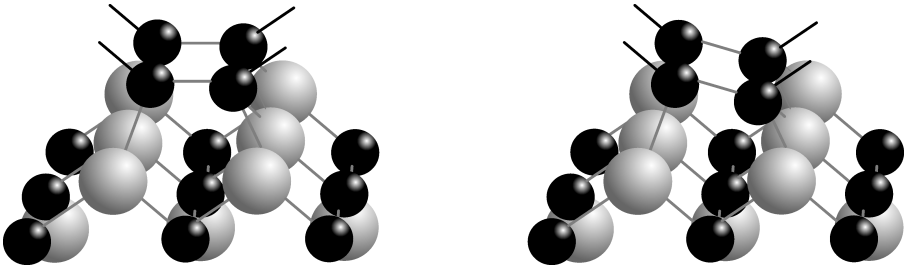

**Figure 2.2:** The schematic difference in the dimer configuration for a symmetric (left) and an asymmetric (right) dimer arrangement. The rearrangement of the atoms in the second layer because of the buckled dimer has been neglected in this picture.

from a group V-rich to a group III-rich surface. This is, for example on GaAs, also accompanied by a change in the surface symmetry which can introduce different compressive or tensile strains on the surface which has to be taken into account for the resulting adsorption structures of the organic molecules. The surface dimer itself can also have different stoichiometries since it can consist either of atoms of the same type ('homo'-dimer) or different atomic species ('hetero'-dimer).

## 2.2. Electronic Levels and Bonding Configurations

For the adsorption of organic molecules on such surfaces different bonding configurations can result. In general two main adsorption processes can appear, chemisorption and physisorption. During chemisorption a chemical bond to the surface occurs while in the case of physisorption no covalent bond between the surface and the adsorbate is formed. This interaction is weak and dominated by forces which are similar to the 'van der Waals' force in molecules. Thus they can be attributed to dipole- or multipole-interaction.

In relatively high surface distances ($d > 0.3\ nm$) for the physisorption a weak minimum can be observed before the strong repulsive forces, the overlap of the electron densities, lead to a strong increase of the interaction energy. The bonding of physisorbed molecules is very weak and not comparable to the one in chemisorption. Typically the bonding energy for a physisorbed molecule is in the range of a few meV. No significant charge rearrangement for the molecule or the surface occur during the physisorption and it is possible to get multilayers of molecules on the surface kept by the van der Waals force [21].

### Chemisorption

Chemisorption appears if a chemical bond between the organic molecule and the surface is formed. In this case a significant charge transfer occurs for the molecule and the surface. Accordingly the adsorption energy in the range of a few eV is higher than for physisorption.

Chemisorption only takes place in the first monolayer and has often to be activated. Different chemical bond formations are possible: e. g. ionic-, covalent-, dissociative- or dative- bonds. In the case of a covalent bond formation for example, both the surface and the molecule contribute electrons to build the new bonds.
During a dissociative molecule adsorption, parts of the molecule split and the molecule is not bound as a whole to the surface whereas in a dative bond formation, the electrons are provided either by the molecule or by the surface. In contrast to physisorption, chemisorption is not always reversible.

In the case of chemical bond formation of a monolayer, charge is arranged in such a way that new bonds can be formed. This results in a saturation of empty surface or molecule states. Thus the electronic structures of both, the surface and the molecule, is modified.
Three charge transfers are possible:

- The ionization energy of the molecules is smaller than the work function of the substrate.
- The electron affinity of the molecules is larger than the work function. Thus the molecules takes the charge from the surface
- The ionization energy of the molecules is larger than the work function of the substrate and the work function is larger than the electron affinity.

With the overlap of the wave functions of the adsorbate and the substrate new orbitals can be formed. This results during a weak bonding, in a broadening of the adsorbate orbitals compared to the width of the conduction band. With the formation of a strong bond new bonding-antibonding states appear.

## 2.3. Adsorption Structures of Organic Molecules

The formation of the first bondings appear most likely during a chemisorption. Different adsorption sites are possible for each surface depending on the dimer configuration and surface stoichiometry. The dimer configuration is an important parameter for the resulting adsorption structure of the organic molecules on the surface. Thus if the dimer is asymmetric or symmetric can be a supporting factor for the adsorption of the molecules or not. Due to the resulting strain after the adsorption of the organic molecules on a dimer different adsorption structures of organic molecules can result. The surface dimer bond can not be arbitrarily stretched during the adsorption. It can be possible either that the dimer remains intact in a so called ‘dimerized’ adsorption configuration or the dimer is cleaved in a ‘dimer-cleaved’ configuration. Both will be explained in detail in this section. Additional to this consideration the molecules can form one, two or even more bonds to the topmost atoms of the surface.
The change in the strain at the bonds of the surface atoms is not the only important parameter which has to be considered for the suggestion of the first bonding sites of organic molecules

on a surface. Important is also the strain which is induced into the bonds of the molecule during the adsorption. Regarding the strain these bonds can not be arbitrarily stretched, too.

Overall the total surface energy should result in a minimum after the adsorption process thus remaining dangling bonds at the surface or the molecule are energetically unfavored. Charge transfer between the topmost atoms of the surface or between the surface and the molecule can play a role for the resulting adsorption structure.

Concluding from all these considerations it follows that the adsorption process of organic molecules on a reconstructed surface is a complex process. Nevertheless it is possible to summarize from these basic considerations general rules which have to be taken into account when suggesting adsorption structures of organic molecules:

- the strain which is induced onto the surface
- the strain which is induced into the molecule
- the electron-counting-rule should be fulfilled
- a rehybridization can occur
- the surface stoichiometry and dimer configuration has to be taken into account.

All of the general points which have been explained in this chapter are based on experimental and theoretical studies and are sufficient to explain the ideas of the resulting adsorption structures. In the following a more detailed overview about possible reactions and the possible adsorption sites will be given.

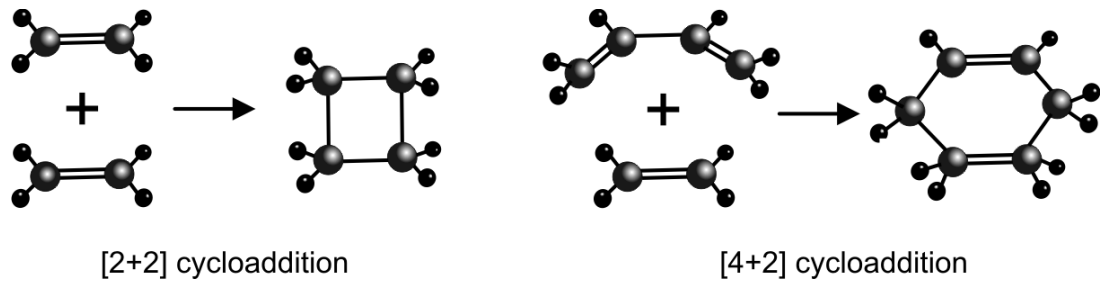


**Figure 2.3:** On the left: $[2+2]$ cycloaddition reaction of two alkenes, ethylene molecules. On the right: a $[4+2]$ cycloaddition reaction between an alkene and an diene which form a six-members ring. The number of $\pi$ bonds involved in the reaction refer to the designations [3].

## Cycloaddition Chemistry on Semiconductor Surfaces

Organic reactions like cycloaddition reactions could be applied to explain surface functionalization [3]. For the formation of carbon-carbon bonds, during the synthesis of new molecules, cycloaddition reactions are widely used because of their high stereoselectivity and versatility [22–24]. During a cycloaddition reaction two $\pi$ bonded molecules form a new cyclic

molecule while losing two $\pi$ bonds and creating two new $\sigma$ bonds. Designated are the reactions by how many $\pi$ electrons are involved in the reaction. In Fig. 2.3 an example for the $[2+2]$ and the $[4+2]$ cycloaddition reactions are depicted. One line represent a single bond while a double line indicate a double bond between the atoms, respectively. In the $[2+2]$ reaction two $\pi$ electrons of each ethylene molecule are involved in the reaction. The $[4+2]$ reaction (Diels-Alder reaction [22] [1]) is shown in Fig. 2.3 on the right for a 'diene' molecule with two conjugated $\pi$ bonds, butadiene, and one alkene, ethylene, to form a six-member ring.

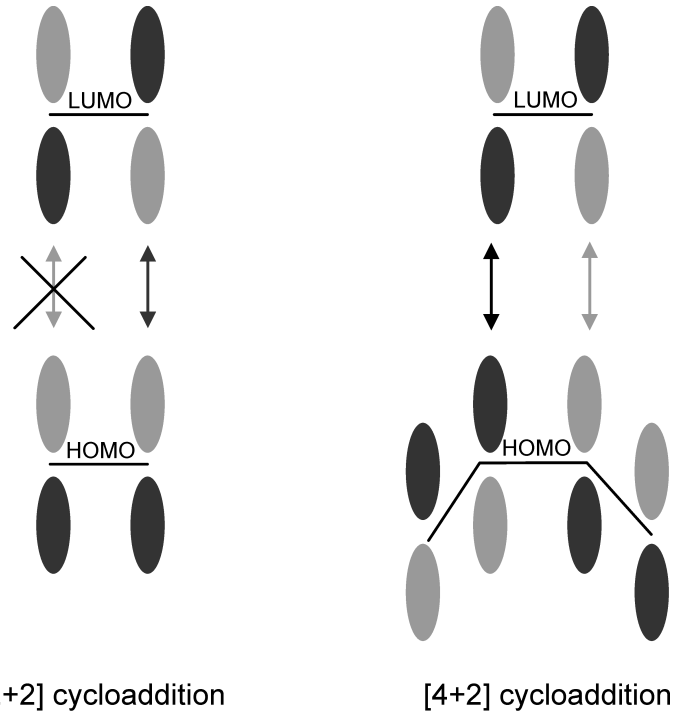


**Figure 2.4:** The highest occupied (HOMO) and lowest unoccupied (LUMO) molecular orbital for the frontier orbitals. The dark and light gray lopes represent the mathematical sign of the molecular orbital. Only the combinations of orbitals with the same color is possible and other combinations are symmetry forbidden, as it is the case for the $[2+2]$ cycloaddition reaction [3].

Cycloaddition reactions are following the 'Woodward-Hoffman' selection rules which stem from an analysis based on the frontier orbital theory. It deals with the symmetries of the highest occupied (HOMO) and the lowest unoccupied molecular orbital (LUMO) of the reactants during the formation of a new reaction product. This theory about the frontier orbital theory was composed by Woodward and Hoffman and they are widely used for the prediction how readily an organic reaction will occur, see [25].

Regarding the 'Woodward-Hoffman' selection rules the light and dark gray lobes in Fig. 2.4 represent positive and negative lobes and have to overlap 'in phase'. This means

[1] Otto Diels and Kurt Alder received the Nobel Prize in Chemistry in 1950 for their studies of this reaction.

for a symmetry allowed reaction the lobes must have the same color.
This is not the case for the $[2+2]$ cycloaddition reaction which is 'symmetry forbidden' because of the particular properties of the $[2+2]$ reaction (see Fig. 2.4). This reaction do not occur without a significant activation energy and is in organic chemistry largely limited to synthesis involving photochemical activation.

The $[4+2]$ cycloaddition instead is allowed by the frontier orbital symmetry. For the formation of new $C-C$ bonds the Diels-Alder reactions are commonly used in organic synthesis [3].

For the analogy discussion of a cycloaddition reaction occurring between an organic molecule and the $Si(001)(2\times1)$ reconstructed surface see section 2.5 and the next section.

## The 'Dimerized' and 'Dimer-cleaved' Adsorption Structures

Prerequisite for a $[2+2]$ cycloaddition reaction between an organic molecule and a semiconductor surface is an asymmetric dimer configuration. As mentioned before regarding the 'Woodward-Hoffman' rules this cycloaddition reaction is without a significant activation energy forbidden. If double bonds between dimer atoms exist analogies can be drawn to a carbon-carbon double bond. Through the asymmetry of the dimer the $[2+2]$ cycloaddition reactions at room temperature is possible because it has been proposed that the molecule approaches in an asymmetric pathway. The asymmetric approach results in a lower symmetry and thus the energy barrier is little or non existent [3]. The resulting adsorption structure is called 'dimerized' adsorption and is shown on the left in Fig. 2.5 for the adsorption of cyclopentene as a template.

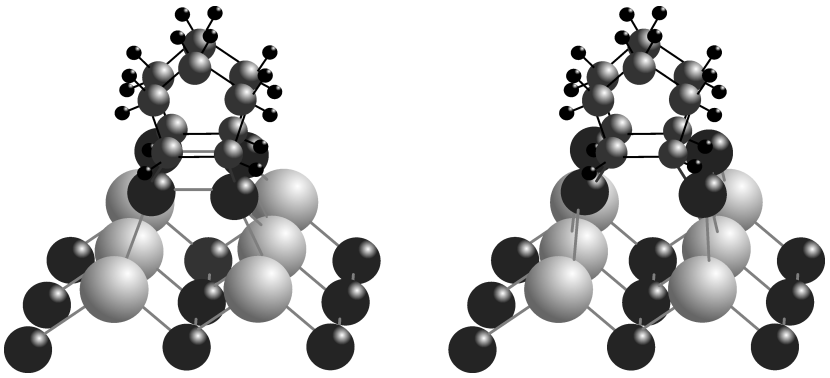

**Figure 2.5:** The different dimer configurations for the adsorption of organic molecules (an example shown for cyclopentene) called 'dimerized' (left) and 'dimer-cleaved' (right) structure. Both structures have general validity for other organic molecules.

On the right in Fig. 2.5 the 'dimer-cleaved' adsorption structure is shown. In this configuration the dimer bond between the dimer atoms at the surface does not remain intact after the adsorption of the molecule.

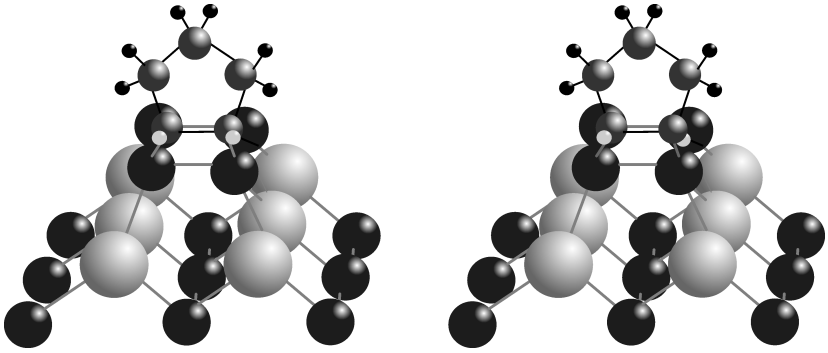

**Figure 2.6:** On the left: the cis-type adsorption configuration of the organic molecule on the surface. On the right: the trans-type adsorption structure. In the cis-type configuration the two hydrogen atoms (light gray) at the $C-C$ atoms which are bonded to the surface are on the same side of the $C-C$ bond and on different sides in the trans-type configuration.

Different sub-configurations for these adsorption structures ('dimerized' and 'dimer-cleaved') are possible like the cis-type or the trans-type adsorption configuration. These two types are depicted in Fig. 2.6 on the left and right, respectively. In the cis-type configuration the two hydrogen atoms at the carbon atoms, which are bonded to the surface, are on the same side of the $C-C$ bond and on alternating sides in the trans-type configuration.
Beside these adsorption possibilities a single bond formation between the organic molecules and the surface can alternative occur which is presented in the following.

## Single Bond Adsorption Structures

A single bond formation of an organic molecule during the adsorption on a semiconductor surface can occur. One possibility for this adsorption structure is depicted in Fig. 2.7 (left). During the bond formation the dimer bond could remain intact or not. This single bond can occur beside a dissociation of the organic molecules. For example one hydrogen atom is dissociated and because of the missing bonding partner the molecule can form a bond to the semiconductor surface. Additional hydrogen atoms which are separated from the molecules can bond beside the molecule to the surface.

It has to be mentioned that these configurations which were introduced here are just a few examples and not all of the possible different adsorption structures. To find the energetically favored adsorption structures several investigations with different complementary methods are necessary. Therefore the monitoring by measuring the chemical composition of the surface (SXPS), as well as the electronic (valence band spectroscopy) and optical properties (RAS) can be applied.

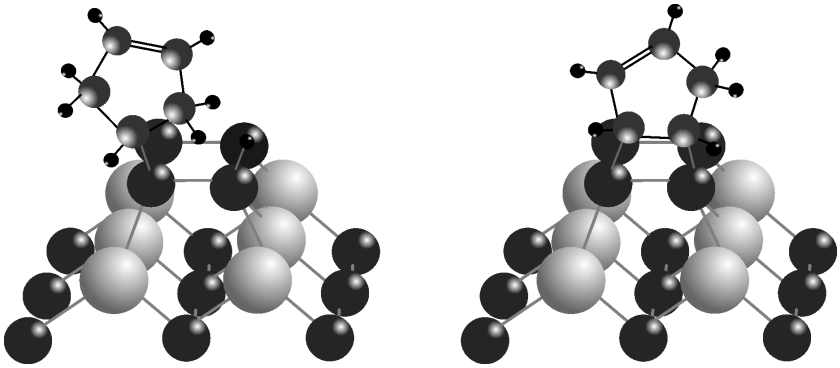

**Figure 2.7:** Dissociative adsorption structures are shown. In both cases hydrogen atoms are separated from the molecules to create empty bonds where the molecule can bind to the surface with. Two (left) or one bond (right) to the surface are formed while two or one hydrogen atoms are dissociated.

## 2.4. Desorption

The desorption of the organic molecules is not always a possible process. In the case of chemisorption two different desorption processes can appear. The first one is called non-dissociative, and the second one dissociative desorption. In the latter case the molecules can not be desorbed as a whole but only in parts. By increasing the desorption energy the remaining parts of the molecule can be further removed.
Physisorption is a completely reversible process which can be realized for example by thermal annealing.
The desorption processes can be monitored by observing the chemical composition (SXPS), the electronic (valence band spectroscopy) or the optical (RAS) properties of the surface. Additionally the clean surface reconstruction can be determined with low energy electron diffraction (LEED).

## 2.5. Organic Molecules on Semiconductors

Only very few publications exist about investigations of small organic molecules on GaAs or InP$(001)$ surfaces [18, 26, 27]. In most existing publications, thick layers of organic molecules or large molecules are discussed but not the systematical interface formation of the first organic layer on the surface [14–17, 26, 28, 29]. Several investigations of organic molecules on silicon are available especially on the Si$(001)(2\times1)$ reconstructed surface. From the structural configuration, the Si$(001)(2\times1)$ is comparable to the $(001)$ surfaces which were used in this work, but it consists of an asymmetric 'buckled' dimer [11–13] which is prerequisite for a cycloaddition reaction [3]. The dimers are attached by a weak $\pi$ bond and strong $\sigma$ bond with a bond length of $\sim$2.4 Å [13,30], a dimer buckling of $\sim$0.56 Å [13] and half filled dangling bonds at the dimer atoms [31, 32]. Hence the Si$(001)(2\times1)$ is a very reactive surface.

As it was explained in section 2.3 the $[2+2]$ cycloaddition reaction of an organic molecule with the Si$(001)(2\times1)$ surface is after the 'Woodward-Hoffman-rule' without a significant activation energy forbidden. Thus a true $[2+2]$ cycloaddition reaction would not occur. Because of the double bonds between the Si dimer atoms and since C and Si are in the same group (IV) of the periodic table the analogies explained in section 2.3 can be drawn for this system. Through the asymmetry of the dimer the $[2+2]$ cycloaddition reactions at room temperature is possible because it has been proposed that the molecule approaches in the asymmetric pathway which enables the $[2+2]$ cycloaddition reaction ( [3] and references therein).
For the discussion of the resulting adsorption structures of molecules on the GaAs and InP$(001)$ surfaces a small overview about the adsorption of cyclopentene, 1,4-cyclohexadiene and benzene adsorbed on the Si$(001)(2\times1)$ surface is given here, respectively.

## Benzene Adsorption on Si$(001)(2\times1)$

Different experimental methods like high resolution electron energy loss spectroscopy (HREELS) [33], RAS [34], fully polarization-resolved near edge x-ray-absorption fine-structure (NEXAFS) [35], thermal desorption spectroscopy (TPD) and angle-resolved photoelectron spectroscopy (ARUPS) [36], ultraviolet photoelectron spectroscopy (UPS), scanning tunneling microscopy (STM) [37] as well as calculations [38–40] have been used to determine the adsorption structure of benzene on the Si$(001)(2\times1)$ surface.

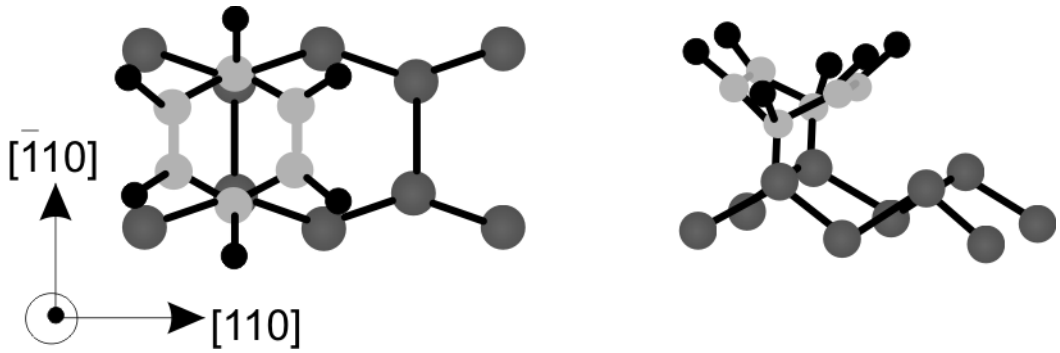


**Figure 2.8:** Favored adsorption 'butterfly-like' structure of benzene on the Si$(001)(2\times1)$ reconstructed surface. On the left is the top- and on the right the side view. Black, gray and light gray balls represent the hydrogen, silicon and carbon atoms, respectively. A light gray line between the carbon atoms indicate a double bond, other colors refer to single bonds.

These results lead to different adsorption structures, like the pedestal tetra-$\sigma$ [38], the butterfly-like [33–36] or the tilted dimer structure [35, 41], which are possible and in discussion. All these models have in common that the dimer bond remains intact during the adsorption of benzene. In [40] the minimum in total energy for dimer-cleaved models were

calculated too but it was found that all of the total energies for these optimized geometries were larger than for the dimerized models. In the case of all structure configurations the delocalized $\pi$ electron system is destroyed. One or two $\pi$ bonds remain in the pedestal or the butterfly-like structure, respectively.
Additionally it was found that the structure changes with the coverage. In [42] the change from the pedestal tetra-$\sigma$ at a very initial coverage up to the di-$\sigma$ structure at the quasisaturation coverage is shown.
In Fig. 2.8 the favored butterfly-like adsorption structure is shown in the top- and side view. In this structure two di-$\sigma$ bonds to the surface are formed and the orientation of the remaining double bonds within the molecule is along (parallel to) the Si dimers with the coordinating atoms showing $sp^3$ hybridization. This stable geometry was found at room temperature and no other stable adsorption geometry was found at higher temperatures or after annealing [35].

## 1,4-Cyclohexadiene Adsorption on Si$(001)(2\times1)$

Several investigations were also performed for the adsorption of 1,4-cyclohexadiene on the Si$(001)(2\times1)$ surface such as HREELS, STM and PES [28, 43, 44], UPS [45] and also first-principles density-functional calculations [46]. From this, two main structures are under discussion, the pedestal model, similar to the case of the adsorption of benzene, and the di-$\sigma$ model as shown in Fig. 2.9.

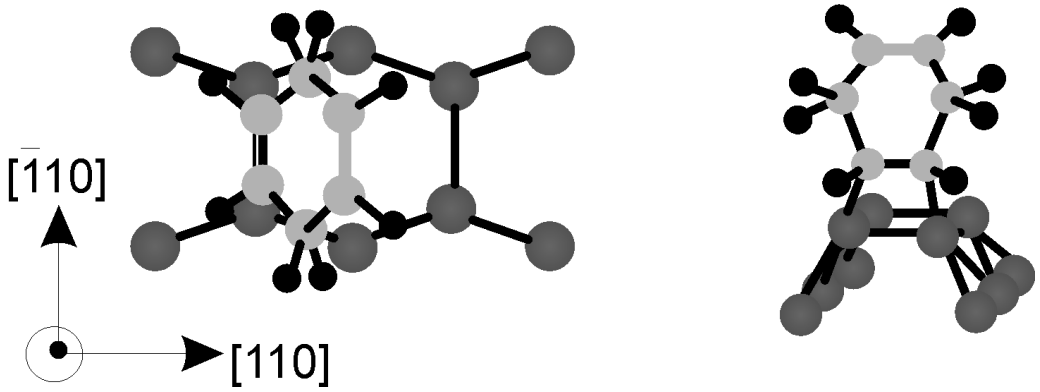


**Figure 2.9:** Favored adsroption di-$\sigma$ structure of 1,4-cyclohexadiene adsorbed on the Si$(001)(2\times1)$ reconstructed surface. On the left in the top- and on the right in the side view. Black, gray and light gray balls represent the hydrogen, silicon and carbon atoms, respectively. A light gray line between the carbon atoms indicate a double bond other colors refer to single bonds.

In the di-$\sigma$ model two $\sigma$ bonds to the silicon surface are formed in a $[2+2]$ cycloaddition-like reaction [44]. One double bond ($\pi$ bond) remains intact during the adsorption process and the molecules are ordered along the Si$(001)(2\times1)$ dimer rows. The molecular plane during this interface formation is tilted from the surface normal, and thus the unreacted $\pi$ bond sticks out into the vacuum side.

## Cyclopentene Adsorption on Si$(001)(2\times1)$

The adsorption structure of cyclopentene on Si$(001)(2\times1)$ was for example investigated with XPS [47], UPS [48, 49], STM [6] and RAS [7]. Additional first-principles density-functional calculations were done [7, 50]. Concluding from the experimental and theoretical results the most common accepted structure model of cyclopentene adsorbed on the Si$(001)(2\times1)$ (and Si$(001)$c$(4\times2)$) is the cis-type dimerized structure, see Fig. 2.10 [6,7,51,52].

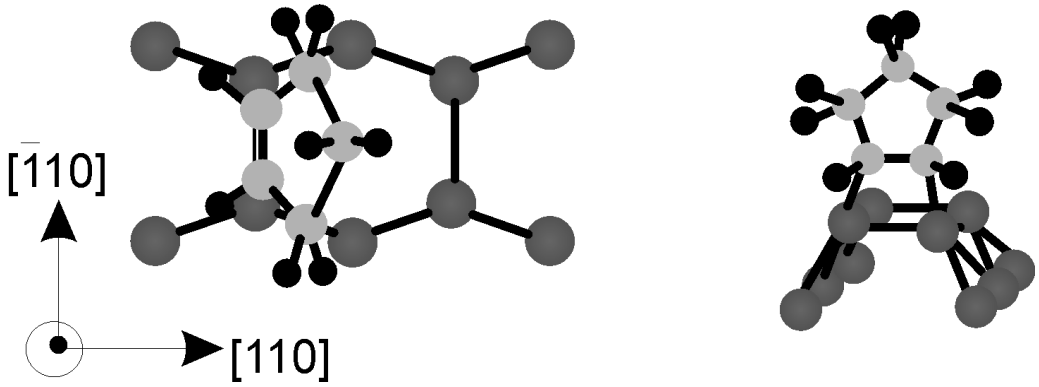


**Figure 2.10:** Schematic structures of the cis-type adsorption of cyclopentene on the Si$(001)(2\times1)$ surface. This is the favored structure for the adsorption of cyclopentene on the Si$(001)(2\times1)$. On the left in the top- and on the right in the side view. Black, gray and light gray balls represent the hydrogen, silicon and carbon atoms, respectively. Only $\sigma$ bonds remain after the adsorption (black).

Thus the dimer bond between the two topmost silicon atoms remains intact during the $[2+2]$ cycloaddition-like reaction of cyclopentene on Si$(001)(2\times1)$. The $\pi$ bond splits during the adsorption and only the $\sigma$ bonds within the molecules remains intact.

# Chapter 3: Molecule Properties

The molecules which were used in this work consist only of hydrogen and carbon atoms arranged in ring structures. They contain no special functional group but they have a different number of double bonds which can be interpreted as functional groups. A functional group in a molecule determines the molecule properties and the behavior during a reaction.
With the different number of intra-molecular double bonds the influence of the intra-molecular double bonds to the adsorption process can be investigated. Therefore in this work only unsaturated hydrocarbons, cyclopentene, 1,4-cyclohexadiene and benzene, were used to characterize the first adsorption sites of these molecules on different surface reconstructions. To understand the functionalization of the surface, the molecules and their properties will be discussed in this chapter. The molecular orbitals and structures which are shown in this work have been calculated on the basis of geometry optimization by DFT/B3LYP [1] with a 6-31**G(d,p) basis set [53].

## 3.1. Hydrocarbon Ring Molecules and their electronic structure

The development of molecular orbitals can be understood in that way that the discrete energy levels of the atomic orbitals of the respective atoms in a molecule interact and thus split in molecular orbitals, see Fig. 3.1.

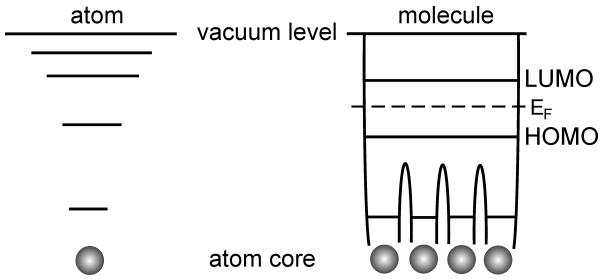


**Figure 3.1:** Discrete atomic energy levels (left) compared to the orbitals in a molecule (right).

[1] In the B3-LYP functional, the exchange term is replaced by an exchange functional retaining a percentage of the so-called 'exact' exchange. This functional contains a mixture of 20% exact exchange with 80% of a pure exchange functional.

The interaction of the atomic orbitals of the bonding atoms of a molecule lead to the formation of two different types of bond symmetries. The first one is the $\sigma$ bond. Here the electrons are with a high probability between the two bonding atoms. They are attracted by both atom cores and at the same time rejected by each other. Thus in a $\sigma$-orbital the electrons are nearly in a stationary position between the atomic cores. According to this the $\sigma$ bond is very strong because the kinetic energy of the electrons is very low.
In contrast to that, the $\pi$ bond is delocalized over the participating atoms. In this kind of bonding the electrons are not located between the atom cores but around the cores. $\pi$ bonds can couple more than two atoms. If a molecule consists of conjugated double and single bonds a delocalization over the hole molecule can occur. In the case of for example benzene, the $\pi$ orbitals couple all of the six carbon atoms so that the electrons are delocalized over the whole molecule for this conjugated system. For cyclopentene and 1,4-cyclohexadiene there is no delocalization over the whole molecules.
If two carbon atoms bond to each other both bond configurations, $\sigma$ and $\pi$, are possible. Each of the carbon atoms in the ground state has four valence electrons, two in the $s$ state, one in the $p_x$ and one in the $p_y$ state. The interaction of these two carbon atoms results in a hybridization to minimize the bond energy by promoting one electron from the $s$ state into the $p_z$ state. Due to the overlap of the four atomic orbitals this results in a $sp^3$ hybridization. A $sp^2$ hybridized bond results due to a mixing of the $s$ and the $p$ orbitals and one electron at each carbon atom remains in the $p_z$ orbital. Due to the overlap of the $p_z$ orbitals the electrons are no longer limited to the $\pi$ orbital of a certain double bond. This results in a delocalization of the electrons of the $p_z$ states over the hole molecule in the $\pi$ orbital.

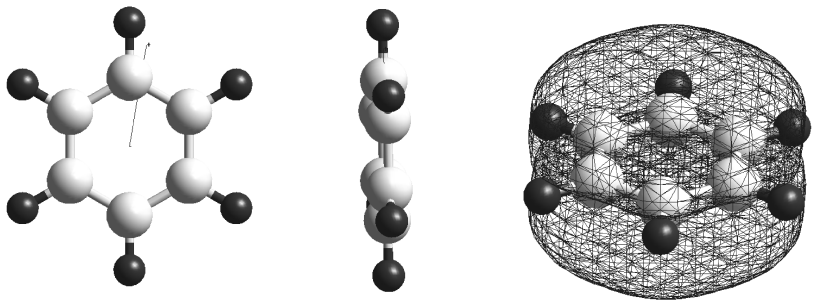

**Figure 3.2:** Schematic structures of benzene $(C_6H_6)$: The localized $\sigma$ orbitals are shown on the left together with the resulting dipole moment of the molecule. In the middle the side view is shown. The planar shape of benzene can be seen. On the right the $\pi$ orbitals with the highest density above and below the plane of the ring are depicted.

The visualization of the $sp^2$ hybridized molecule benzene with a delocalized $\pi$ orbital over the whole molecule is shown in Fig. 3.2.

## Benzene

Benzene $(C_6H_6)$ is an aromatic ring shaped molecule with alternating single and double bonds. After the 'Hückel rule' a molecule is called an aromatic if it consists at least of one closed cyclic system with a delocalized $\pi$ electron system with $(4n+2)$ $\pi$ electrons. All atoms of the flat ring have to be $sp^2$ hybridized. This is the case for benzene. Effectively all $C-C$ bonds are equivalent because of the delocalization. According to the LCAO (linear combination of the p-atom orbitals) the overlap of the atomic orbitals leads to a formation of three binding $\pi$ and three anti-bonding $\pi^*$ orbitals [54].
In most cases the highest $\pi$ state gives rise to the highest occupied molecular orbital (HOMO) while $\pi^*$ is the lowest unoccupied molecular orbital (LUMO). Additionally 12 $\sigma$ and 12 $\sigma^*$ orbitals exist in benzene originating from the carbon-carbon and hydrogen-carbon bonds. The orientation of the $\sigma$ bonds lies within the plane of the ring and the $p_z$ states are perpendicular to this plane. The bonding angle for all $C-C$ bonds is 120° and all bond lengths are equal with 1.4 Å [53,54]. Because of this all of the twelve atoms of benzene are in one plane (see Fig. 3.2).

## 1,4-Cyclohexadiene

The 1,4-cyclohexadiene $(C_6H_8)$ molecule includes only two double bonds as can be seen in Fig. 3.3. The electrons of the $\pi$ orbitals are not delocalized over the whole molecule because the single and double bonds are not alternating.

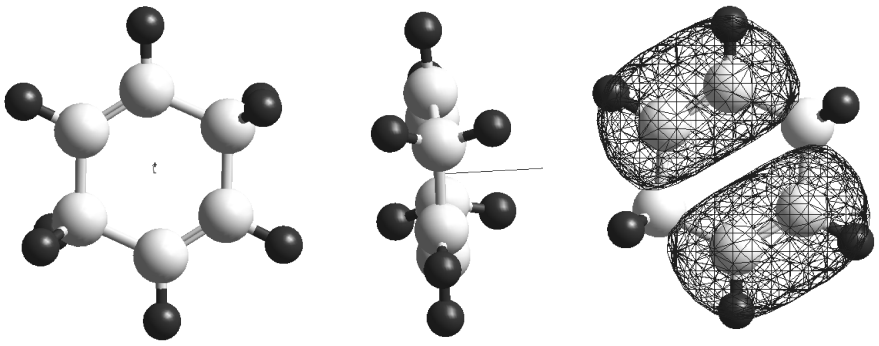

**Figure 3.3:** Schematic structures of 1,4-cyclohexadiene $(C_6H_8)$: The $\sigma$ and $\pi$ bonds are indicated by single and double bonds on the left along with the dipole moment of the molecule. The side view is displayed in the middle and on the right the $\pi$ orbitals of 1,4-cyclohexadiene are shown.

The term '1,4' means that the double bonds are between the first and second as well as at the fourth and fifth carbon atoms as can be seen in Fig. 3.3. With four $\pi$ electrons 1,4-cyclohexadiene does not follow the Hückel rule $(4n+2)$ and it has no flat configuration because the parts where the double bonds are located are moved out of the plane, as

can be seen in Fig. 3.3. 1,4-cyclohexadiene is no conjugated system and hence no aromatic molecule. The bond lengths of the $C-C$ and $C=C$ bonds are 1.53 Å and 1.32 Å , respectively [53].

## Cyclopentene

Cyclopentene, as shown in Fig. 3.4, is a ring shaped molecule like benzene and 1,4-cyclohexadiene but the ring only consists of five carbon atoms. The $\pi$ orbital in cyclopentene is located at two of the five carbon atoms. Thus there is no delocalization of the $\pi$ electrons over the whole molecule and cyclopentene is not an aromatic molecule.

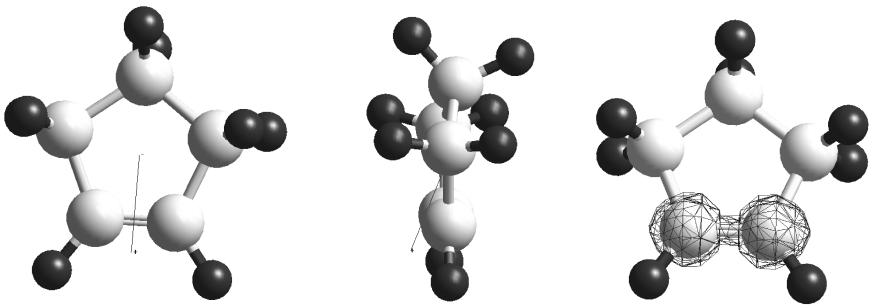

**Figure 3.4:** Schematic structures of cyclopentene $(C_5H_8)$: The $\sigma$ and $\pi$ bonds are indicated by single and double bonds on the left in combination with the dipole moment of the molecule. The side view is displayed in the middle and on the right the $\pi$ orbital of cyclopentene $C_5H_8$ is presented.

The carbon atom which is on the opposite of the carbon atoms involved in the double bond is moved out of the plane. The bonds lengths of the $C-C$ and $C=C$ bond are similar to the bond lengths for 1,4-cyclohexadiene 1.54 Å (for the $C-C-C$), 1.52 Å (for the single bond in $C-C=C$) and 1.34 Å (for the double bond), respectively. The $C-H$ bond length is found to be 1.10 Å [53, 55].

In Fig. 3.5 the comparison between the HOMO-LUMO gap (comparable to the band gap in an inorganic semiconductor like GaAs) is shown. The gap of each molecule was calculated on the basis of geometry optimization by DFT/B3LYP with a 6-31**G(d,p) basis set. A gap of 7.23 eV is found for cyclopentene while for 1,4-cyclohexadiene and benzene 6.83 eV and 6.47 eV were calculated, respectively [53].

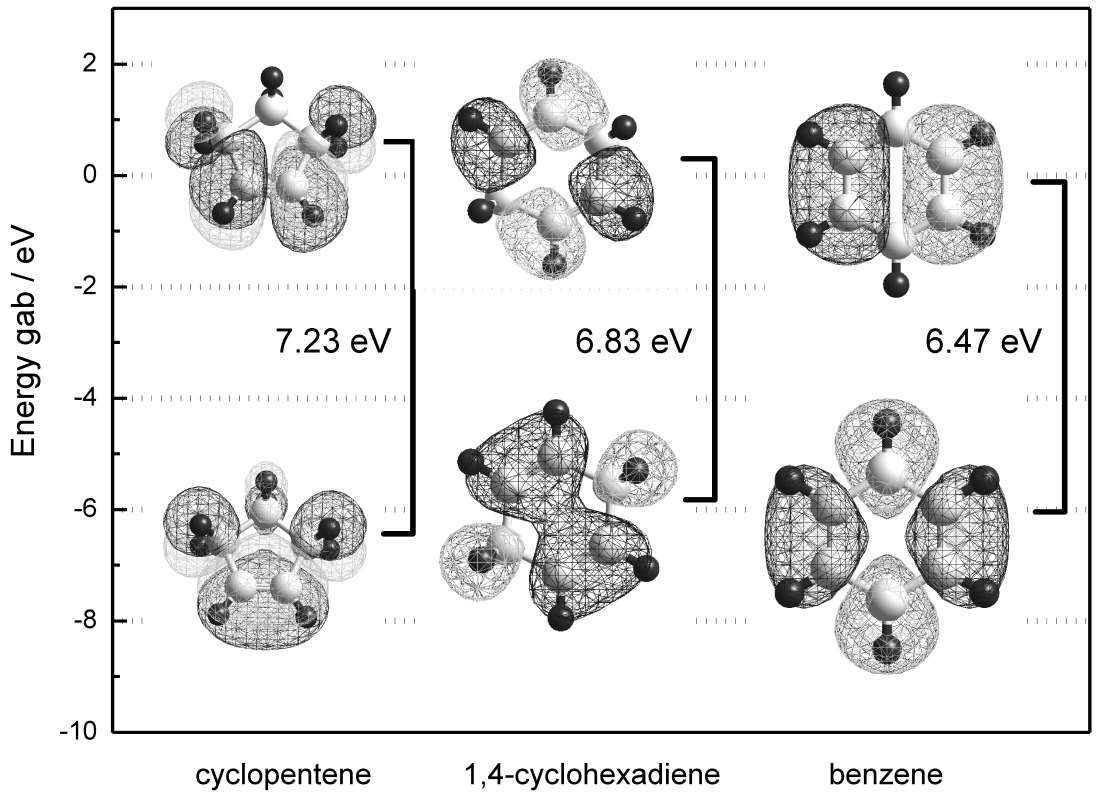


**Figure 3.5:** The HOMO-LUMO gap of cyclopentene, 1,4-cyclohexadiene and benzene are shown. The molecular orbitals which are presented here have been calculated on the basis of geometry optimization by DFT/B3LYP with a 6-31**G(d,p) basis set [53].

# Chapter 4: Experimental Methods and Sample Preparation

In the previous chapter the formation and characteristics of hybrid structures consisting of organic molecules and III-V$(001)$ surfaces have been discussed. For each adsorption structure different methods of investigations can be used to determine the atomic arrangement within the topmost layer of the surfaces. This chapter will give an overview of these methods and will introduce the surface preparation methods as well as the deposition parameters.

## 4.1. Experimental Methods

All experiments were carried out in ultra high vacuum (UHV) to investigate defined surfaces and adsorption structures without contamination. The electronic properties were investigated with scanning tunneling microscopy (STM), scanning tunneling spectroscopy (STS) and synchrotron based photoemission spectroscopy (SXPS). Additionally SXPS gives an overview of the chemical content of the surface topmost layers. The changes in the optical anisotropy were monitored with Reflectance Anisotropy Spectroscopy (RAS). Low electron energy diffraction (LEED) measurements were performed since it is sensitive to a change in the periodicity of the surface atoms arrangement or the surface symmetry.

### 4.1.1. Scanning Tunneling Microscopy (STM)

Scanning tunneling microscopy was invented in the 1980's by G. Binnig, H. Rohrer, C. Gerber and E. Weibel and has become an invaluable and powerful method for the investigation of surfaces and interfaces [56–58]. G. Binning and H. Rohrer received together with E. Ruska for his contribution to the development of electron microscopy, the Nobel Prize in physics in 1986. The idea of scanning tunneling microscopy is based on a quantum mechanical tunneling current. This means that an electron has a finite probability of entering a classically forbidden region.
Atomic resolution is achieved by a very sharp metal tip, ideally consisting of only one atom, which scans the surface in $x$- and $y$- direction measuring the current between tip and sample at each surface position while the voltage applied between the tip and the sample is fixed. Thus an image for the whole surface can be taken. The reproducible positioning and the movement of the sample is obtained by piezo drives which can move the tip in sub-atomic

steps. The atomic resolution in the images can be achieved because of the strong exponential dependence of the tunnel current on the distance between the two electrodes. It is possible to run the STM in two ways: the 'constant current mode' and the 'constant height mode'. In the 'constant current mode' the current between tip and sample is kept constant and the distance is changed by a $z$-piezo. The change in the voltage for the piezo driving as a function of the tip position gives then the information for the image. In the 'constant height mode' the tip/sample distance is kept constant while scanning the surface. In this mode the current measured between tip and sample gives the topography information for the image of the surface.
To describe the transmission probability of an electron with energy E by assuming a rectangular barrier $V_b$ between tip and sample, the Schrödinger equation has to be solved. The tunneling current, which is proportional to the probability density $|\Psi(z)|^2$ of finding an electron at a distance $z$ from the barrier, is then given by:

$$I \approx |\Psi(z)|^2 = |\Psi(0)|^2 e^{\frac{\sqrt{8m(V_b-E)}}{\hbar}\cdot z} \tag{4.1}$$

This approach works well for a resolution in the nanometer scale but not for atomic resolution because the main fraction of the tunneling current arises from electrons at the Fermi level. This problem can be solved by taking the first order of perturbation into account. Therefore low temperatures and only elastic tunneling (energy conservation) are considered additionally:

$$I = \frac{4\pi q_e}{\hbar}\int_0^{q_eV} d\varepsilon \rho_{tip}(E_F^{tip} - q_e + \varepsilon)\rho_{sample}(E_F^{sample} + \varepsilon)\,|M|^2 \tag{4.2}$$

where $\rho_{tip}$ is the density of states of the tip and $\rho_{sample}$ of the sample. $E_F^{tip}/E_F^{sample}$ are the respective Fermi energies. So $I$ depends on the density of states of the tip and the sample and the matrix $M$ of which Bardeen showed that the matrix elements can be simplified [59].

However it is still necessary to express the wave function of the tip and the sample. This is a large problem because the atomic structure of the tip is completely unknown. Tersoff and Hamann recommended a solution in which the tip consists of a mathematical point source of current [60, 61]. From this approximation a tip-independent formulation for the tunneling current results:

$$I(\mathbf{r}_t) \approx \int_{E_F}^{E_F+q_eV} \rho_S^{local}(\mathbf{r}_t, E)dE \tag{4.3}$$

$\rho_S^{local}$ is the local density of states, which gives the density of states of the sample at a position $r$ of the tip above the sample.

By this approximation STM can simply be understood as a portrait of the electron density of states integrated over a chosen energy range. If a positive voltage is chosen with respect to the tip, the STM image shows the filled surface states of the electrons. Measuring with a negative voltage, the electrons tunnel into empty states of the sample, showing the unoccupied orbitals. Even though 4.3 was obtained by a significant simplification, Tersoff and Hamann showed that 4.3 remains valid regardless of the tip size. Further details concerning experimental and theoretical aspects of STM can be found in a textbook, as for instance [62–64].

In this work STM was used to determine the resulting adsorption structures of the organic molecules on each surface, the layer thicknesses and the roughness of the surfaces. With the help of complementary methods, models of the adsorption structures of the molecules on the surfaces were suggested in the discussion of the results. Depicted in the work are always the filled state STM images of each investigated surface. Additionally STS was performed on the clean surface and during the deposition of organic molecules. STS will be explained in the next section.

## Scanning Tunneling Spectroscopy (STS)

Scanning tunneling spectroscopy is a method performed complementary to the results obtained by conventional topographic imaging (STM). By measuring the detailed dependence of the tunneling current on the applied voltage, it is possible to measure the electronic density of states of a sample ( 4.3). The spectroscopic data gives information about the local electronic structure. The Differential conductivity can be described by:

$$\frac{dI(eU)}{dV} \approx \rho_S^{local}(\mathbf{r}_t, E_F + q_e V)dE \tag{4.4}$$

Equation 4.4 is valid under the assumption that $\rho_{tip}(E) = const$. According to this $\frac{dI}{dU}$ is directly related to the LDOS of the sample surface. STS provides information about the electronic band structure of semiconductors or metals [62,65]. In the case of a semiconductor also the surface band gap can be determined by STS. The fact that the unoccupied and occupied molecular orbitals can be measured is a very interesting point for this work. After the molecule deposition additional molecular orbitals could contribute to the surface band structure and thus the HOMO-LUMO gap could be modified [66]. This modification can be monitored between the different deposition steps. In fact, it could be possible to determine whether a surface becomes metallic during the adsorption of organic molecules by lowering the surface band gap.
One problem exists for the interpretation of the data obtained by STS because in 4.4 the tip structure is disregarded and the LDOS of the tip is assumed to be constant. Several tip conditions have to be chosen for a reliable interpretation of STS measurements. In this work STS is basically used to prove whether a surface is metallic or semiconducting or whether it

changes its behavior during the modification with organic molecules. Also the surface band gap was determined. For these interpretations small variations of the tip can be neglected. More information about experimental and theoretical aspects of STM and STS can be found in textbooks, e. g. [62–64].

### Molecule Influence on the Tip

During a STM/STS measurement in principle always an exchange of material between tip and surface can appear. This is problematical because in this case the electronic density of the tip is not constant anymore. Therefore changes during the measurement can occur because the tip can not be approximated by a mathematical point source of current. This results in a degradation of the resolution and electronic effects like 'contrast reverse' can occur.
These effects might be amplified due to the molecule adsorption. If additional physisorption appear molecules can be picked up by the tip because of a weaker bonding of the molecules to the surface. Due to these effects it can be very difficult to provide an atomic resolution constantly.

## 4.1.2. Photo-Emission Spectroscopy (PES)

Photoemission spectroscopy or photo-electron spectroscopy is widely used to investigate the electronic structure and properties of solids such as semiconductors or metals. In this work it will be used to identify the clean surface and characterize new surface related components, which results due to a bond formation of the organic molecules to the surface.

The effect of electron emission after irradiation with light was first discovered by Hertz in 1887 [67, 68]. The first correct explanation was given by A. Einstein in 1905 [69] for which he was awarded the Nobel Prize in physics in 1921. In this section only a brief description of the facts which are relevant for photoemission spectroscopy will be given. Further explanations can be found in [70, 71].

Electromagnetic radiation impinges on the solid sample and the electrons excited by the photoelectric effect are then analyzed with respect to their energy $E_{kin}$ in an electronic analyzer (see Fig. 4.1). By knowing the energy of the electromagnetic radiation and the work function, the binding energy $E_B$ of the electrons in the sample can be determined from the following equation:

$$E_{kin} = \hbar\omega - \phi - |E_B| \tag{4.5}$$

where $E_{kin}$ is the kinetic energy of the emitted electron, $\phi$ is the work function of the analyzer,

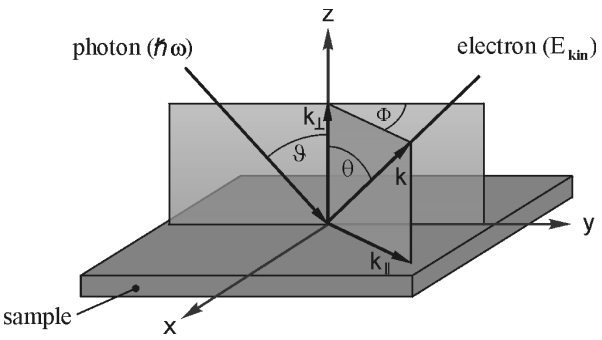


**Figure 4.1:** The experimental geometry for photoemission (SXPS and ARPES) measurements in a schematic view. Light with energy $E_{photon} = \hbar\omega$ is incident on the sample and excites a photo-electron with a wave vector $k$ comprising two components: $k_{||}$ (parallel to the surface) and $k_{\perp}$ (normal to the surface). The kinetic energy of the electrons is measured as a function of $E_{photon}, \Phi, \vartheta$ and $\Theta$.

$|E_B|$ is the binding energy of the electron and $\hbar\omega$ is the excitation energy.
However the work function of the analyzed sample does not contribute to $E_{kin}$ but cancels out in the total energy balance.
Fig. 4.1 also shows the angular dependence which can be used for Angular Resolved PES (ARPES). In this work the angle of incidence is always set to $\vartheta = 45°$ and $\Phi = 0°$ and $\Theta = 0°$ if not mentioned otherwise.

## Three Step Model of the Photo Emission Process

The photoemission process can be described in three steps. The so called 'three-step model' is schematically shown in Fig. 4.2. In the first step photoionization occurs after the photon is locally absorbed and an electron is excited from its initial state $E_i$ (initial) into a final state $E_f$ (final). The transition is given by Fermi's Golden Rule:

$$\omega \propto \frac{2\pi}{\hbar} \left| \langle \Psi_f | \, \mathbf{A} \cdot \mathbf{p} \, | \Psi_i \rangle \right|^2 \delta(E_f - E_i - \hbar\omega) \tag{4.6}$$

if the Hamiltonian of the dipole approximation of the electron-photon interaction (e. g., in the solid in the absence of an electromagnetic field) is

$$H = \frac{e}{mc} \mathbf{A} \cdot \mathbf{p} \tag{4.7}$$

For an easy description it can be assumed that the remaining orbitals (passive orbitals) after the excitation of an electron are the same in the final state as they were in the initial state. This so called 'frozen-orbital approximation' or 'Koopmans's approximation' neglects

relaxations energies. It states that the binding energy equals the negative energy of the orbital from which the photo-electron is emitted. It assumes that the photoemission process does not produce any changes in the remaining N-1 orbitals (N: number of the orbitals). This reduces the transition matrix element to just one matrix element. With this approximation the measured binding energy is approximated with the binding energy of the initial state which leads to 4.5.

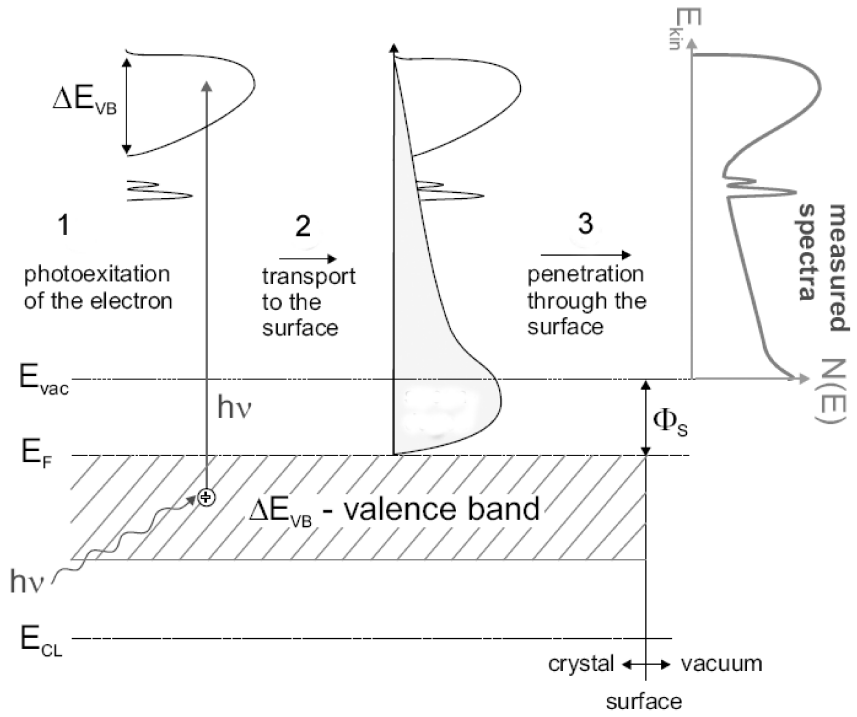


**Figure 4.2:** Photoemission as a three step process: (1) photo excitation of electrons; (2) travel to the surface with concomitant production of secondary electrons (shaded); (3) penetration through the surface (barrier) and escape into the vacuum.

The second step describes the propagation of the photo-excited electrons to the surface. The probability for the electron to reach the surface is proportional to the electron mean free path which depends on the kinetic energy of the electrons (see Fig. 4.3). Beside this a background of secondary electrons exists underneath the original photo-electron spectra (see Fig. 4.2). These secondary electrons are photo-electrons which are scattered by plasmons, phonos or other inelastic effects thus they do not contribute to a certain feature.

In the third step only electrons, with an energy higher than the work function and a velocity component normal to the surface can escape through the sample surface into the vacuum.

Therefore $k_{||}$ is conserved whereas $k_{\perp}$ is not conserved due to the translational symmetry break.

## Electron Mean Free Path

The excited electrons have a certain kinetic energy and their probability to reach the surface depends on the electron mean free path. This dependency of the kinetic energy on the electron mean free path $\lambda$ is shown in Fig. 4.3 as measured for various materials.

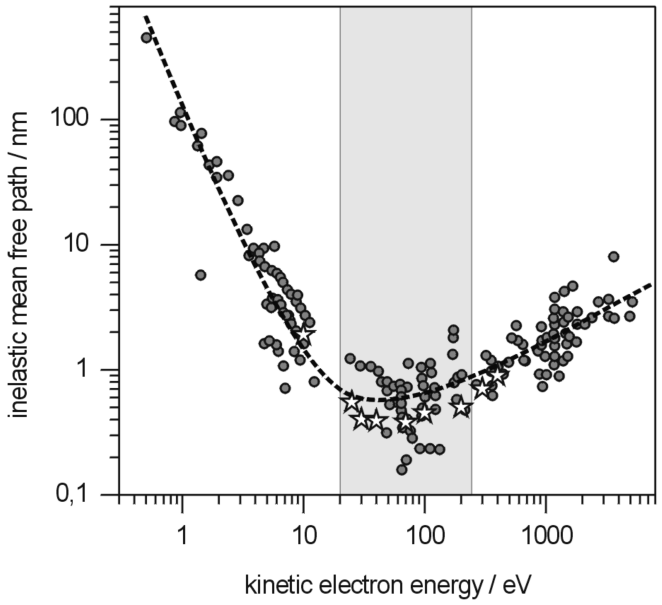


**Figure 4.3:** Electron mean free path (escape depth) of photo-electrons as a function of their kinetic energy for various materials [72]. The stars represent data for GaAs obtained from oxidation processes [73]. The data indicate a nearly universal curve with a minimum of 2-5 Å for kinetic energies around 50 eV.

The dashed curve in Fig. 4.3 is a guide for the eye of the mean free path independent of the material and the points are measured data from many elemental solids. The curve is therefore often called the universal curve. The reason for this universality is that the inelastic scattering of electrons in this energy range mostly involves excitations of conduction electrons, which have more or less the same density in all elements. Note that at lower energies other scattering mechanisms will be important, like scattering from phonons. The mean free path between 20 eV and 200 eV amounts to only a few $\mathring{A}$. The minimum of the universal curve is around 50 eV. This results in an information depth of only a few atomic layers. Therefore a change of the excitation energy can exhibit different information because the respective kinetic energy of the photo-electrons is different. The dependence of the electron mean free path on the kinetic energy of the electrons is mainly caused by electron-electron interactions. This dependence therefore can be used to distinguish between contributions from the surface and those which originate from bulk atoms.

Beside the fact that there is a universal curve for the electron mean free path which is more or less independent of the material, it has to be taken into account that the cross section of the emitted electrons differs slightly for the elements. This is important for the comparison of core level emission lines of different elements.
The thickness of the organic molecular layers investigated in this work were estimated this way:

$$d \sim -\lambda\sigma ln(1-\frac{I_1}{I_0}) \tag{4.8}$$

where d is the thickness of the molecule layer, $I_0$ and $I_1$ are the intensities of the core level bulk components before and after the deposition, $\sigma$ is the photo ionization cross section of the element and $\lambda$ is the mean free path of the electrons of the different atom species.

## Core Level Spectroscopy

Core electrons have binding energies of more then $E_B > 10\ eV$. Usually they are not taken into account during the consideration of the bond formation of neighbor atoms in a solid. However, the binding energies of core electrons do show dependence of the electronic and chemical environment of the atom they belong to. Those bonding sites can be analyzed by measuring the core level emission line shape with photoemission spectroscopy. Core levels are classified by their principal quantum number $n(n = 1,2,3,...)$ and their secondary quantum number $l(l = 0,1,2,3,... \longrightarrow s,p,d,...)$. For $l \geq 1$ due to the spin-orbital interaction the total spin quantum number $s$ and the momentum quantum number $l$ couple to a total angular momentum $j = l \pm s$. The resulting core levels show a splitting into doublets (or multiplets for higher atomic numbers). The intensity ratio $R$ between two levels (also called branching ratio) in the core level line shape is given by their respective populations $(2j+1)$:

$$R = \frac{2(l+s)+1}{2(l-s)+1} = \frac{l+1}{l}. \tag{4.9}$$

Due to the electron diffraction of the photo-electrons at periodically ordered surfaces this ratio $R$ can deviate in realistic measurements up to 20% [74–77]. This is expecially the case if the electrons escape with a different angle than normal emission. Also the difference in the photoionization cross section can lead to deviations from the theoretical value of R [78]. Additional the absolute binding energy $(E_B)$ of an element can be determined by the position of the core level emission line. Therefore the Fermi edge can be measured at a metal surface and gives the reference point $E_B = 0$. It can be obtained in normal emission if the sample is in electrical contact with this metal surface.

During the investigation of molecules and solids it is not only interesting to determine the absolute binding energy of a particular core level. Even more important is a thorough

understanding of the factors affecting the chemical shifts and the type of physical and chemical information which can be obtained by these shifts. The basic physics underlying the change in binding energy is simple. The energy of an electron in a tightly bound core state is determined by the repulsive core Coulomb interaction with all the other electrons and the attractive potential of the nuclei. A spatial rearrangement of the valence charges of a particular atom and a different potential created by the core and electronic charges on all the others atoms in the compound are the reasons for a change in the chemical environment of an atom. These rearrangements can occur for example on a reconstructed surface or during the adsorption of organic molecules. The resulting energy difference is called surface core level shift (SCLS). It is explained by the ionicity of the different atom species, i. e. cations and anions. In a bond formation the cation loses electrons while the anion attracts those electrons. That lowers the screening of the core potential of the cations thus increasing the binding energies of the core levels.

These surface components can be differentiated by changing the excitation energy or varying the takeoff angle (see Fig. 4.1). If the excitation energy is changed the kinetic energy of the photo-electron changes which changes the surface sensitivity (Fig. 4.3) and thereby the ratio between the bulk and surface related components. If the takeoff angle is varied between 30° and 60°, the information depth is obtained by multiplying with $cos\Theta$ which leads to an increase of the surface related components [70, 79].

## Numerical Curve Fitting

The analysis of the core level line shape is done by numerical analysis by fitting the line shape with a theoretical model based on the non-linear least-square curve fitting algorithm of Marquardt [80]. The background of inelastic scattered electrons is fitted with a $3^{rd}$ order polynomial. The program used in this work is 'BFIT' and a detailed description can be found in [81]. The core level itself with the spin-orbital doublets is fitted with a Lorentzian and a Gaussian broadening (Voigt profile). This Voigt profile corresponds to the limited lifetime of the core hole state, the broadening caused by the experimental setup as well as to the sample inhomogeneities. The scope during the fit procedure is to obtain a residuum (the residuum shows the difference between the measured spectrum and the model function) without any structures. The residuum is shown in each plot below the core level emission line.
The fit parameters which can be varied are the surface core level shifts (SCLS) with respect to the bulk component and the corresponding intensities of the components. The values for the lifetime broadening $\gamma$, the experimental broadening $\sigma$, the branching ration R and the spin orbital-splitting *SO* are the same for all components of a certain core level.

## Influence of Radiation on the Molecules

At the synchrotron facility BESSY II in Berlin and DELTA in Dortmund the SXPS measurements were performed. At the (RG-PGM) German-Russian beamline in BESSY the stability

| | $\gamma/eV$ | $\sigma/eV$ | R | $SO/eV$ |
|---|---|---|---|---|
| $As3d$ | 0.08±0.03 | 0.46±0.03 | 1.54±0.05 | 0.69±0.01 |
| $C1s$ | 0.1±0 | 0.9±0.1 | - | - |
| $Ga3d$ | 0.08±0.03 | 0.37±0.03 | 1.66±0.05 | 0.44±0.01 |
| $In4d$ | 0.1±0 | 0.46±0.06 | 1.47±0.08 | 0.86±0.01 |
| $P2p$ | 0.061±0.03 | 0.41±0.06 | 2.07±0.07 | 0.86±0.01 |

**Table 4.1:** Fit parameters for the As3d, C1s, Ga3d, In4d and P2p core levels obtained on the different surfaces. In the table the values for lifetime broadening $\gamma$, experimental broadening $\sigma$, branching ratio R and spin orbit-splitting $SO$ are shown.

of the molecule layer on the surface was tested because it is possible that sensitive parts of organic molecules can be destroyed or desorbed by the irradiation. Thus the initial real surface adsorption structure would not be investigated but only a modified one. The RG-PGM beamline is a dipole beamline and exhibits a spectral range of nominal 30 to 1500 eV and keeps a resolution (beamline and analyzator) of about 120 meV at an excitation energy of 75 eV. The analysis chamber (MUSTANG) was equipped with a hemispherical Omicron phoibos 150 detector.
To determine whether such a degenerative process appears, several transients were taken at the maximum kinetic energy of the C1s core level.

In Fig. 4.4 an example for a transient with a duration of three minutes is shown for the cyclopentene saturated InP$(001)(2\times4)$ reconstructed surface. It can be seen that within the signal-to-noise ratio no changes in the intensity can be found. If no instantaneous change of the molecule structure on the surface appears (in a time $<<$ 1 s) it can be concluded that the molecules stay intact during the irradiation with synchrotron light and the adsorption structure does not change.

### 4.1.3. Reflectance Anisotropy Spectroscopy (RAS)

Reflectance Anisotropy Spectroscopy is a non destructive surface sensitive optical tool to characterize the change in the optical anisotropy of the topmost layers of the surface [82,83]. The origin for anisotropies on the surface could be for instance surface reconstructions or surface roughness caused by adsorbed layers [83, 84]. Comprehensive reviews of the theoretical and experimental aspects of RAS together with its application to the characterization of semiconductor and metal surfaces can be found in [82, 83, 85–101]. RAS was first used in 1966 [102] and has developed since then as a commonly used experimental method by the work of Berkovits [103] and Aspnes [104]. Details of the RAS setup are described elsewhere [98, 105, 106].

RAS measures the difference between the optical reflectance of light polarized along two perpendicular axes of the surface at nearly normal incidence as a function of the photon energy. In Fig. 4.5 a schematic sketch of the RAS setup used in this work is shown. The

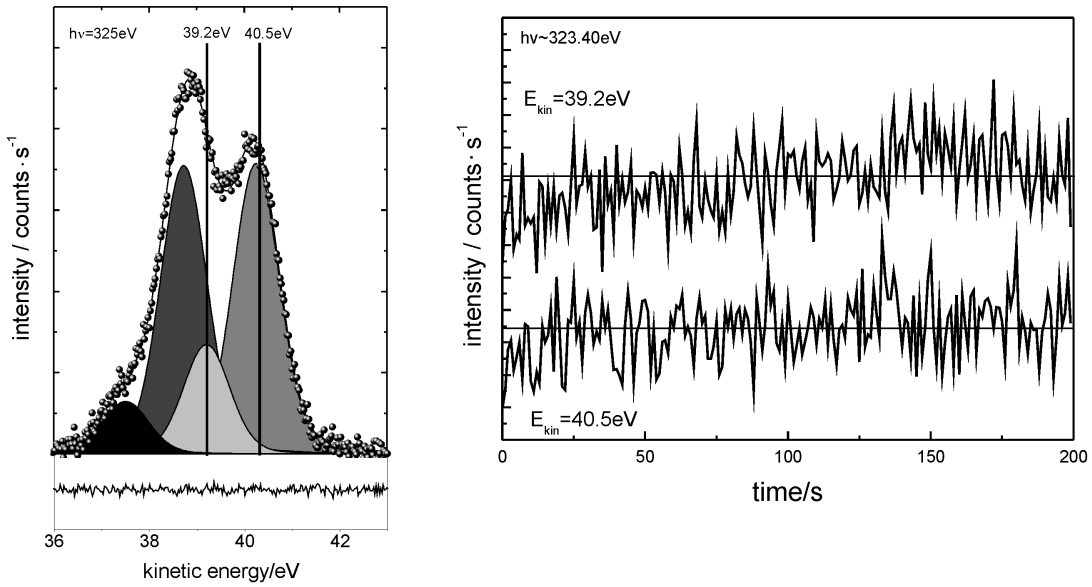


**Figure 4.4:** On the left: the C1s core level of the cyclopentene saturated InP$(001)(2\times4)$ reconstructed surface. Indicated are the energy positions at which the transients were taken. On the right: transients taken at 39.2 eV (top) and 40.5 eV (down) at an excitation energy of $h\nu \approx 323.4$ eV. The stability of the signal for 3 min irradiation is shown.

main part of RAS is a photoelastic modulator for the analysis of the reflected light of the sample. The RAS signal is normalized to the total reflectivity and the complex RAS signal is given by:

$$\frac{\Delta r}{< r >} = 2\frac{r_x - r_y}{r_x + r_y} \tag{4.10}$$

where $r_x$ and $r_y$ are the complex reflectivities for light polarized linearly in the corresponding directions. In the case of the (001) planes these directions lie along [110] and $[\bar{1}10]$. The RAS signal consists of a real and a imaginary part of the reflectance anisotropy. In this work the real part of the RAS signal will be discussed which is related to differences in the amplitude of the reflectivity in each direction.

In the case of a zincblende-type III-V semiconductor, like GaAs or InP, the bulk contribution is in the first approximation isotropic as discussed in chapter 2 and the different surface reconstructions can be identified by their characteristic RAS spectra (fingerprint). The main RAS features in the spectra result from the characteristic dimer configuration of the topmost layers and thus results in an anisotropic signal. So the RAS signal is dominated by transitions

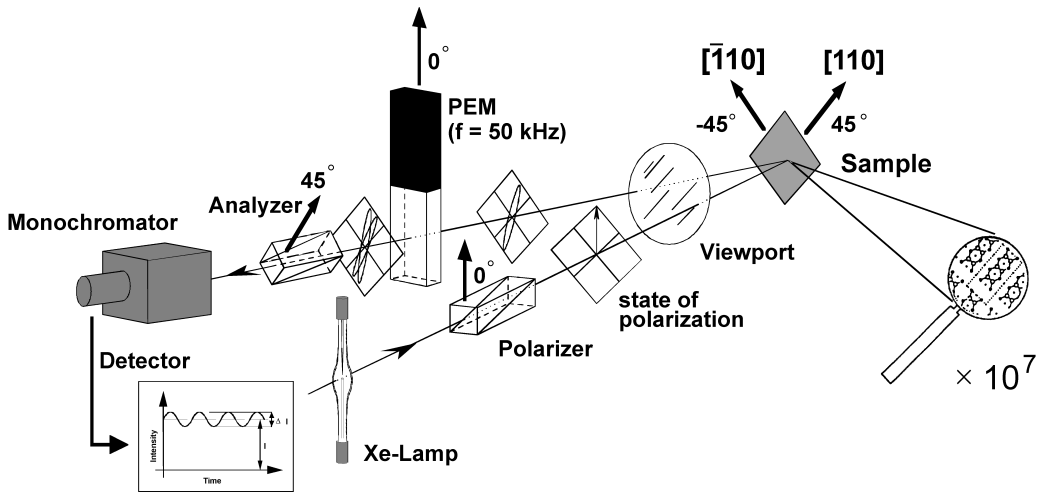


**Figure 4.5:** The experimental RAS setup used for the RAS measurements in the work according to Aspnes et al. (figure from [85]).

between occupied and unoccupied surface states. These transitions normally can be identified in the spectra above the band gap $E_0$ and below the $E_1$ critical bulk energy at energies between 1.45 eV and 3 eV.

With the adsorption of organic molecules on the surface the electronic structure of the surface is modified. Interactions between the molecular orbitals and the electron bands of the substrates appear. Therefore transitions within the molecules (see chapter 3) for instance between the HOMO (highest occupied molecular orbital) and the LUMO (lowest unoccupied molecular orbital) can appear as well as transitions between the surface and the unoccupied states of the molecule. To excite an electron from the HOMO to the LUMO the lowest energy is necessary.
In the spectral range between 1.5 eV and 6 eV, which is investigated here, the HOMO-LUMO transition estimated from theoretical calculations (this was discussed in chapter 3) as well as from gas phase measurements is out of the spectral range [7, 53, 107]. Thus no intramolecular transitions are observable. Due to the fact the RAS spectra exhibits contributions which can be assigned to transitions related to the surface atoms the modifications of the surface transitions during the adsorption of the organic molecules are monitored with the RAS. Therefrom conclusions can be drawn for the bonding sites of the organic molecules on the surface.

### 4.1.4. Density Functional Theory

Based on the experimental methods (SXPS, STM, STS, RAS and LEED) which provide information about the optical, geometrical and electronic properties, it is possible to suggest structural models. The totally relaxed adsorption structures cannot be obtained only by the results of experiments, however, first suggestions for the resulting structures are possible.

These suggestions can be used to limit the number of possible adsorption structures for the theoretical calculations. With total energy (TE) calculations based on the density functional theory (DFT) the models can be verified. The model with the lowest TE is than considered energetically favorable. Relaxed geometries and the charge transfer are the result of these calculations. Additional the optical anisotropy of the adsorption structures can be obtained and compared to the experimental results. Further theoretical background and applications can be found in [108].

The basis for the DFT is the Hohenberg-Kohn-theorem which indicate that instead of the wave function for a many electron system the electron density can be chosen. The ground state of the system can be defined by the electron density distribution. Further, they showed that if the ground state electron density is known all other ground state properties follow, i. e. lattice constant, cohesive energy, etc. This minimizes the computational effort. W. Kohn and L. J. Sham found in 1965 that the time-independent Schrödinger equation took a very simple form if the potential experienced by the electrons was formally expressed as a function of the electron density. $E[n]$ which is the energy for a system with N interacting electrons in an external field as a functional of the electron density $n(r)$ and with a ground-state energy $E_0$ which is also a functional $n(r)$ can be expressed by:

$$E[n] = T_e[n] + \int d\mathbf{r}\; v_{ext}(\mathbf{r})n(\mathbf{r}) + \int d\mathbf{r}dr' \frac{n(\mathbf{r})n(\mathbf{r}')}{|\mathbf{r}-\mathbf{r}'|} + E_{XC}[n] \tag{4.11}$$

where $T_e[n]$ is the kinetic energy of non-interacting electrons [109, 110]. The second term in 4.11 describes the interaction with an external potential and the third term the electrostatic energy of the electrons. The term $E_{XC}[n]$ includes all exchange-correlation interactions. Due to the fact that $E_{XC}[n]$ is not known explicitly this theory involves enormous computational effort. Therefore $E_{XC}[n]$ has to be further approximated. One approximation is the local density approximation (LDA). Due to the exchange-correlation interaction in the LDA the energy for an electron at a position $r$ is substituted by the energy of a homogeneous electron density.

$$E_{XC}^{LDA}(n) = \int d\mathbf{r}\; n\; \varepsilon^{LDA}(n) \tag{4.12}$$

This approximation also gives a qualitatively good description of the ground state properties of a variety of highly inhomogeneous systems. However LDA does not always provide accurate results, i. e. it often overestimates the binding energy and underestimates the bond length of molecules and solids [111]. To improve LDA, a dependence of the exchange-correlation energy on the derivatives of the electronic density can be introduced:

$$E_{XC}^{GGA}(n) = \int d\mathbf{r}\; n\; \varepsilon^{GGA}(n, |\nabla n|) \tag{4.13}$$

This approximation is known as the generalized gradient approximation (GGA) and is restricted to first order derivatives.
The DFT calculations shown In this work were performed by W. G. Schmidt (University of Paderborn) and P. Favero (Universidade de Brasilía) for the cyclopentene modified InP(001)$(2 \times 4)$ surface.

## 4.2. Sample Preparation and Experimental Setup

The different experimental setups which were used in this work will be briefly discussed and an overview about the sample preparations will be given in this section.

### Experimental Setup

All samples investigated in this work were prepared in a standard ultra high vacuum (UHV) analysis chamber with a base pressure of approximately $1 \cdot 10^{-10}$ mbar. Each UHV chamber (TU Berlin, BESSY, DELTA) is equipped with resistive filament heating, a quadrupole mass spectrometer (QMS) with a mass range of 1 to 100 amu and a LEED setup. For this work the RAS setup was mounted at the chamber to monitor the sample preparation as a fingerprint method. The gas inlets for the molecule deposition were similar at each chamber. The chamber at the TU Berlin was also equipped with a RT-STM setup. With this setup it was possible to take STM images and STS spectra under UHV conditions of each sample preparation step.
At BESSY beside the measurements at the (RG-PGM) German-Russian (see section 4.1.2) additional measurements were performed at the PGM-3 beamlines. The RG-PGM beamline exhibits a spectral range of nominal 30 to 1500 eV and the PGM-3 a range of nominal 20 to 1900 eV. Both keep a resolution (beamline and analyzer) of about 120 meV at an excitation energy of 75 eV. The analysis chamber (MUSTANG) was additionally equipped with a hemispherical SPECS phoibos 150 detector. The core level spectra at DELTA were taken at the PGM beamline 11. Besides the QMS and LEED the chamber was equipped with a hemispherical CLAM detector. In this case the samples were attached to a silicon sample with indium which was mounted in a direct heating assembly.

The core level spectra were taken in normal emission using photon energies between 70 eV and 630 eV. The excitation energies were corrected by the Fermi edge of the molybdenum sample holder in electrical contact with the samples. Binding energies are referred to the Fermi edge. The line shape of the core level spectra are deconvoluted with a 'best-fit' (see chapter 4.1.2). From this a fit including one bulk and more surface related components results.

To identify the surface reconstruction and to monitor the modification of the surface during the deposition with the organic molecules different RAS setups were used in this work. One with a spectral range from 1.45 eV to 5 eV called MBE-RAS at the TU Berlin during the

STM measurements and another one called UV-RAS with a spectral range from 1.45 eV up to 6 eV for the measurements at the TU Berlin and also for the measurements at BESSY and DELTA.

### Sample Preparation

The preparation process was monitored by quadrupole mass spectroscopy (QMS) and RAS, in order to obtain reproducible, well ordered surfaces. The surface symmetry of each surface reconstruction was determined after preparation by LEED.
Reflectance anisotropy spectroscopy (RAS) was then used to monitor the molecular deposition and to analyze the surface optical properties after the modification.

### GaAs(001) surfaces

The GaAs$(001)$ samples used in this work were grown by by molecular-beam epitaxy (MBE) with different Si-doping levels of nominal $n = 3-4\cdot 10^{17}\ cm^{-3}$ as well as $n = 5\cdot 10^{17}\ cm^{-3}$ and $n = 1\cdot 10^{18}\ cm^{-3}$. To protect the surfaces from contamination during transfer through air the samples were capped with an amorphous arsenic protection layer directly after growth [112, 113]. The amorphous protection layer was thermally desorbed at 350°C inside the UHV chamber to yield a $c(4\times 4)$ As-rich surface [113]. The error for all the temperature measurements amounts to ($\pm$20°C).
Further annealing to 430°C and 520°C leads to the less As-rich $(2\times 4)$ or the Ga-rich $(4\times 2)$ reconstruction, respectively [113].

### InP(001) surface

The InP$(001)$ surfaces were Sb-doped grown by metal-organic-vapor-phase-epitaxy (MOVPE). The samples were capped with an amorphous phosphorus and an amorphous arsenic protection layer directly after growth [112]. An arsenic layer deposited straight onto the surface would lead to exchange reactions with the surface phosphorus atoms and thus a change of the surface stoichiometry.
The amorphous arsenic protection layer was thermally desorbed at 350°C inside the UHV chamber. After that the phosphorus layer was desorbed at 420°C to yield a $(2\times 4)$ P-rich surface.

## 4.3. Molecule Deposition

Cyclopentene with a purity of at least 97%, 1,4-cyclohexadiene as well as benzene with a purity of more than 99% were used in this work. The liquid molecules were introduced into

the chamber through a variable gas-inlet valve. The deposition of the molecules onto each surface reconstruction if not mentioned otherwise was carried out at room temperature (RT). In order to avoid decomposition of the molecules all filaments inside the chamber, e.g. ion gauges, were switched off during the whole deposition procedure. The effective molecule layer thicknesses for the saturated surfaces estimated from SXPS and STM measurements is around one monolayer for each molecule deposition and reconstruction.

For the adsorption of the organic molecules on the GaAs$(001)$ and InP$(001)(2\times4)$ surfaces higher pressures were necessary compared to the deposition on the Si$(001)(2\times1)$ reconstructed surface. A typical deposition amount of cyclopentene until saturation on the Si$(001)(2\times1)$ was 30 L ($1L = 1,33\cdot10^{-6} mbar\cdot s$) [47, 114] while on the InP$(001)(2\times4)$ reconstructed surface round 50000 L had to be offered until the surface was saturated. On the GaAs$(001)$ surface reconstructions this value was even higher with $\sim$200000 L.
The process of saturation is shown for the deposition of cyclopentene on the GaAs$(001)(4\times2)$ reconstructed surface in Fig. 4.6. It has to be mentioned that the point where the surface related features did not change anymore during the deposition of the organic molecules is called 'saturation' in this work. This point is represented by the thick line spectrum in Fig. 4.6.
Additional adsorption beyond this point is still possible to occur, for example by physisorption, but can not be further observed by RAS because in the spectral range investigated here no intra-molecular transitions can be observed (see section 4.1.3). Therefore at this point the deposition was stopped.

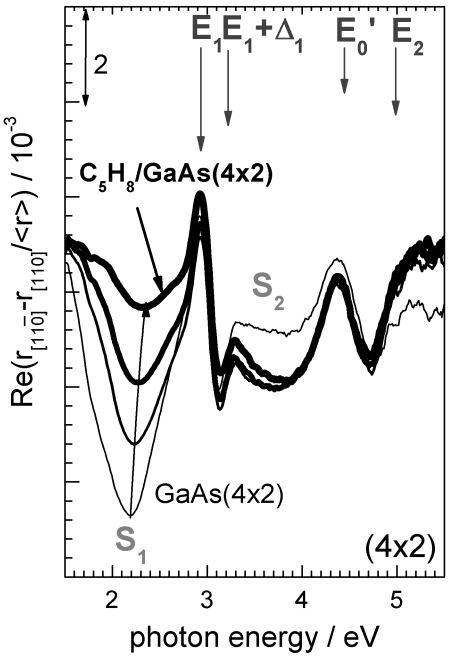


**Figure 4.6:** Saturation process shown for the deposition of cyclopentene on the GaAs$(001)(4\times2)$ reconstructed surface measured with the RAS.

# Chapter 5: The reconstructed III-V Semiconductor Surfaces

In this chapter the optical, electronical and geometric properties of the InP$(001)(2\times4)$ reconstructed surface will be introduced as well as the properties of the three 'main' GaAs$(001)$ surface reconstructions. The relaxed geometries will presented followed by a discussion of the experimental results concerning the optical and electronical characteristics.

## 5.1. The InP$(001)(2\times4)$ Surface

The InP$(001)$ samples were grown in MOVPE and then transferred into UHV. For the preparation the samples were annealed up to 420°C and then cooled down as described in section 4.2.
After the preparation the topmost layer of the InP$(001)(2\times4)$ reconstructed surface consists of an asymmetric 'hetero'-dimer, denoted as 'mixed-dimer'. This dimer configuration is similar to the one of Si apart from the facts that the Si$(001)(2\times1)$ surface has half filled dangling bonds at a 'homo'-dimer atoms while the InP$(2\times4)$ reconstructed surface exhibits a 'hetero'-dimer with a filled dangling bond at the P atom and an empty dangling bond at the In atom [115, 116]. Experimental results obtained by STM, RAS, SXPS and ARPES as well as results from DFT-LDA calculations are discussed in detail in [117, 118]. The resulting structure configuration is shown in Fig. 5.1. The asymmetric dimer bond length for the In-P bond is ∼2.6 Å and a vertical buckling of ∼2.59 Å for the In-P bond and ∼2.8 Å for the second layer In-In bond is found, indicating a tilt angle of ∼91° and ∼118° respectively, which is in agreement with previous work [119].

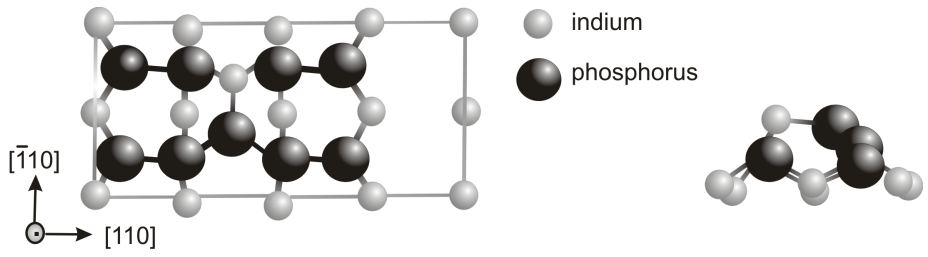


**Figure 5.1:** The InP$(001)(2\times4)$ 'mixed-dimer' reconstructed surface in the top-(left) and sideview (right). Shown are the relaxed geometries as obtained by DFT-LDA from [120].

SXPS measurements of the clean reconstructed surface are shown in Fig. 5.2 and confirm the commonly accepted 'mixed-dimer' structure model for this surface. It was introduced in chapter 4.1.2 that higher binding energy refer to lower kinetic energies and the other way around. Therefore kinetic energies will be used to display the core level emission lines while the binding energies will be discussed. With a best fit the data obtained by the SXPS measurements are reproduced. The residuum below each spectrum is a measure for the quality of the fit. The solid line component in the spectra belongs to the emission line of the bulk coordinated atoms. The dashed small components shifted with respect to the bulk component are related to atoms located at the surface.

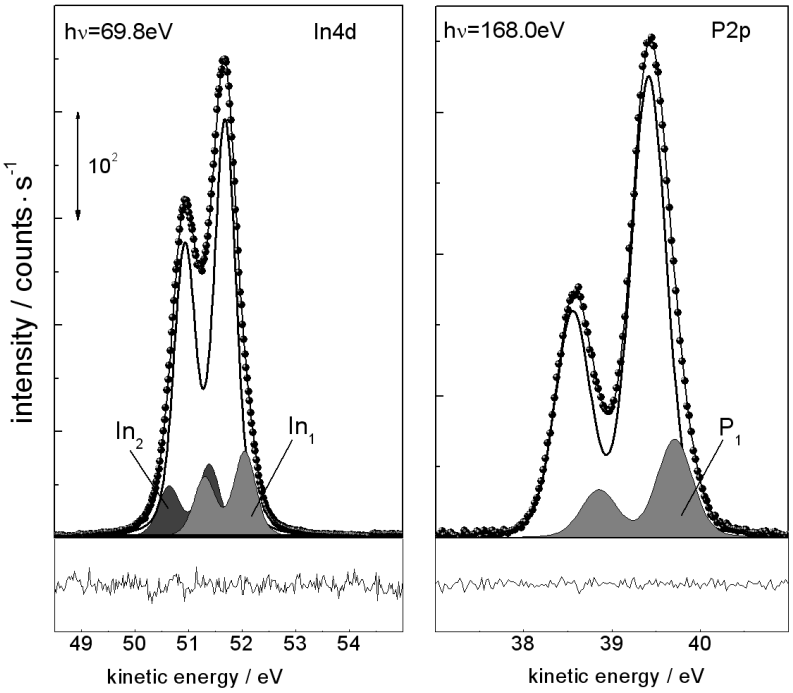


**Figure 5.2:** In4d (left) and P2p (right) core level for the clean InP$(001)(2\times4)$ reconstructed surface taken at photon energies of 69.8 eV and 168.0 eV, respectively. Depicted are the measured data (fits) in the dotted (solid) lines. The shaded areas belong to the surface components. In the In4d core level two surface components are found, shifted by -0.42 eV (+0.45 eV) toward lower (higher) binding energies with respect to the bulk related component. In the P2p core level one surface component can be seen shifted by -0.30 eV.

For the In4d core level two surface related components (shaded) can be revealed with the numerical analysis. With respect to the bulk component these surface related features are shifted by -0.42 eV ($In_1$) and +0.45 eV ($In_2$) towards lower and higher binding energies, respectively. In the P2p core level, one surface component (shaded) shifted by -0.30 eV can

be derived by numerical analysis. These results are in a good agreement with previous work in [118, 119, 121] and the small energy shifts are within the resolution of 120 meV.
According to the 'mixed-dimer' model [119] the surface related component in the P2p core level can be assigned to the topmost P atom contributing to the 'mixed-dimer'. The two surface related components in the In4d core level can be explained by two inequivalent group-III sites in the surface unit cell which have a threefold and fourfold coordination (high and low binding energies) [118, 119]. The $In_1$ component is related to In atoms which have fourfold coordination and this results in a relative charge accumulation, whereas In atoms which contribute to $In_2$ are located in the second layer of the surface unit cell and have empty dangling bonds. The topmost In atom of the 'mixed-dimer' contributes to $In_2$ because it has threefold coordination as well.

The RAS signal of the clean reconstructed InP$(001)(2\times4)$ is depicted in Fig. 5.3. Corresponding to [116, 122] the RAS spectrum shows surface related transitions denoted with $S_1, S_2$ and $S_3$ and bulk related ones are designated $E_1$ and $E_0^{'}$.

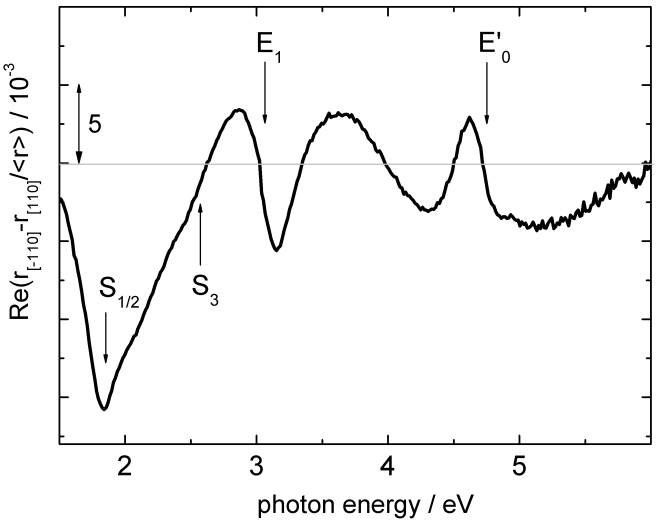


**Figure 5.3:** The RAS spectrum for the clean reconstructed InP$(001)(2\times4)$ surface. Denoted are the surface related transitions with $S_1, S_2$ and $S_3$ as well as the bulk related contributions $E_1$ and $E_0^{'}$.

The origin of $S_1, S_2$ and $S_3$ are the topmost four atomic layers [116]. $S_1$ is caused by transitions between electronic states localized at the bonds between the first- and second-layer $In-In$ bonds whereas $S_2$ arises from transitions mainly involving electronic states localized at the second layer $In-In$ bonds. The symmetry break which is caused by the 'mixed-dimer' on the $In-In$ bonds of the second atomic layer together with the dimer bond itself are the origin of $S_3$ [116]. The strongly surface localized P dangling bond, on the other hand, contributes only weakly.

In the case that organic molecules adsorb on the surface by chemisorption, those surface related contributions in the RAS spectrum should change during the deposition as well as the surface related components in the core level spectra.

## 5.2. The GaAs(001) Surface Reconstructions

Depending on the surface stoichiometry a variety of surface reconstruction are known for the GaAs$(001)$ surface [123]. Three so-called 'main' reconstructions are the very As-rich c$(4\times4)$, the As-rich $(2\times4)$ and the Ga-rich $(4\times2)$. They have been investigated by several experimental and theoretical methods (see [124–128] and references therein). In this chapter the results of RAS, STM and XSPS measurements will be shown for these three reconstructions.

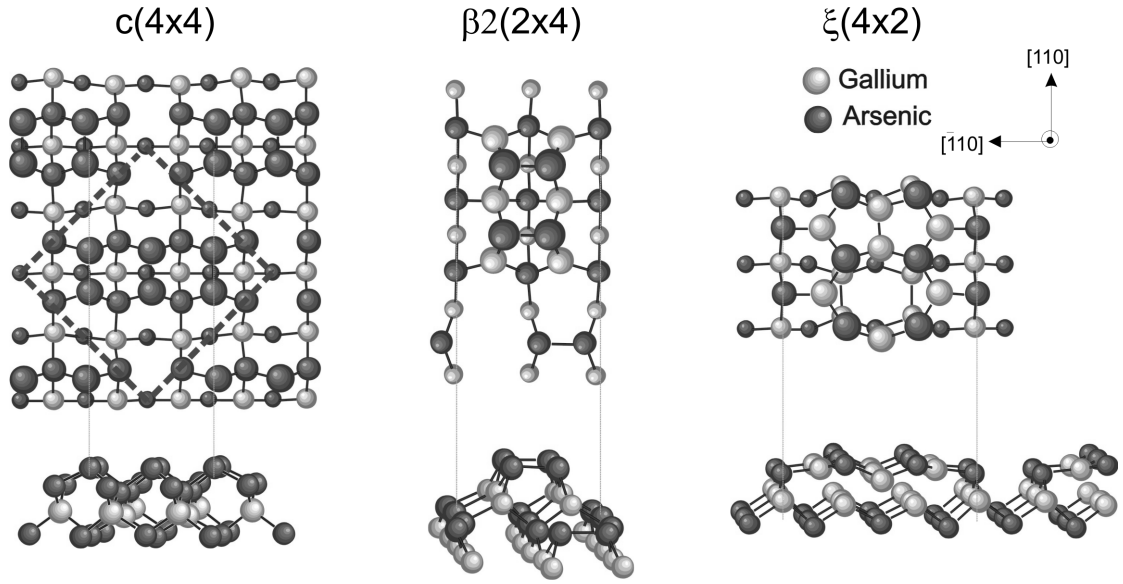


**Figure 5.4:** The relaxed geometries for the three 'main' GaAs surface reconstruction derived from DFT-LDA calculation performed by W. G. Schmidt et al. [127,129]. On the left: very As-rich c$(4\times4)$, As-rich $(2\times4)$ and Ga-rich $(4\times2)$.

In Fig. 5.4 the three different structure models are presented which are found to be the energetically favorite ones for the given chemical environment (displayed are the relaxed geometries from DFT-LDA calculations by W. G. Schmidt et al. [129, 130]). In the first row the top views of the structure models are shown while in the second row the side views along [110] are depicted.

The topmost layer of the GaAs$(001)c(4\times4)$ surface consists of three arsenic dimers per surface unit cell bonded to a complete second arsenic layer (Fig 5.4 left). The $As-As$ dimer bond is oriented along the $[110]$ direction [131]. The three As dimers are grouped in a row as triplets which are separated by a missing dimer. The dimer triplet of two adjacent rows are shifted by half a surface lattice constant with respect to each other resulting in a c$(4\times4)$ surface symmetry. The dimer bond length is $\sim 2.13$ Å which is a similar value as for the Si$(001)(2\times1)$ surface [13, 30] and the outer ones have a length of $\sim 3.02$ Å [132].
The GaAs$(001)(2\times4)$ reconstruction is less As-rich than the c$(4\times4)$, although two As dimers are still linked to a incomplete Ga layer underneath with a dimer bond length of

$\sim$2.5 Å [132] which is comparable to the length of the $Si-Si$ dimer on the Si$(001)(2\times1)$ surface with $\sim$2.4 Å [13, 30]. In the middle of Fig 5.4 the $\beta2(2\times4)$ structure is presented and was first proposed by Northrup and Froyen [133]. Confirmed by total energy calculations [134, 135] this structure was found to be the one with the lowest total energy. With several experimental technics like in situ grazing incidence X-ray diffraction measurements [136], dynamical RHEED analysis [137] and high resolved STM images [126] the $\beta2(2\times4)$ structure was demonstrated to be the best model for the $(2\times4)$ surface.

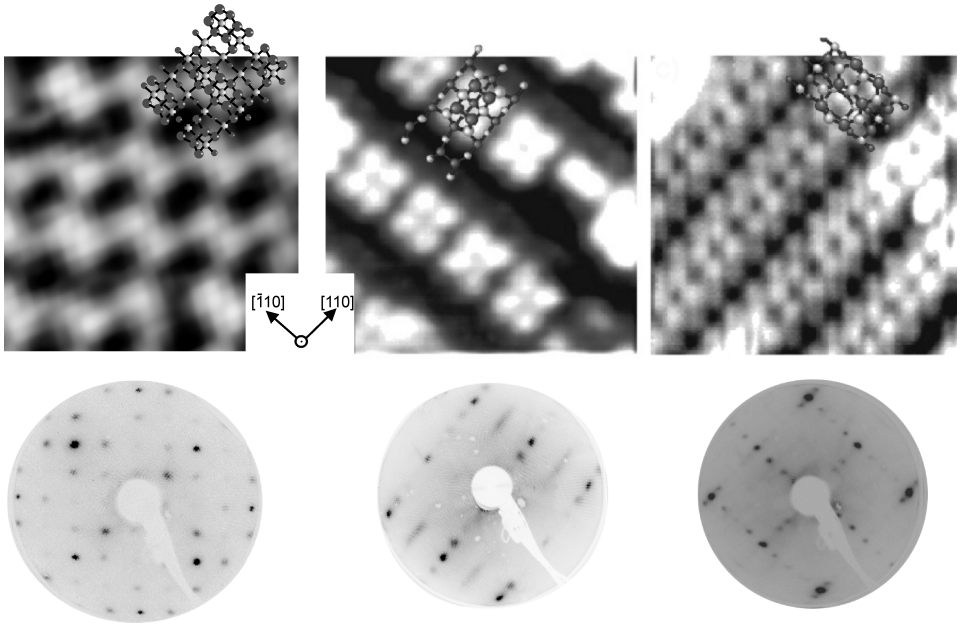


**Figure 5.5:** In the first row: the filled state $5.6\times5.6$ $nm^2$ STM images of the three main GaAs$(001)$ surface reconstructions. On the left the c$(4\times4)$ (measured at U=-2.4 V), in the middle the $(2\times4)$ and on the right the $(4\times2)$ [138]. In the second row the corresponding LEED pattern taken at $\sim$42 eV.

The Ga-rich GaAs$(001)(4\times2)$ surface has been a subject of extensive discussion. Biegelsen et al. [139] discussed their STM images in terms of the $\beta2(4\times2)$ as well as Yue et al. [140]. Nevertheless no confirmation of this structure model by an independent experimental technique has been obtained. The $\xi-(4\times2)$ was discussed by Lee et al. [127] and calculated by DFT calculations. The obtained atomic arrangement for the topmost layers of this surface is shown in Fig 5.4 on the right [130, 141]. This surface consists of subsurface Ga dimers in the second bilayer and linear chains of atoms on non bulk like sites at the surface along [110]. In comparison to other models this arrangement is rather unusual but confirmed by grazing incidence XRD measurements of Kumpf et al. [142]. These Ga dimers are surrounded by single As atoms with filled dangling bonds.

The filled states STM images of the three GaAs$(001)$ surface reconstructions prepared by MBE and subsequent annealing at 350°C, 430°C and 520°C are depicted in Fig 5.5. With these annealing steps the amount of As desorbing from the surface changes and thus the surface stoichiometry with the sample temperature. The white structures represent the posi-

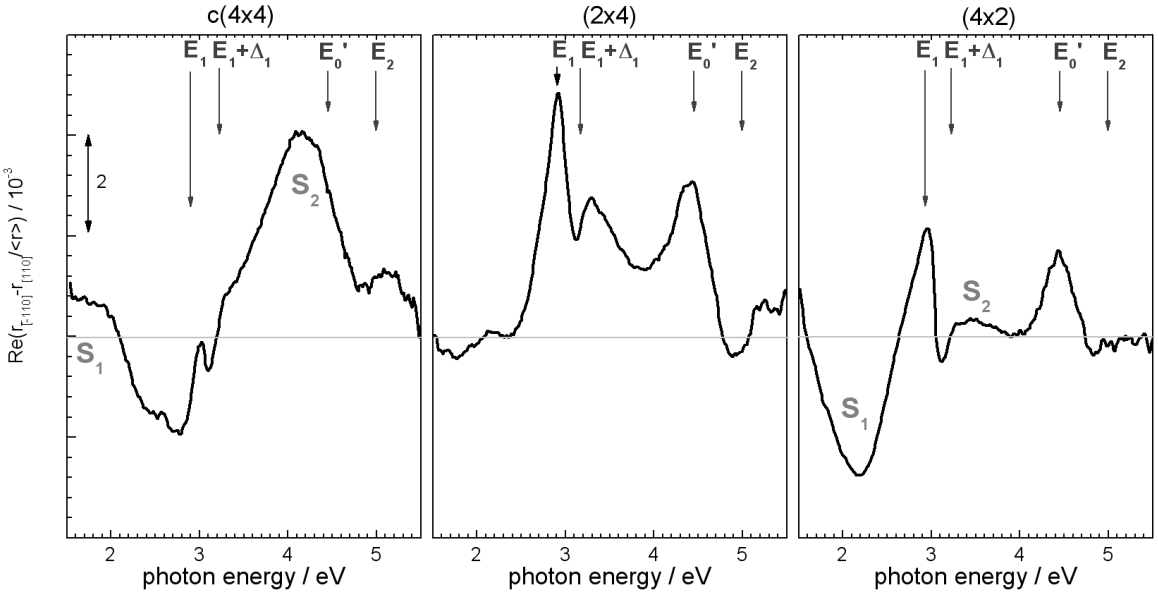


**Figure 5.6:** RAS spectra of the three 'main' clean reconstructed GaAs$(001)$ surfaces ($n = 5 \cdot 10^{17}$ $cm^{-3}$ Si-doped), the c$(4\times4)$, the $(2\times4)$ and the $(4\times2)$, respectively. $S_1$ and $S_2$ are surface related transitions. Bulk related contributions are denoted with $E_1$, $E_1+\Delta_1$, $E_0^{'}$ and $E_2$.

tions where the filled dangling bonds of the As atoms are located. Below the STM images in Fig 5.5 the LEED pattern of each surface reconstruction is shown which exhibits the periodicity of the surface.

In Fig. 5.6 the RAS spectra for the three stable GaAs$(001)$ surfaces are depicted and display several transitions which are either surface ($S_1$ and $S_2$) or bulk ($E_1$, $E_1+\Delta_1$, $E_0^{'}$ and $E_2$) related. The difference in the spectra results from the anisotropic arrangement of the topmost atoms. They are well understood and in good agreement with the literature. Additionally these spectra are simulated by DFT-LDA calculations [143,144]. All three RAS spectra have the bulk related peaks in common which have their origin in the bulk dielectric properties. They are labeled in the RAS spectra according to the interband transitions, $E_1$, $E_1+\Delta_1$, $E_0^{'}$ and $E_2$ [145].

Beside the $(4\times2)$ a second surface reconstruction with a $(n\times6)$ periodicity, can occur. Both can coexist at the same time as it is shown in Fig. 5.7.

The $(n\times6)$ has also a slightly different RAS signature which is shown in Ref. [128]. In comparison to the $(4\times2)$ the minimum around 2.2 eV, $S_1$, shifts towards lower photon

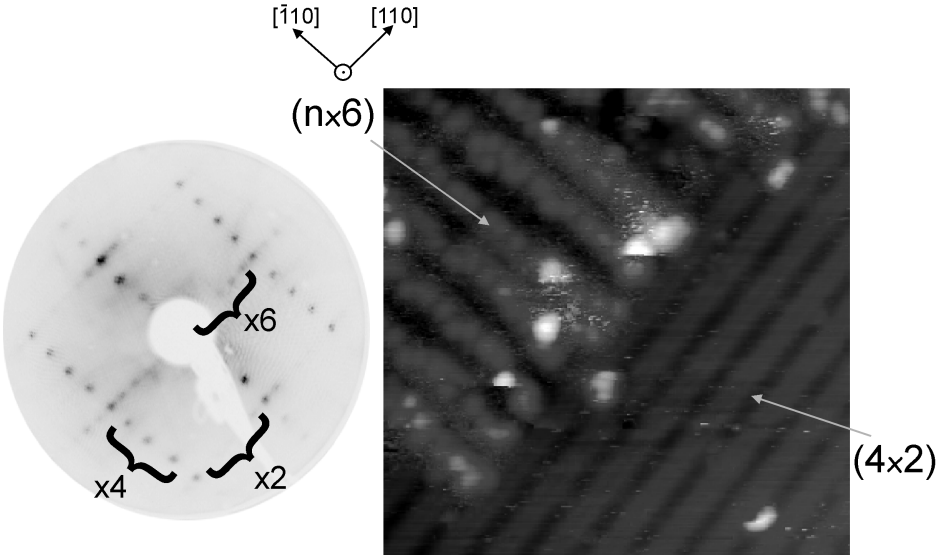


**Figure 5.7:** $25 \times 25\ nm^2$ STM images (right) and LEED pattern (left) taken at an energy of $\sim$42 eV of the $(4 \times 2)$ and the coexisting $(n \times 6)$. The STM image was taken at a gap voltage of -3.727 V and a tunneling current of 0.228 nA.

energies. The relation between the $(4 \times 2)$ and the $(n \times 6)$ coverage depends on the wafer and the MBE growth. It seems that for higher preparation temperatures the $(n \times 6)$ becomes more likely, hence the temperature range between 480°C and 550°C is critical. It is still under discussion if this $(n \times 6)$ reconstruction has a $(1 \times 6)$ or a $(2 \times 6)$ periodicity [139]. The RAS signal calculated with DFT-LDA of the $\xi$-$(4 \times 2)$ surface reproduces well the features in the measured spectrum [144].

The core level emission lines of Ga3d and As3d for the three surface reconstructions are presented in Fig 5.9 as a function of the kinetic energy of the detected electrons. Additionally the relative intensity ratios ($I_{surf}/I_{bulk}$) have been analyzed as a function of the photon energy. A maximum is found below 75 eV photon energy, shown in Fig. 5.8, which is reasonable because the escape depth of the electrons is a function of their kinetic energy. In Fig. 5.8 the reciprocal graph of Fig. 4.3 is plotted and due to this a maximum is found.

The surface components in Fig. 5.9 can be related to atoms which have a different chemical environment compared to the bulk coordinated atoms. For atoms which have a relative charge accumulation this results in a shift towards lower binding energies and, for atoms which have a relative charge depletion this results in a shift to higher binding energies. Thus the surface components shown in Fig. 5.9 can be interpreted as follows:
For the As3d core level of the c$(4 \times 4)$ three surface components are be revealed in the best fit. One, shifted towards lower binding energies, is assigned to defect structures. That means atoms which deviate in their position from the perfect arrangement of the surface reconstruction. The two large components shifted to higher binding energies are related to As atoms of the first and second layer. In the Ga3d core level line shape only two small components

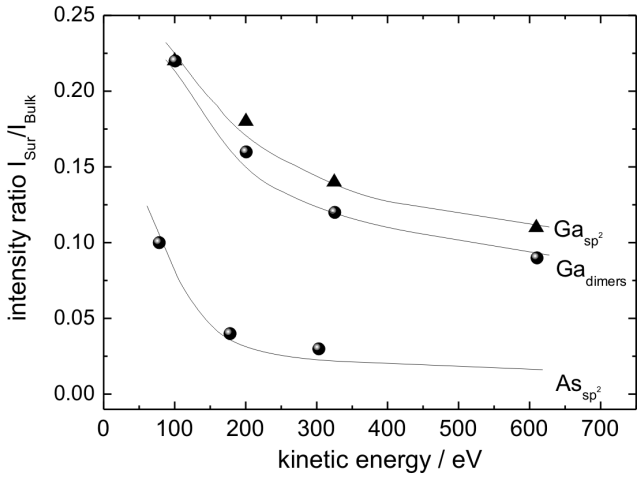


**Figure 5.8:** The relative SXPS intensities for three different surface components of the GaAs$(001)(4 \times 2)$ reconstructed surface.

can be revealed, $Ga_1$ and the $Ga_{defects}$. $Ga_1$ is not yet clearly assigned and the $Ga_{defects}$ component can be related to defect structures on the surface. There is no specific surface assigned Ga component because the topmost layers of the c$(4 \times 4)$ reconstructed surface consists of arsenic atoms. The assignments and the shifts of the components are consistent with previous work [146, 147].
With the change to the $(2 \times 4)$ in the Ga3d core level emission line, a new component emerges $Ga_{2ndlayer}$ which is shifted towards higher binding energies. The two other components $Ga_2$ and $Ga_3$ are not yet related to specific atoms of the surface. In the As3d core level emission line the components at the high binding energy side disappear while a new component shifted by -0.48 eV show up. This component can be related to the As dimers of the $(2 \times 4)$ which are bonded to second layer Ga atoms. These Ga atoms have a relative charge depletion compared to the atoms of the bulk. The component $As_1$ as well as $Ga_2$ and $Ga_3$ are not yet assigned. This is the case for the $Ga_4$, too, which show up in the Ga3d core level emission line for the $(4 \times 2)$ in Fig 5.9 on the right.
This surface is characterized by large Ga3d surface components shifted by -0.35 and +0.39 eV, respectively. These components can be assigned to the Ga dimer $(Ga_{dimers})$ and to the Ga $sp^2$ $(Ga_{sp2})$ bonded atoms [148]. One pronounced component in the As3d core level emission line is found and shifted by -0.51 eV. This component is related to the $sp^2$ bonded As atoms of the topmost layer [148]. The $As_2$ component is very small for the clean surface but it will be later shown that it is important for the discussion of the As3d core level after the adsorption of the molecules. It is shifted by +0.46 eV. This component and the small component $As_3$ in the As3d core level emission line are assigned to the parts of the surface which are $(n \times 6)$ reconstructed [146, 149].
The specific fit parameters can be found in the appendix A for each surface reconstruction.

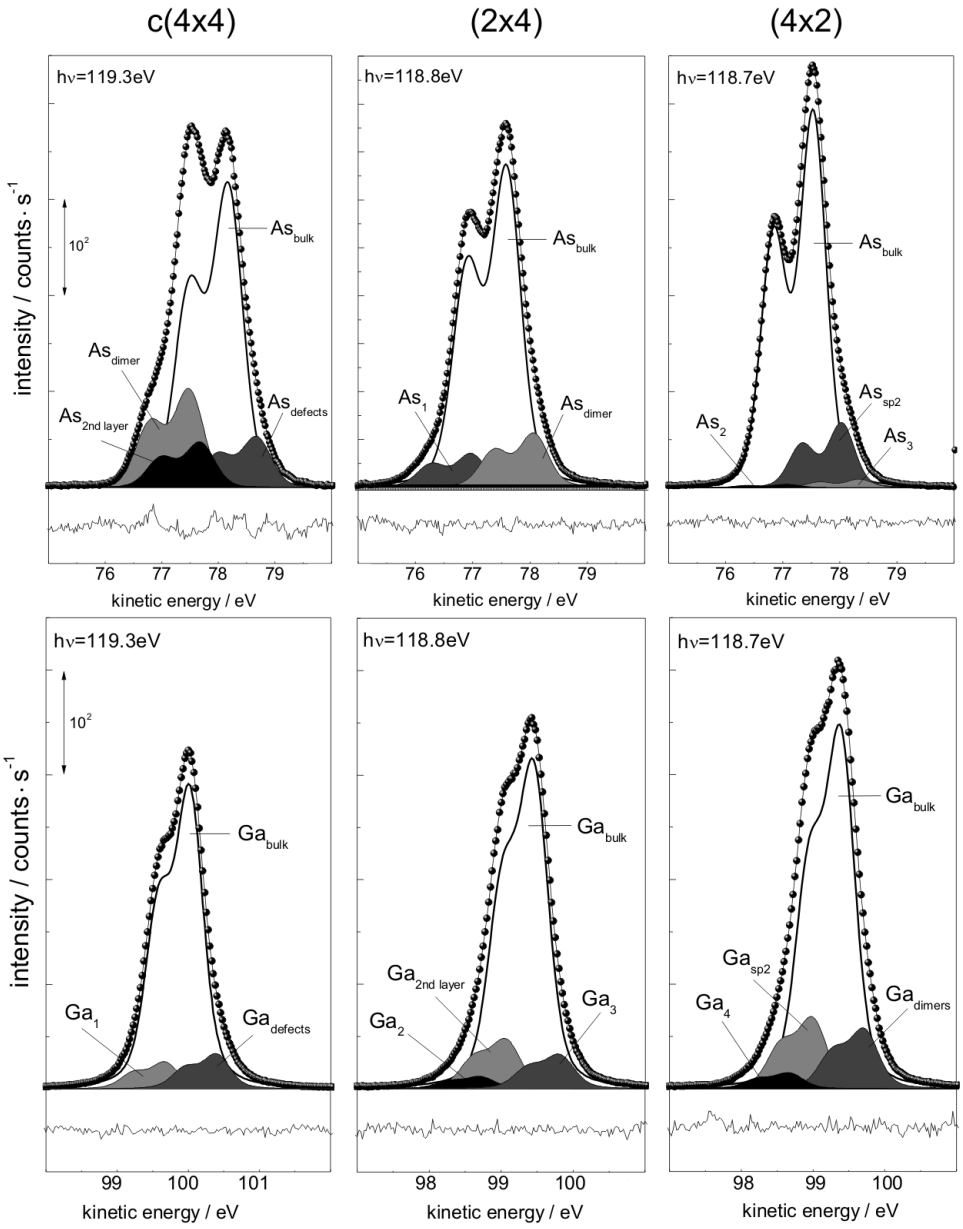


**Figure 5.9:** As3d (first row) and Ga3d (second row) core level emission lines for the three clean reconstructed GaAs(001) surfaces. The filled circles are the background corrected measured data, the thin solid lines are the resulting fits, while the thick solid lines represent the emission line of the bulk atoms and the shaded contributions belong to the surface components. Below each spectrum the corresponding residuum is shown.

# Part II.

# Interface Formation between Cyclopentene and the InP$(001)(2 \times 4)$ surface

# Chapter 6: Adsorption Structure Determination of Cyclopentene on the InP(001)$(2 \times 4)$ surface

In this chapter the adsorption structure of cyclopentene on the InP$(001)(2 \times 4)$ reconstructed surface will be discussed. The main focus is here to determine the role of the surface 'hetero'-dimer ('mixed-dimer') on the adsorption process. Thus the influence of the surface geometry will be analyzed. Therefore RAS, LEED and SXPS measurements were performed and the results will be compared to the results obtained by DFT calculations. Thereby a final adsorption structure of cyclopentene on the InP$(001)(2 \times 4)$ reconstructed surface will be suggested.

## 6.1. Determination of the Optical Anisotropy

The RAS spectrum of the clean reconstructed surface is well understood and was discussed in chapter 5.1.

In Fig. 6.1 this spectrum is shown again (thin line) together with the RAS spectra taken during the deposition with cyclopentene (intermediate lines) up to the saturation (thick line). It is obvious that the RAS line shape clearly changes upon deposition at the pronounced negative peak below 2 eV. The bulk related features between 3 and 5 eV are only reduced in amplitudes.
The change of the surface related contributions below 2 eV could be due to a saturation of the empty dangling bonds of the first layer In atoms with cyclopentene molecules inhibiting transitions between first and second layer In atoms. As a result the structure $S_1$ and $S_2$ within the RAS line shape are reduced [150]. These changes at energies where transition between surface states contribute already indicate a covalent bonding of the cyclopentene molecules.
In Fig. 6.2 (left) the LEED pattern of the clean reconstructed $(2 \times 4)$ surface is shown. This pattern vanishes during the deposition of the cyclopentene molecules as can be seen in the middle in Fig. 6.2 until only bulk spots remain in the pattern (right side in Fig. 6.2).

This indicates the possibility that cyclopentene not only adsorb at the 'mixed-dimer' because if this would be the case the LEED pattern should become weak but not disappear. Two different bonding sites would explain why the LEED pattern vanishes during deposition of cyclopentene on the InP$(001)(2 \times 4)$ surface as there are $In-In$ dimers in the second

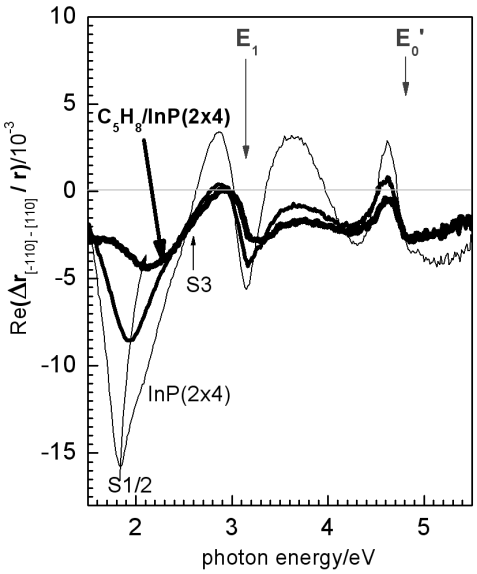


**Figure 6.1:** The RAS spectra taken during the deposition of cyclopentene on the InP$(001)(2\times4)$. Thin, intermediate and thick line: spectrum of the clean, partly covered and saturated surface, respectively.

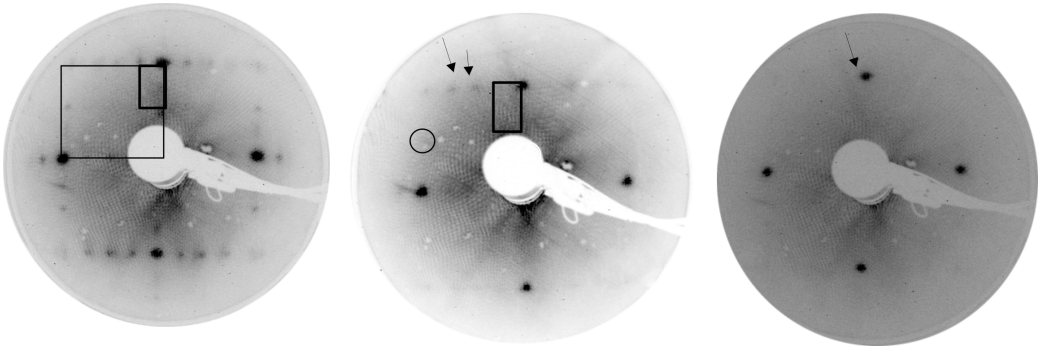

**Figure 6.2:** LEED pattern of the clean InP$(001)(2\times4)$ reconstructed surface on the left, in the middle the partially covered surface with cyclopentene and on the right the saturated surface. All three images were taken at 57 eV. The $(1\times1)$ bulk (thin rectangle) and the $(2\times4)$ surface unit cell (thick rectangle) are indicated. The $(2\times4)$ LEED pattern vanishes during the saturation with cyclopentene until only the $(1\times1)$ bulk spots remain.

layer. A translation invariant arrangement of the cyclopentene molecules on InP$(001)(2\times4)$ like on the Si$(001)(2\times1)$ surface is statistically hindered.
In order to obtain information on the chemical bonding configuration and to determine possible bonding sites of cyclopentene on the InP$(001)(2\times4)$ reconstructed surface SXPS measurements of the In4d, P2p and C1s core level are performed.

## 6.2. Core Level Spectroscopy of the Interface

In Fig. 6.3 SXPS core level spectra of the In4d core levels for the initial, the partly covered and the cyclopentene saturated InP$(001)(2 \times 4)$ surface are displayed.

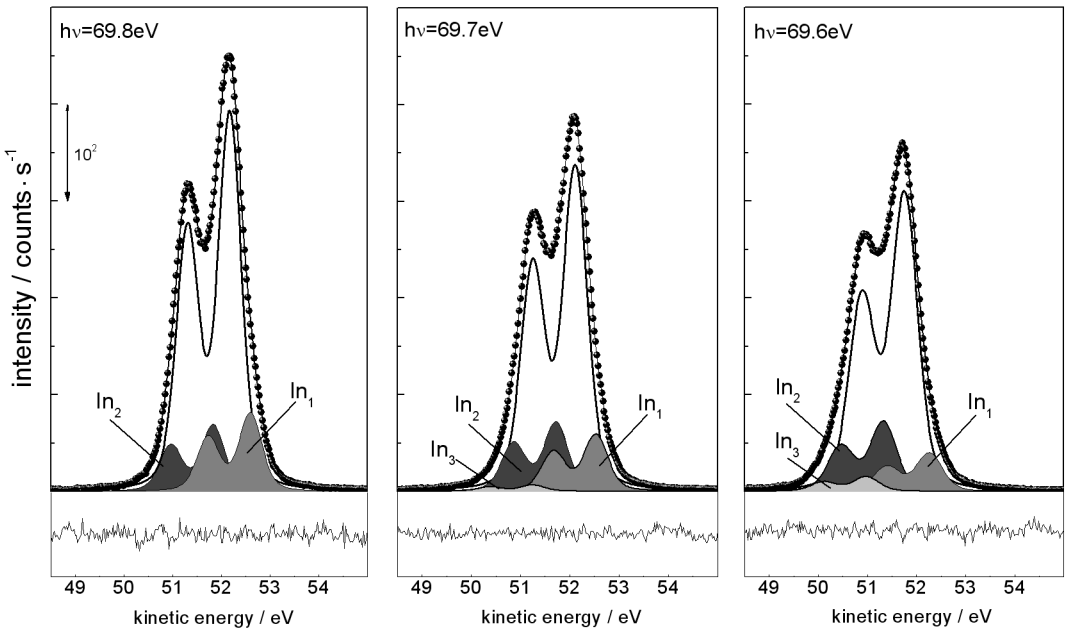


**Figure 6.3:** In4d core level of the clean (left), partly covered (middle) and saturated (right) InP$(001)(2 \times 4)$ reconstructed surface, respectively. For the partly covered surface a new component ($In_3$, light gray) emerges shifted towards higher binding energies of about +0.84 eV with respect to the bulk component which rises for the saturated surface.

The spectra (dotted lines) are shown together with best-fit from numerical analysis (straight lines) and the residuum (bottom) giving the differences between the measured line shape and the fitted one. The fit parameters are shown in table C.1. The fits were performed as long as the residuum contains no clear structures anymore.

As discussed in chapter 5.1 the surface related component ($In_1$) which is shifted toward lower binding energies is related to the fourfold coordinated In atoms of the second layer and the component which is shifted to higher binding energies ($In_2$) was assigned to the outer In atoms of the second layer which are threefold and also to the In atom of the 'mixed-dimer'. As can be seen in Fig. 6.4 $In_1$ decreases clearly with the coverage of cyclopentene. The decrease is stronger in the second deposition step until saturation than in the first one. Therefore it can be concluded that the interaction with the second layer In atoms is stronger

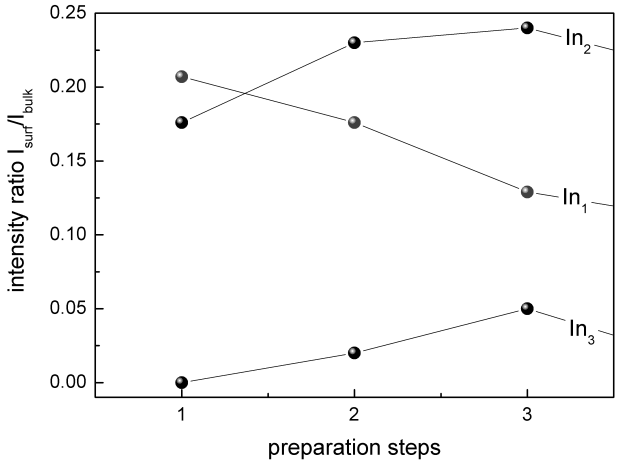


**Figure 6.4:** The development of the intensity ratio of the In4d surface components versus the preparation steps. $In_1$ and $In_3$ increases while $In_2$ decreases with the deposition of cyclopentene.

for a higher coverage. The second surface component, $In_2$, increases strongly in the first deposition step and then slightly more until saturation. A new bond formation of cyclopentene to the topmost In atoms of the surface is the origin for the third component, $In_3$, shifted by +0.84 eV. This component is rising in intensity up to the saturation.
The In4d core level were taken at excitation energies where a maximum surface sensitivity was obtained, as can be seen in Fig. 6.5.

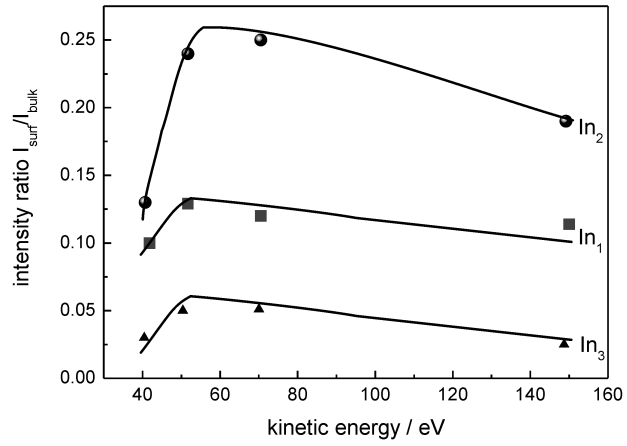


**Figure 6.5:** The relative intensity ratios between the In4d surface and the bulk components versus their kinetic energy. The curves are guides for the eye. At kinetic energies below 60 eV for all of the In surface components, a maximum intensity is found.

The maximum intensity for all three components is found near 55 eV (the reciprocal value corresponding to Fig. 4.3 is plotted). Above and below 55 eV the intensity decreases, exactly the behavior which was expected because of the dependence between the mean free path of the electrons and their kinetic energy. Thus it can be concluded that the new component $In_3$ which appears after the deposition has its origin in the topmost layer of the surface.
The changes in the P2p core level during the deposition are shown in Fig. 6.6. Again all three

steps are shown, the clean (left), the partly covered (middle) and saturated InP$(001)(2\times4)$ surface. The behavior of the intensity ratio for $P_1$ and $P_2$ (not shown) is similar as for the In4d surface components in Fig. 6.5.

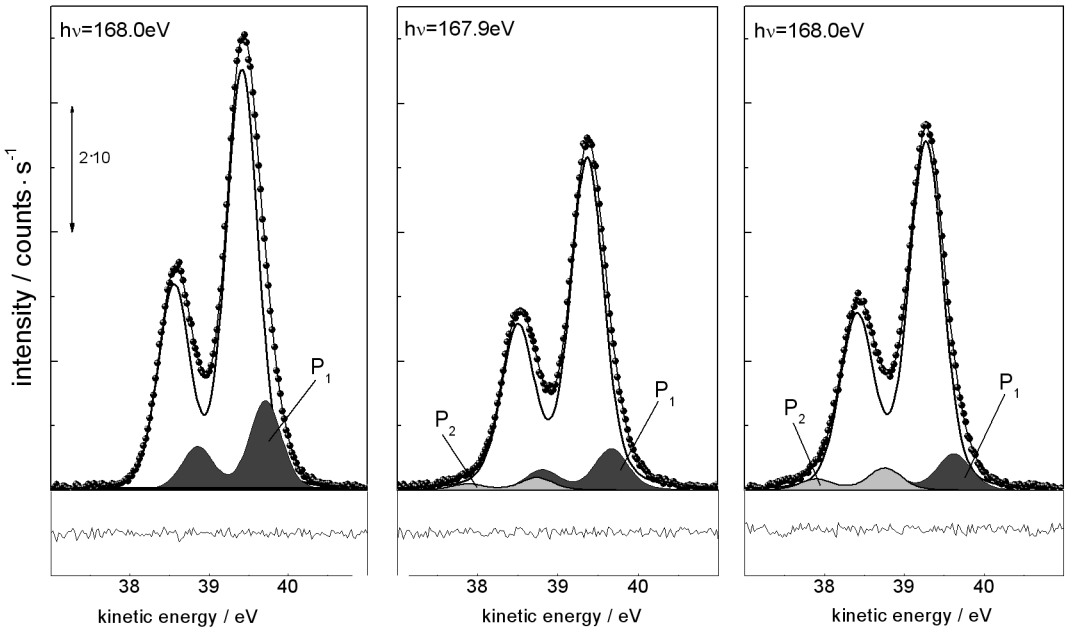


**Figure 6.6:** P2p core level of the clean (left), partly covered (middle) and saturated (right) InP$(001)(2\times4)$ reconstructed surface, respectively. A new component ($P_2$, light gray) emerges shifted toward higher binding energies of about +0.59 eV in the core level of the partly covered and rises for the saturated surface.

As mentioned in chapter 5.1 the P2p core level exhibits only one surface related component ($P_1$) assigned to the P atoms of the 'mixed-dimer' in the topmost layer which is shifted towards lower binding energies with respect to the bulk component. A new component ($P_2$) appears for both the partly covered and the saturated surface which is shifted by +0.59 eV in binding energy due to a lower electronegativity of the P atom compared to the C atom (see table 2.1).

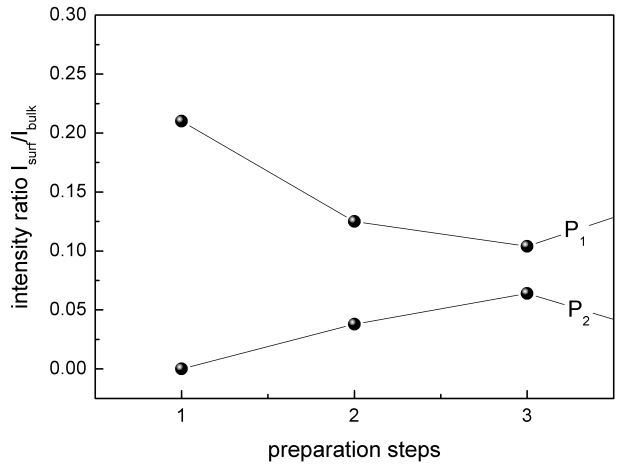


**Figure 6.7:** The development of the intensity ratio of the P2p surface components versus the preparation steps. $P_1$ decreases while $P_2$ increases with the deposition of cyclopentene.

The behavior of the two surface components in the intensity ratios for the different preparation steps is shown in Fig. 6.7. The $P_1$ component decreases until the saturation of the surface with cyclopentene while the $P_2$ component is increasing. From these results it can be concluded that the molecules bond to the P atoms of the 'mixed-dimer' and form a covalent bond which is the origin for $P_2$.

The change in $In_1$ and $In_2$ can be interpreted in that way that the adsorption of cyclopentene occurs not only on the 'mixed-dimer'. During the saturation of the surface the molecules bond to fourfold and threefold coordinated second layer In atoms. As a result of this bonding the $In_1$ component decreases more strongly with the second deposition step. However, for the bonding on the $In-In$ dimers one could also expect a new In4d component which is not the case. An explanation could be that this new component is energetically too close to the first $In-C$ component and both can experimentally not be resolved due to the limited resolution. Another possibility would be that the observed $In-C$ component is related to the bonding on the In-In sites whereas the bonding on the 'mixed-dimer' results in a component which is energetically very close to the $In_2$ component. This would explain why the $In_2$ component gets slightly more intense with the deposition.
The calculated In4d core level shift (calculations performed by P. Favero) for bonding on the second layer $In-In$ dimers amounts to $-0.72$ eV, which is very close to the one for the adsorption on top of the 'mixed-dimer' which was calculated to $-0.65$ eV. Since this two shifts present a small energy difference, it could be possible that they have not been resolved in the SXPS experiments mainly due to the limited experimental resolution.

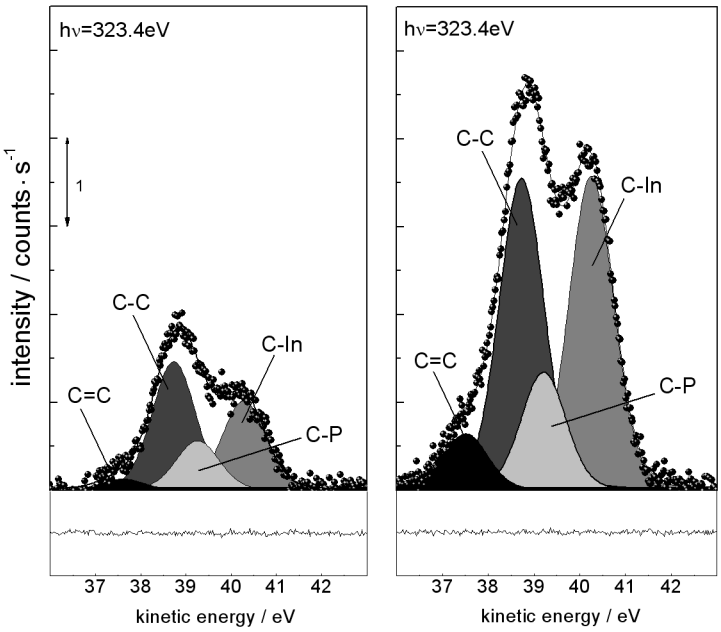


**Figure 6.8:** The C1s core level of the partly covered (left) and saturated (right) InP$(001)(2\times4)$ reconstructed surface, respectively. On the clean surface no C1s contribution was found.

The C1s core levels are shown in Fig. 6.8. Four components are evaluated. The main component is assigned to stem from C atoms which are involved in a single bonding to another C and hydrogen atom. The second component is shifted about +1.17 eV toward higher binding energies with respect to the $C-C$ component. This component is assigned to atoms participating in a $C=C$ double bond. Two other contributions were evaluated in the 'best-fit' and is assigned to stem from C atoms which are bonded to In and P in a $C-In$ and a $C-P$ bond formation. These two other components are shifted toward lower binding energies, by -1.54 eV and -0.50 eV, respectively, with respect to the first $C-C$ contribution. The $C-In$ component is weaker in the first deposition step but in the second one the $C-In$ component becomes more pronounced for the saturated surface than the $C-P$ component. Therefore it can be concluded that the surface exhibits a second adsorption site. More In atoms are involved in the bond formation to cyclopentene than P atoms. This is in agreement with the additional components $In_3$ in the In4d and $P_2$ in the P2p core level.

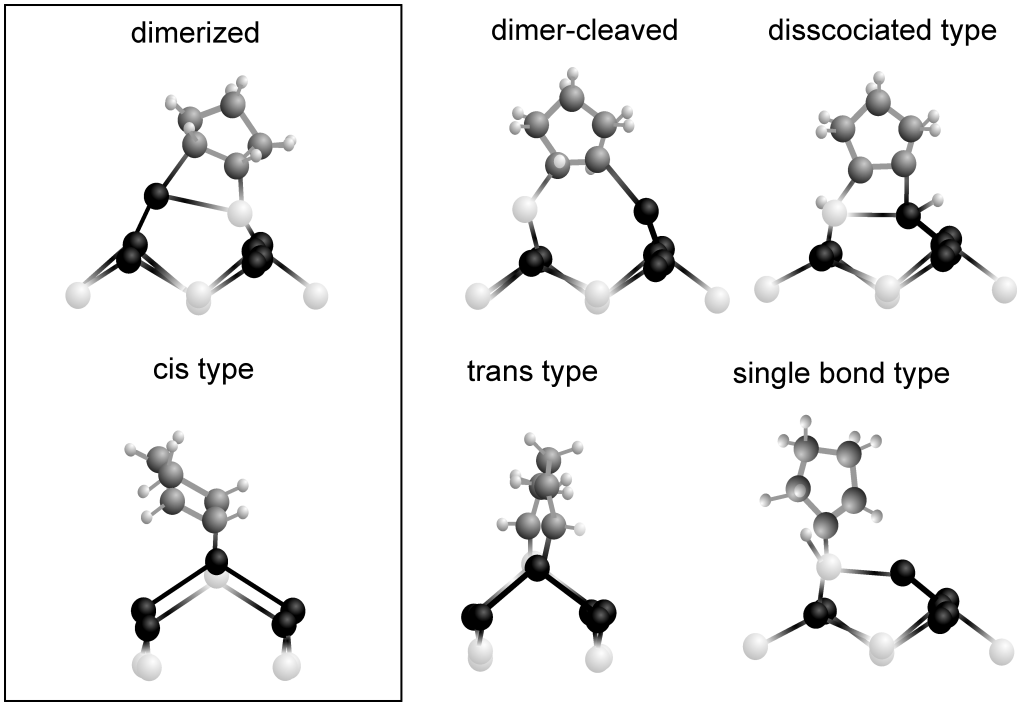


**Figure 6.9:** A few examples of the possible adsorption structures found for cyclopentene on the InP$(001)(2\times4)$ reconstructed surface including the dimerized and dimer-cleaved structures as well as dissociated adsorption configurations. The DFT calculations were done by P. Favero.

## 6.3. Discussion of Resulting Adsorption Structures

The experimental results presented here indicate an adsorption of cyclopentene in a two step process. In atoms of the first and second layers are involved as well as the topmost P atoms. Based on these experimental results DFT calculations were performed and a few examples for adsorption structures of cyclopentene on the InP$(001)(2\times4)$ surface reconstruction derived from DFT-GGA calculations are depicted in Fig. 6.9.

Within this calculations is was found that only the cis-type dimerized structure has an exothermic adsorption process. Thus only this adsorption structure is possible to occur without an additional activation energy. To further support the cis-type dimerized model for the cyclopentene adsorption on InP$(001)(2\times4)$ the optical anisotropy was calculated for different adsorption sites. Due to the computational method the resulting RAS spectra, presented in Fig. 6.10, are difference spectra of the saturated and the clean surface.
The first spectrum show the calculation for the adsorption of cyclopentene on the 'mixed-dimer' and the second one the resulting RAS difference spectrum after the adsorption on the second layer $In-In$ bonds. The most likely one is depicted in the third panel and shows the RAS signal after the adsorption at both, the 'mixed-dimer' and the second layer $In-In$ bonds. For a final determination of the bonding sites of cyclopentene on the InP$(001)(2\times4)$ reconstructed surface the SXPS measurements have to be discussed again.

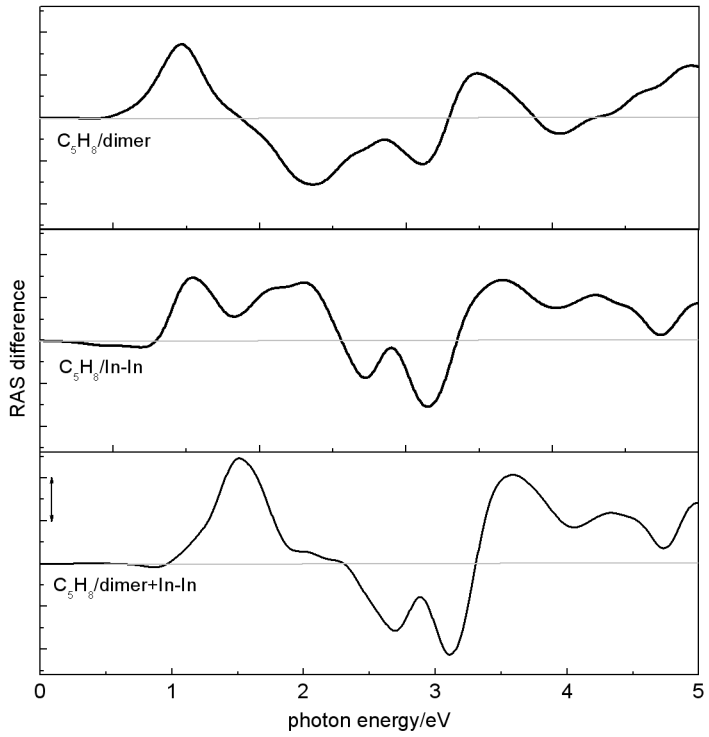


**Figure 6.10:** The calculated RAS difference spectra for the adsorption of cyclopentene on the dimer atoms (top), on the second layer In-In atoms (middle) and on both, the dimer and the second layer In-In atoms. The difference means that the spectrum of the clean reconstructed InP$(001)(2\times4)$ surface was subtracted from the one saturated with cyclopentene. The DFT calculations were done by P. Favero.

Due to the higher electronegativity (see table 2.1) of C compared to P and In the bonding would lead to relative charge depletion at the P and In atoms, respectively. Therefore the new component in the P2p as well as in the In4d core level is shifted towards higher and in the corresponding C core level towards lower binding energies. It is reasonable that the $C-In$ component is shifted more than the $C-P$ component based on to the different electronegativities.

The outermost P atom has a filled dangling bond. If the atom loses electrons a new component shifted towards higher binding energies should appear which is the case ($P_2$, see Fig. Fig. 6.7). Thus this new component $P_3$ is a direct hint for the bond formation of the outermost P atoms to the C atoms of the cyclopentene molecules while $P_1$ decrease.

The interpretation of the changes for the In4d components $In_1$ and $In_2$ (in Fig. 6.4) is not as straight forward as in the case of the change for the P2p surface related component ($P_1$). Here, in the first step, the topmost In atoms of the 'mixed-dimer' also form a bond to the cyclopentene molecules. In this step $In_1$ decreases while $In_2$ increases slightly. This trend is stronger in the second step until saturation. Due to the fact that two adsorption sites exists

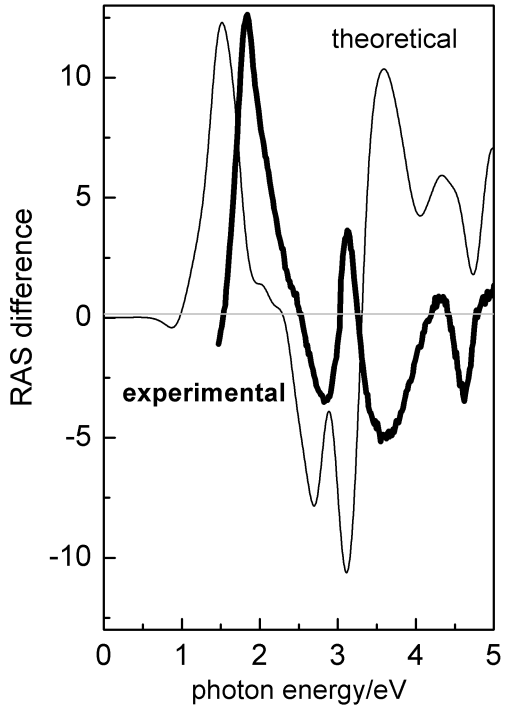


**Figure 6.11:** The RAS difference spectrum of the saturated InP$(001)(2\times4)$ reconstructed surface for the cis-type dimerized adsorption structure with additional adsorption of cyclopentene at the second layer $In-In$ bonds derived from DFT-LDA calculations done by P. Favero (thin line). The RAS difference spectrum depicted from the measurements is presented for comparison (thick line). The calculated spectra are not GW corrected which would reduce the shift between the measurements and the calculated data.

at the surface In atoms a second component should be revealed in the In4d core level after the adsorption of cyclopentene. This is not the case but an increase for $In_2$ is found. As mentioned before it could be the case that a new contribution can not be resolved due to the experimental resolution. Therefore the increase of $In_2$ results.
Thus it can be concluded that there are two adsorption sites on the InP$(001)(2\times4)$ reconstructed surface. This is in agreement with the C1s core level where the $C-In$ component is more pronounced than the $C-P$ component after saturation. Hence more In atoms are involved in the interface formation than P atoms.
Additionally the RAS spectrum Fig. 6.1 show a strong change of $S_1$ and $S_2$ which are mainly caused by transitions between states at the first and second layer In atoms.
From the DFT-GGA calculation three RAS difference spectra were obtained, depicted in Fig. 6.10. The one for the adsorption on the 'mixed-dimer' and additionally on the $In-In$ bonds is plotted again together with the RAS difference spectrum of the clean reconstructed surface subtracted from the cyclopentene saturated one in Fig. 6.11. This calculated spectrum reproduces the measurements very well. The main features are identified in both spectra regardless of the fact that the calculated results are red shifted by 0.4 eV. The reason is the underestimation of excitation energies which is well known. The same holds for the underestimation of the calculated RAS magnitude, see [116].

According to all these results it can be concluded that the first adsorption site for cyclopentene on the InP$(001)(2\times4)$ surface is the 'mixed-dimer' in a cis-type adsorption geometry [150]. This is a similar adsorption geometry as for the adsorption for cyclopentene

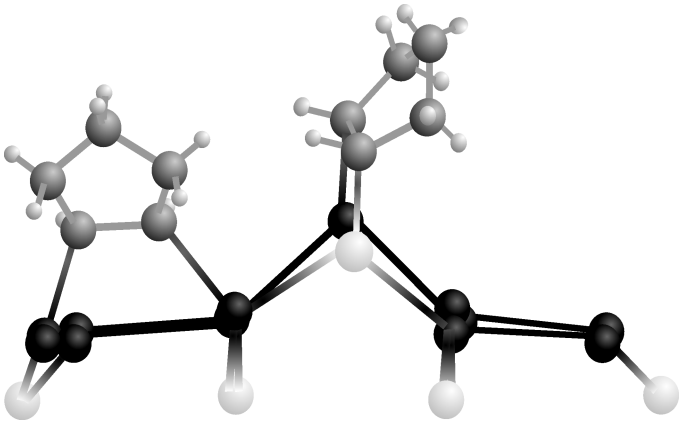

**Figure 6.12:** Suggested adsorption structure of cyclopentene adsorbed on the InP$(001)(2\times4)$ reconstructed surface.

on the Si$(001)(2\times1)$ surface where a $[2+2]$-cycloaddition reaction occurs, see chapter 2.5. The resulting adsorption structure of cyclopentene on the InP$(001)(2\times4)$ reconstructed surface is presented in Fig. 6.12.
Upon cyclopentene adsorption the buckling of the 'mixed-dimer' changes into the opposite direction and decreases by 0.53 Å, whereas the second layer $In-In$ dimer buckling increases by 0.43 Å [150]. This dimer rearrangement suggests a charge transfer between In and P atom in analogy to the $Si-Si$ dimer tilting of the bare silicon surface. Indeed, a comparison of the second highest occupied molecular state from the bare InP surface and the adsorbed system (not shown here) clearly indicates a charge redistribution due to the interaction between cyclopentene and the surface [150]. Although a second molecule adsorption does not result in the lowest energy configuration, it is interesting to emphasize that the adsorption on a $In-In$ dimer within a surface unit cell is only possible after a previous adsorption of cyclopentene on the neighboring 'mixed-dimer' which is consistent with the interpretation of the C 1s core level evolution upon deposition.
The theoretical calculated adsorption energy for cyclopentene at the 'mixed-dimer' is $-0.28$ eV which is much lower than the one found for cyclopentene on the Si$001(2\times1)$ surface reconstruction which is ∼-1 eV [51,151]. This corresponds to a high desorption temperature of around 900°C [3,51]. The adsorption of cyclopentene at the second layer $In-In$ bonds is an energetically favorable process with an adsorption energy of $-0.1$ eV. Therefore two processes occurring for the adsorption of cyclopentene on the InP$(001)(2\times4)$ reconstructed surface were found. This could also result in two different desorption temperatures of cyclopentene on this surface.

## 6.4. Desorption Experiments

In this work it was not possible to determine exact desorption temperatures therefore only the possibility of restoring the $(2\times4)$ surface reconstruction was investigated.

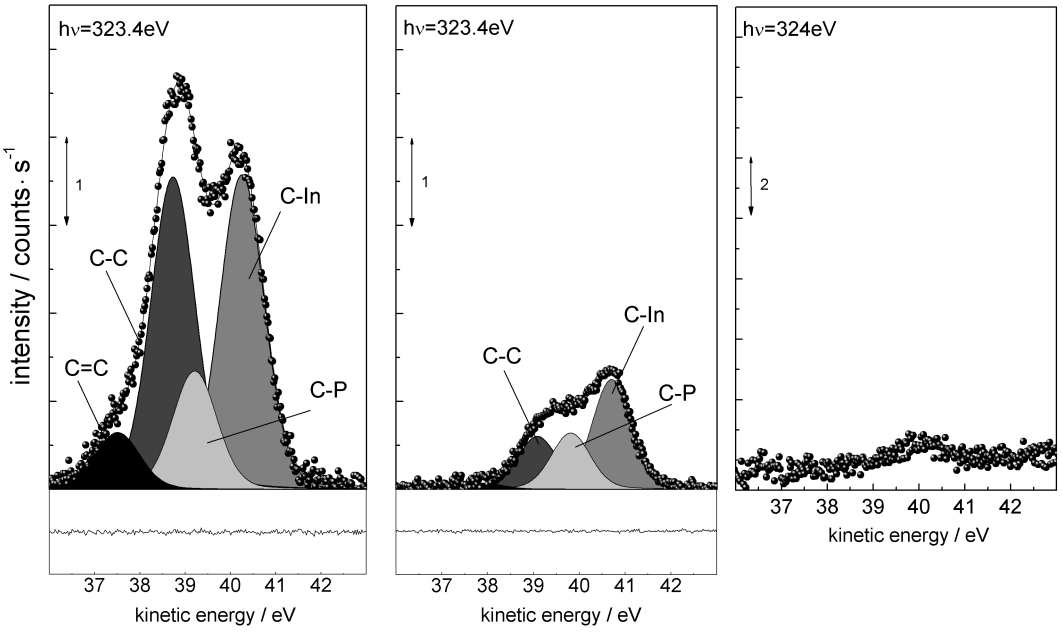


**Figure 6.13:** C1s core level of the cyclopentene saturated surface (left) and the core level after the first heating to 300°C (middle). After this heating step not all of the C was removed from the surface. The $C-In$ component is now more pronounced than the $C-C$ contribution. The $C=C$ component has nearly vanished. This is a hint for additional physisorbed molecules which are removed from the surface after this heating step. After a second heating to 430°C for ∼15 min no C1s core level was detected anymore (right).

In order to desorb cyclopentene the cyclopentene saturated InP$(001)(2\times4)$ reconstructed surface was heated to 300°C. In Fig. 6.13 the C1s core level emission lines for the cyclopentene saturated surface (left) and the core level emission line taken after the first heating step to 300°C are shown. It is obvious that the whole C1s emission line is significantly reduced in its intensity. The line shape reveal that the $C-C$ component is strongly reduced, as well as the $C=C$ component which nearly vanished completely after this procedure. This is a hint that the $C=C$ component can be related to additional physisorbed cyclopentene which are removed at lower temperatures than chemisorbed cyclopentene molecules. These physisorbed cyclopentene molecules contribute to the $C-C$ component, too, which is now reduced. Due to the fact that the C1s core level emission line is still detectable and that the

LEED pattern of the $(2\times4)$ reconstructed surface was not restored an additional heating procedure to 430°C for approximately 15 min was applied. After this heating no C1s core level emission line was detected anymore (Fig. 6.13 right). The corresponding contributions in the In4d and P2p core levels vanished, too, and the initial core level line shape was restored.

This and the fact that no carbon C1s core level contributions has been detected anymore is a proof for the desorption of cyclopentene and the restoring of the surface reconstruction.

These results are confirmed by RAS and LEED measurements. The RAS line shape with the surface related features was restored (see Fig. 6.14) after the second heating step to 430°C for 15 min and a LEED pattern of the $(2\times4)$ was observed.
Small changes in the intensity of the RAS signal after the desorption compared to the initial prepared InP$(001)(2\times4)$ reconstructed surface appear which can be explained by a degradation of the surface after heating. This effect can be observed for clean surfaces heated several times without molecule deposition, too. Therefore this change is not related to cyclopentene molecules or their desorption behavior.
The desorption temperature of 430°C (-0.28 eV derived from DFT-LDA calculations) is much lower than for the cyclopentene adsorbed on the Si$(001)(2\times1)$ [3, 51, 151].

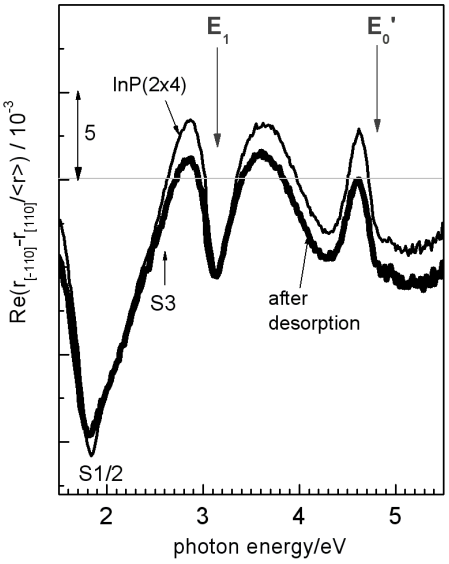


**Figure 6.14:** RAS spectrum of the initial clean InP$(001)(2\times4)$ surface (thin line) depicted together with the spectrum taken after desorption of the cyclopentene molecules. It is obvious that the line shape of the clean surface was restored.

# Part III.

# Interface Formation between Small Organic Molecules and GaAs$(001)$ Surfaces

# Chapter 7: Interaction of Cyclopentene with the GaAs$(001)$ Surfaces

In this chapter the bond formation between the model molecules, the small hydrocarbon ring molecules, and the $(001)$ GaAs surfaces upon adsorption is discussed. The main focus will be the role of the intra-molecular double bond on the one hand and on the other the surface dimer structure on the bonding configuration. The results will be presented for the adsorption of the three different molecules one after another and all three GaAs$(001)$ surfaces in each case. Therefore, firstly, the RAS signal is presented after that the results obtained by core level spectroscopy and the surface morphology measured by STM. In the last part of this chapter the results and possible adsorption structure models will be discussed for all the different hybrid structures and general trends for an understanding of the adsorption mechanism will be suggested.

## 7.1. Change in the Optical Anisotropy

In Fig. 7.1 the RAS spectra of the three different GaAs$(001)$ surface reconstructions after deposition of cyclopentene (thick lines) up to saturation are depicted together with the ones of the initial surfaces (thick lines).

The saturation conditions of the surfaces are explained in chapter 4.3. It is obvious that the RAS line shape clearly changes for the GaAs $c(4\times4)$ and the $(4\times2)$ (Fig. 7.1 left and right) with respect to the ones for the clean surfaces upon deposition. In the case of the $(2\times4)$ the amplitude at bulk related transitions is reduced but it has to be mentioned that the RAS spectrum of the $(2\times4)$ is dominated only by bulk related features.

After the deposition of cyclopentene on the $c(4\times4)$ reconstructed surface, the surface related contribution $S_1$ which is below 1.5 eV is reduced in intensity. This could be due to a saturation of an unsaturated surface state by the molecule after adsorption so that the RAS feature vanishes. The change in $S_2$ is even more obvious as the decrease of this feature is very strong. Since both features are assigned to transitions between states localized at the As dimers, it can be concluded that cyclopentene adsorbs during a chemical bond formation at the As dimer because $S_1$ has vanished and a strong reduction for the feature $S_2$ is obvious.

As mentioned before no surface related contribution is evident in the RAS spectrum of the $(2\times4)$ reconstructed surface. The shoulder around 2.5 eV however could be due to a

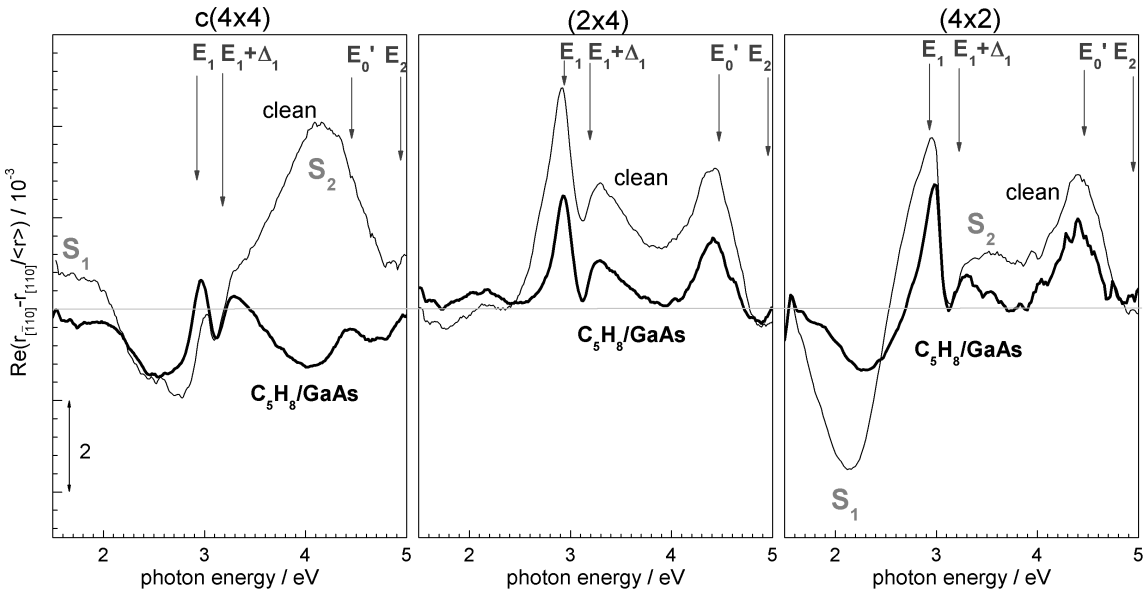


**Figure 7.1:** RAS spectra of the three 'main' clean reconstructed GaAs(001) surfaces (thin lines), the c$(4\times4)$, the $(2\times4)$ and the $(4\times2)$, respectively, compared to the spectra taken after the saturation with cyclopentene (thick lines).

surface contribution [144]. That could be underlined by the change in the spectrum after the saturation with cyclopentene (thick line) because this shoulder shifts slightly to higher photon energies. This could be an indication for a change at the surface after the adsorption of cyclopentene.

For the GaAs $(4\times2)$ reconstructed surface the surface related contribution $S_1$ also changes due to the cyclopentene deposition. The transition which is related to $S_1$ is reduced and a small shift to higher photon energies could be observed which can be associated to a change of the surface structure.

However, for both the GaAs $c(4\times4)$ and the GaAs $(4\times2)$, the RAS spectra change clearly at those energies where transitions between surface states contribute. Thus it can be concluded that the changes in the optical response, and therefore the electronic surface properties, are related to changes in the atomic surface structure. It seems reasonable that cyclopentene bonds to the top surface dimers or atoms and thereby lead to the observed changes. In the case of the $c(4\times4)$, which is terminated by $As-As$ dimers on top of a complete As layer, it can be expected that the bonds are formed with the As atoms of this dimers. In the case of the $(4\times2)$ surface such an assignment is more difficult due to the complicated surface

structure model as discussed in chapter 5.2 where several bonding sites exist.
The spectral changes for the cyclopentene deposition on the GaAs$(001)(2\times4)$ reconstructed surface (Fig. 7.1 middle) are much less significant and show a amplitude decrease of the bulk related transitions. Since clear contributions from surface states are not found in the RAS spectrum of the $(2\times4)$ reconstruction, it is difficult to deduce interactions of cyclopentene with the surface. To find the final bonding sites of cyclopentene a determination of the electronic properties is necessary.

## 7.2. Core Level Spectroscopy at the Interface

In the following the results obtained by core level spectroscopy at the saturated surfaces will be presented. In Fig 7.2 the core level emission lines for the three 'main' GaAs$(001)$ surfaces saturated with cyclopentene are shown. For a better comparison the spectra of the clean reconstructed surfaces (first shown in Fig. 5.8) are plotted above the ones of the corresponding saturated surfaces.
As discussed in chapter 5.2, surface related contributions are revealed in each emission line. After the saturation for the $c(4\times4)$ (see Fig 7.2 left) one new surface related component (light gray) can be found shifted by +1.35 eV$\pm$0.05 eV toward higher binding energies. This shift towards higher binding energies is reasonable due to a bond formation between cyclopentene and the topmost As atoms of the c$(4\times4)$ reconstructed surface. These atoms would show a relative charge depletion due to the higher electronegativity of C compared to As (see table 2.1). Thus the $As-C$ component can be attributed to As atoms which form a covalent bond to the C atoms of the cyclopentene molecules.
Except for the $As_{defect}$ contribution the shifts of the As3d core level components of the c$(4\times4)$ reconstructed surface are increased by a factor of 1.35. Beside this the $As_{dimer}$ component is reduced by $\sim$50%. This can be caused by an adsorption of cyclopentene at the dimer atoms and thus this could be an indication that the dimer bond splits. The $As_{defects}$ component increases by $\sim$47%. The $As_{2ndlayer}$ component is constant because the second layer should not be affected during adsorption of the cyclopentene molecules on the surface.
Similar as for the c$(4\times4)$ for the GaAs $(2\times4)$ a new component (light gray) can be revealed in the fit which is shifted toward higher binding energies by +1.05 eV$\pm$0.1 eV. Due to this shift the component, $As-C$, can be assigned to a bond formation between the C and the As atoms. The carbon atoms have a higher electronegativity and therefrom a shift towards higher binding energies results. Within the experimental resolution the shifts of the two As components, $As_1$ and $As_{dimer}$, do not change compared to the initial shifts for the components of the clean reconstructed surface. The intensities for the two surface related components change in such a way that the $As_{dimer}$ component is slightly reduced to $\sim$75% of the initial value and the second As component ($As_1$) increases by approximately 65%. Due to the fact that the decrease of the $As_{dimer}$ component is not as strong as it was the case for the $As_{dimer}$ component after the adsorption of cyclopentene on the c$(4\times4)$ reconstructed surface it can be concluded that the dimer bond remains intact. Accordingly to the increase of $As_1$ after

the adsorption of cyclopentene it could be concluded that this component is defect related. A fourth component ($As-C$, light gray) was derived from the 'best fit' as can be seen in Fig 7.2 on the right for the cyclopentene adsorption on the $(4\times2)$ reconstructed surface.

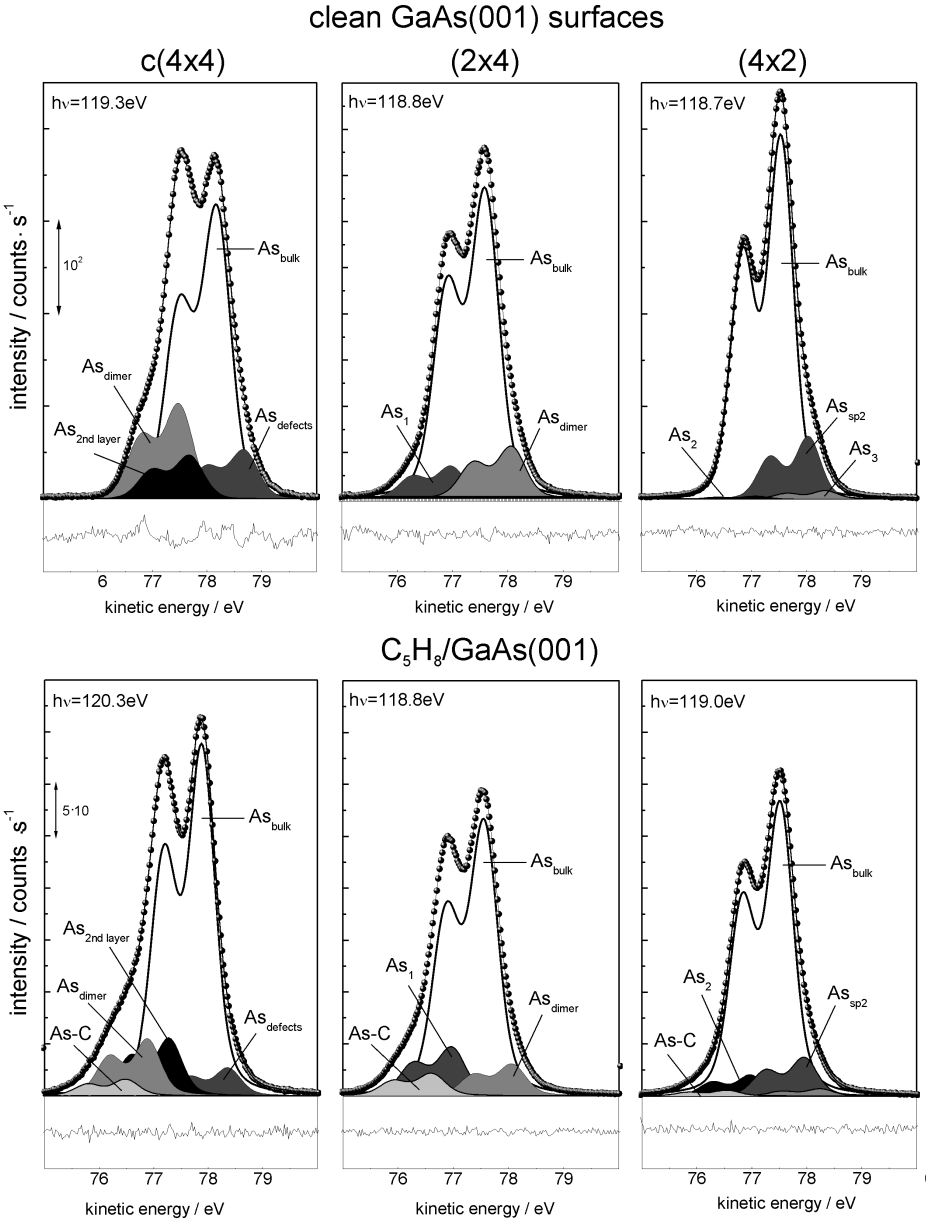


**Figure 7.2:** The As3d core level emission lines before and after adsorption of cyclopentene on the three main GaAs(001) surfaces at excitation energies of ∼120 eV. A new component assigned with $As-C$ can be revealed in each of the core level emission lines shifted toward higher binding energies. For comparison the As3d core level emission lines of the clean reconstructed surfaces are shown.

This component is shifted by +1.0 eV±0.09 eV towards higher binding energies which is comparable to the shift of the $As-C$ component found on the $(2\times4)$. Within the experimental resolution the initial As surface components show no change in the shifts. It is obvious that the $As_2$ component shifted towards higher binding energies increases by a factor of 5 while the $As_{sp2}$ component decreases. Thus on the one hand the increase could be caused by atoms which initially contribute to $As_{sp2}$ and are now involved in a bond formation to cyclopentene. This results in an increase for the $As_2$ component because a slight difference in the shifts can not be resolved. On the other hand due to the fact that the $As_2$ component is related to the As atoms of parts on the surface which are $(n\times6)$ reconstructed it can be concluded on the other hand that cyclopentene bonds to this As atoms, too. The $As_3$ component does not change within the experimental resolution. For all of the three surface reconstructions a new component $As-C$ shifted towards higher binding energies is found because of the higher electronegativity of carbon compared to As. This component can be assigned to a chemical bond formation of cyclopentene and the topmost As atoms of the surface. The surface components in the Ga3d emission line for the c$(4\times4)$, $Ga_{defects}$ and $Ga_1$ show no obvious change compared to the ones of the clean reconstructed surface, see Fig. 7.3 left. The shifts of the surface contributions compared to the clean surface are equal. The same results for the $(2\times4)$ reconstructed surface. No change in the shift for the surface related contributions appear and no new component can be evaluated with the numerical analysis. Only a slight reduction of the components is found. Therefrom it can be concluded that no Ga atoms are involved in a bond formation to the cyclopentene molecules so far.

In the case of the $(4\times2)$ reconstructed surface a new component $(Ga-C)$ shifted by +1.08 eV±0.08 eV towards higher binding energies emerges. This component can be assigned to a bond formation of cyclopentene to the Ga atoms of the surface because the shift towards higher binding energies can be explained by a relative charge depletion due to the respective electronegativities. The $Ga_{sp2}$ component is nearly not affected by the adsorption of cyclopentene and the component $Ga_{dimers}$ is reduced to 50%. Therefrom an adsorption of cyclopentene to the $Ga_{dimers}$ can be assumed. The third component, $Ga_4$, shifted by +0.74 eV towards higher binding energies is increased by a factor of 2. It could be the case that during the saturation of the surface cyclopentene bonds to the atoms which are contributing to the $Ga_{dimer}$ and additionally to atoms contributing to the $Ga_{sp2}$ component. Thus two new components should result after the saturation. Now only one new component, $Ga-C$, emerges but $Ga_4$ increases. It could be due to the experimental resolution that the differences in the shifts of $Ga_4$ and a second new component can not be resolved and thus $Ga_4$ increases. This could be the case because both new components have to be shifted towards higher binding energies due to the higher electronegativity of C compared to Ga.
In the C1s core level emission line for the cyclopentene saturated c$(4\times4)$ reconstructed surface three components are revealed, Fig. 7.4 left. These components are denoted with $C-C$, $C-As$ and $C=C$. This assignment is in direct agreement with the bonding configuration of the corresponding atom and with respect to the different electronegativities of the elements, see table 2.1. The main component is denoted with $C-C$ and this component is assigned to atoms which are involved in a $C-C$ single bond. The $C=C$ component is re-

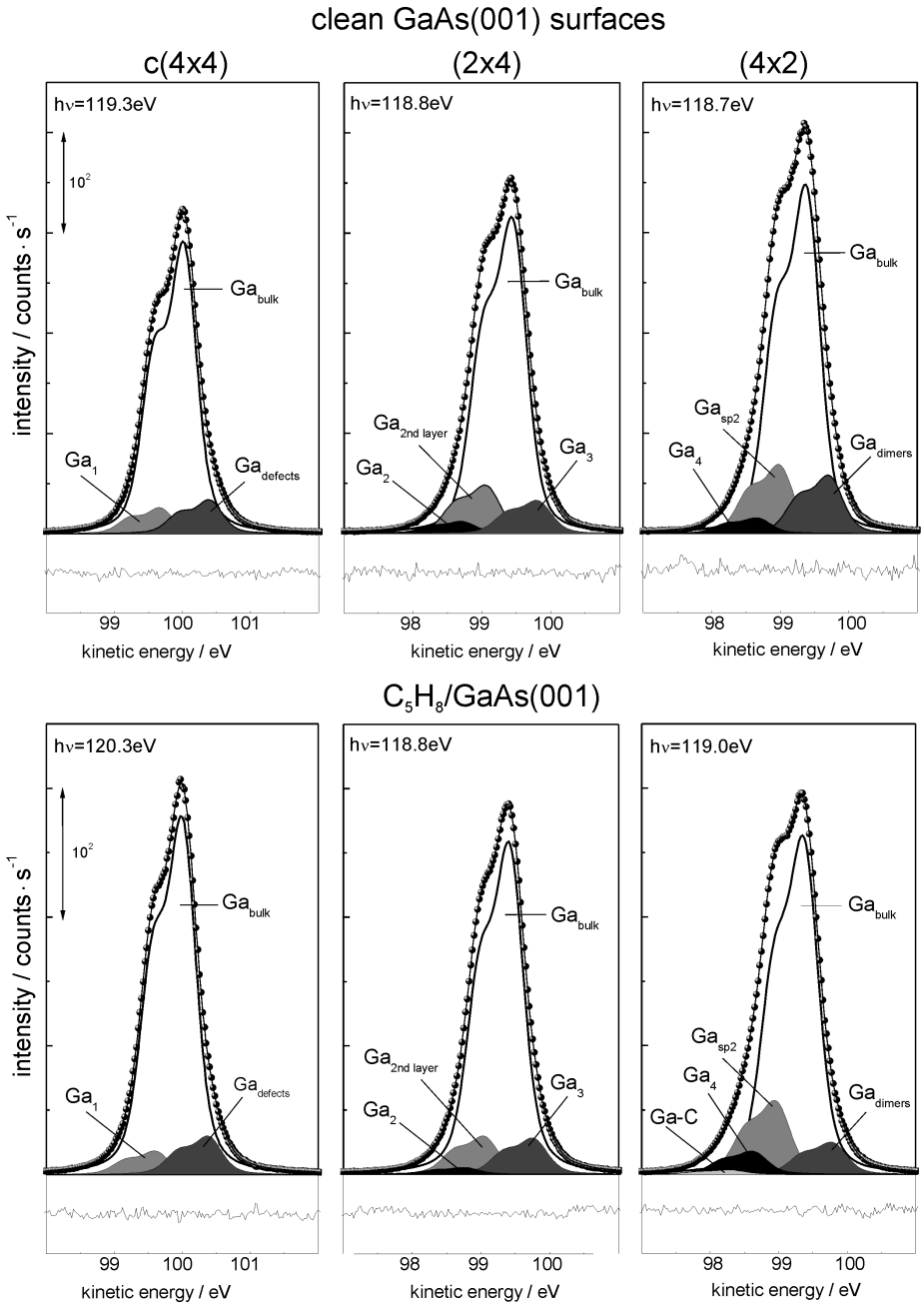


**Figure 7.3:** Depicted are the Ga3d core level emission lines taken after the adsorption of cyclopentene on GaAs(001), c$(4\times4)$ (left), $(2\times4)$ (middle) and $(4\times2)$ (right) at excitation energies $\sim$120 eV. For comparison the Ga3d core level emission lines of the clean reconstructed surfaces are shown above.

lated to C atoms contributing to a double bond. This component is with respect to the $C-C$ component shifted by +0.79 eV in binding energy because of more electrons involved in a

double bonds than in a single bond. Thus a shift to higher binding energies should occur for this component which is the case here. This component should not appear during an adsorption of cyclopentene with an interaction of the $\pi$ bond and the surface. The fact that this component is found indicates that not all cyclopentene molecules bond with a splitting of the double bonds. The third component is denoted with $C-As$ and corresponds to the $As-C$ component in the As3d core level emission line. It is shifted by -0.61 eV in binding energy and related to C atoms which form a covalent bond to As atoms of the surface. This assignment is in agreement with the electronegativity of the bonding partners C and As.

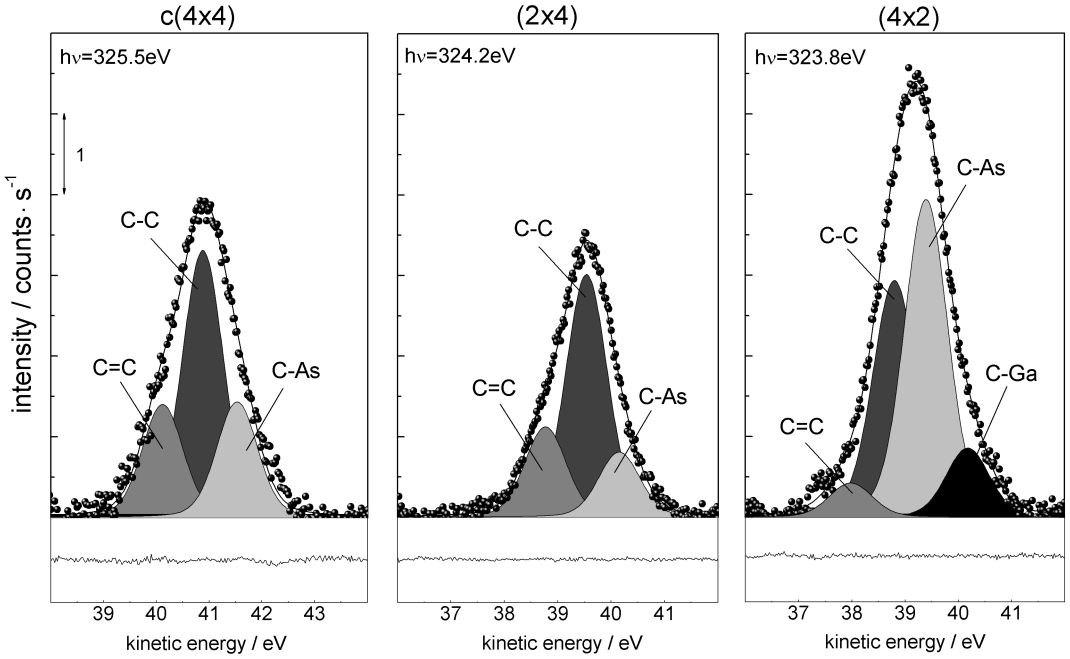


**Figure 7.4:** The C1s core level emission lines for the c$(4\times4)$ (left), $(2\times4)$ (middle) and the $(4\times2)$ (right) after saturation with cyclopentene taken at an excitation energy $\sim$325 eV.

The C1s core level emission line of the cyclopentene saturated $(2\times4)$ reconstructed surface is shown in Fig. 7.4 middle. Again three components are revealed with the line shape analysis. The assignment and the shifts of the components are in direct agreement with the findings for the cyclopentene saturated c$(4\times4)$ reconstructed surface. Thus the $C-C$ and $C=C$ components are related to the single and double bonds cyclopentene contains of, respectively. The occurrence of the $C=C$ component indicates that not all of the double bonds of the cyclopentene molecules split during the adsorption. The $C-As$ component corresponds to the $As-C$ component in the As3d core level.

In the case of the $(4\times2)$ reconstructed surface saturated with cyclopentene the C1s core level emission line exhibits four components. The assignments and shifts of the $C-C$, the

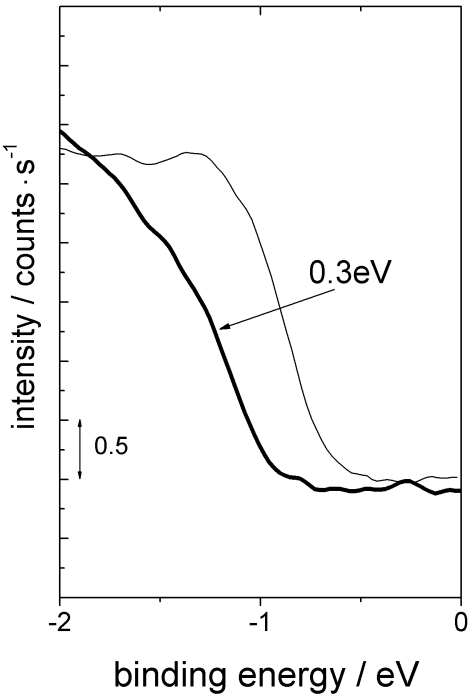


**Figure 7.5:** The valence band edge of the clean reconstructed c$(4\times4)$ surface (thin line) depicted together with the corresponding cyclopentene saturated surface (thick line). It is obvious that the valence band edges of the cyclopentene saturated surface is shifted by 0.3 eV with respect to the valence band edge of the clean surface.

$C=C$ and the $C-As$ are in agreement with the components found for the c$(4\times4)$ and $(2\times4)$. It is obvious in Fig. 7.4 right that the $C-C$ component is less pronounced than the $C-As$ component. Therefore it can be concluded that more C atoms of cyclopentene are involved in a bond to As atoms than in single $C-C$ bonds. The forth component indicates that cyclopentene has an additional bonding partner which should have a lower electronegativity than C and As. This is the case for Ga. Thus the $C-Ga$ component is shifted by -1.38 eV towards lower binding energies. This shift is stronger than for the $C-As$ component which was found to be -0.61 eV towards lower binding energies.
The assignment of the contributions found for the cyclopentene saturated GaAs$(001)$ surface reconstructions is in agreement with results obtained at the Si$(001)(2\times1)$ reconstructed surface saturated with hydrocarbons [42, 47].

In Fig. 7.5 the valence band edge of the clean reconstructed c$(4\times4)$ surface is depicted together with the valence band edge taken after saturation with cyclopentene. The hole spectrum is not shown and new contributions will not be discussed because of the signal-to-noise ratio and the high excitation energy the valence band spectra were taken at ($\sim$60 eV, excitation energies at $\sim$20 eV are more useful). Nevertheless a shift of the valence band edge of the cyclopentene saturated surface with respect to the spectrum of the clean reconstructed

c$(4\times4)$ is found. This is not the case for the valence band edges of the saturated $(2\times4)$ and $(4\times2)$ (not shown here). It will be shown in chapter 8 that this shift is found for the 1,4-cyclohexadiene saturated c$(4\times4)$ surface, too. In this case the shift is also verified within the core levels of As3d and Ga3d. Both exhibit a corresponding shift of the core levels taken before and after saturation.
This shift is an indication for a surface band bending due to the adsorption of cyclopentene and 1,4-cyclohexadiene. An explanation for this shift could be a change of the charge density at the surface and the compensation of this increased surface charges causes a shift in the surface states to higher binding energies in the space-charge-region and thus a surface band bending. Because of the problems discussed above this has to be verified with further measurements. Nevertheless this shift can be an indication for the splitting of the $As-As$ dimer bond during the saturation with cyclopentene or 1,4-cyclohexadiene which induces a change in the surface strain.

## 7.3. Interface Characterization by Scanning Tunneling Microscopy

In Fig. 7.6 (left) the filled-state STM image of a partly covered GaAs(001)c$(4\times4)$ reconstructed surface is shown.

In the case of cyclopentene adsorbed on the c$(4\times4)$ reconstructed surface oval shaped structures are found on the surface which are oriented along the $[110]$ direction of the crystal with a length of 2.4 nm and an average width in the $[\bar{1}10]$ direction of 1.7 nm. They are too big to represent only single molecules which have a dimension of $0.42\ nm\times0.24\ nm$ in the length and width [53]. Thus these ovals can be assumed to be cluster-like cyclopentene structures which are arranged in a local order. Some areas exist denoted by black rectangles in Fig. 7.6 where the c$(4\times4)$ is still present on the surface.
After saturating the c$(4\times4)$ surface with cyclopentene the ovals nearly cover the hole surface, as can be seen in Fig. 7.6 (right). They still have the same dimensions as for the partly covered surface. As it is indicated with the white circle in Fig. 7.6 the local ordering of the molecules along the $[110]$ direction of the crystal is kept during the saturation. Due to the fact that this is only some kind of local ordering no long range order exists and thus no LEED pattern is obtained. Only bulk spots remain in the LEED pattern presented in Fig. 7.6 (middle).

In Fig. 7.7 STS spectra were taken of the clean (dark gray boxes) and the saturated (gray triangles) surface which are depicted in Fig. 7.7. For both surfaces, the clean and the cyclopentene modified one, a band gap of $\sim$1.3 eV is found. No change of the band gap in the STS spectrum of the saturated surface is found. In the contrast to this the spectrum of the saturated surface is very similar to the one measured for the clean reconstructed surface. Therefrom it can be concluded that on the saturated surface mainly chemisorption takes place

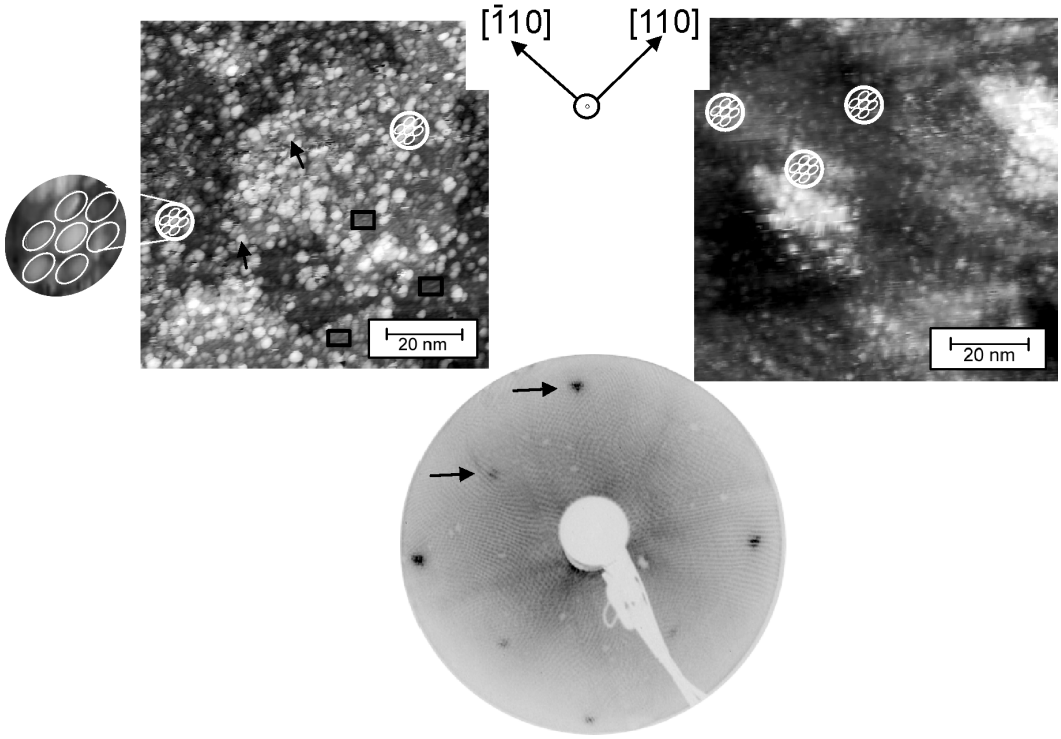


**Figure 7.6:** Filled-state STM images of a partly covered (left) and cyclopentene saturated (right) c$(4 \times 4)$ surface. No long range ordering exists (measured at U=-2.4 V and U=-2.8 V, respectively) but parts with local ordering are identified and indicated by white cycles. The cluster-like structures of cyclopentene molecules result in oval shaped structures measured in the STM images. Beside the STM images the LEED pattern of the saturated surface is depicted in the middle taken at 42 eV. Only bulk sports remain.

where cyclopentene interacts with the surface which results in a covalent bond formation of cyclopentene and the topmost atoms on the surface.

The filled-state STM images in Fig. 7.8 show the partly cyclopentene covered (left) and the cyclopentene saturated (right) $(2 \times 4)$ reconstructed surface. The rows along the $[\bar{1}10]$ direction of the crystal, which represent the position of the As dimers on the clean reconstructed surface, have a distance of 1.55 nm which is in agreement with previous work [128, 130]. These rows are still present on the partly covered and saturated surface which can be seen in Fig 7.8 and have the same distance of 1.54 nm as it was the case on the clean reconstructed surface. Only the height of the lines are different, which is an indication of an adsorption of cyclopentene on the surface.
The apparent periodicity in the STM images is reproduced in the LEED pattern which is depicted in Fig. 7.8 (middle, taken at an energy of 42 eV). The pattern exhibits spots indicating a $(1 \times 4)$ symmetry like reconstruction because the spots in the $[110]$ direction remain after the saturation with cyclopentene. This shows an ordering of cyclopentene along the rows of the clean reconstructed surface during the adsorption.

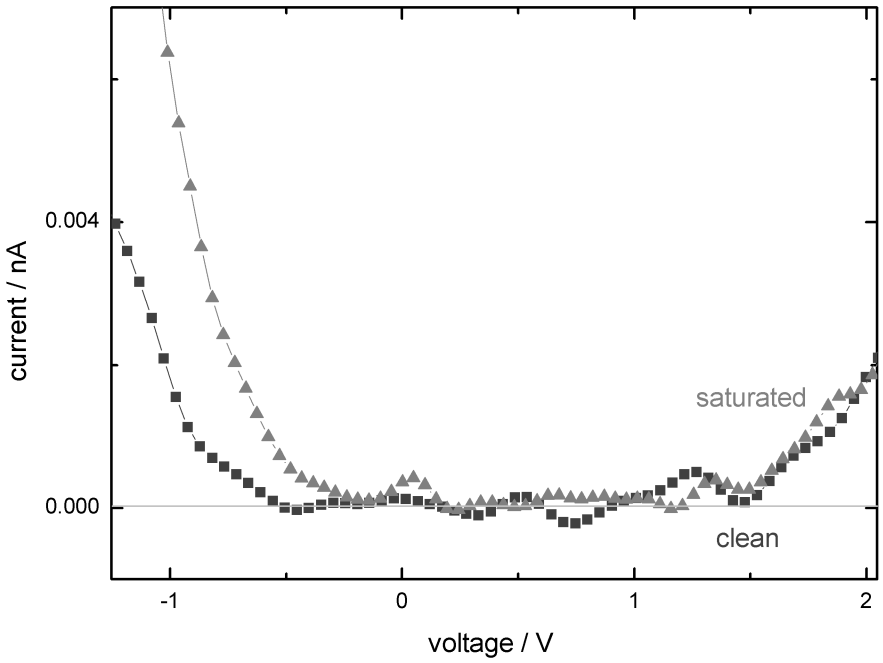


**Figure 7.7:** STS measurements of the band gap before (clean) and taken after the adsorption of cyclopentene (saturated) on the c$(4\times4)$ surface. The STS measurement of the clean surface is shown in dark gray boxes, the saturated in gray triangles and a over-saturated surface in black spots.

STS measurements (not shown here) indicated that no change for the band gap occurs after the saturation with cyclopentene. The band gap was for the clean reconstructed and cyclopentene saturated surface determined with $\sim$1.3 eV.

In Fig. 7.9 the filled-state STM images of the partly cyclopentene covered (left) and the cyclopentene saturated (right) $(4\times2)$ reconstruction are shown. No local or long range ordering of cyclopentene is observed in the STM images. Parts where the clean surface reconstruction can still be found are indicated with black rectangles and structures where molecules adsorbed on the surface (brighter spots) with black arrows. These formations are not small enough to represent only one molecule hence they could represent cluster-like structures of cyclopentene molecules.
The absence of ordering is consistent with the corresponding LEED pattern shown in Fig. 7.9 (middle). This LEED pattern shows no spots thus no long range order of cyclopentene on the surface is observed.
For the adsorption of cyclopentene on the $(4\times2)$ reconstructed surface it can be concluded that preferred adsorption sites exists because of the brighter spots in the STM images but no ordering is found.

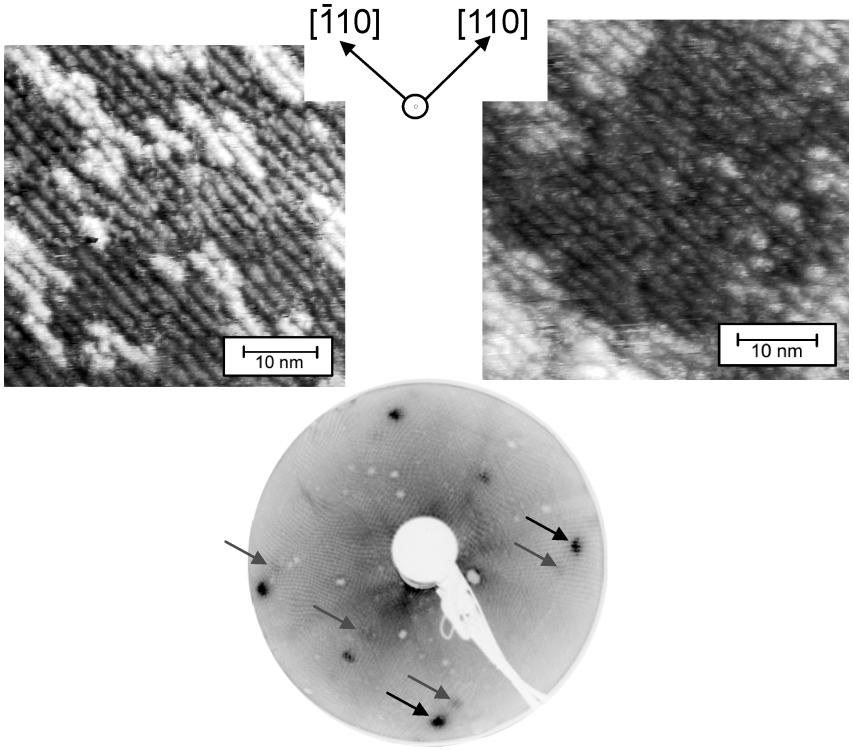


**Figure 7.8:** Filled-state STM images of a partly covered (left) and cyclopentene saturated (right) GaAs(001)$(2\times4)$ surfaces. For the $(2\times4)$(measured at U=-2.8 V) an alignment along the dimer rows of the surface reconstruction is visible. Beside the STM images the LEED pattern of the saturated surface is depicted in the middle taken at 42 eV. A $(1\times4)$ periodicity remains in the pattern.

For the cyclopentene saturated $(4\times2)$ reconstructed surface the STS spectrum (not shown) indicate no change in the band gap compared to the spectrum of the clean surface. The band gap is determined with $\sim$1.3 eV for both surfaces as it was the case for the c$(4\times4)$ and $(2\times4)$.

## 7.4. Discussion: Adsorption Structure of Cyclopentene on the GaAs$(001)$ Surfaces

After saturation of the three GaAs(001) surface reconstructions, each RAS spectrum for the several surface reconstructions exhibits no surface related contributions anymore. These surface related features were quenched during the adsorption of the cyclopentene molecules as it was shown in Fig. 7.1. Only bulk related structures are still visible in the spectra.

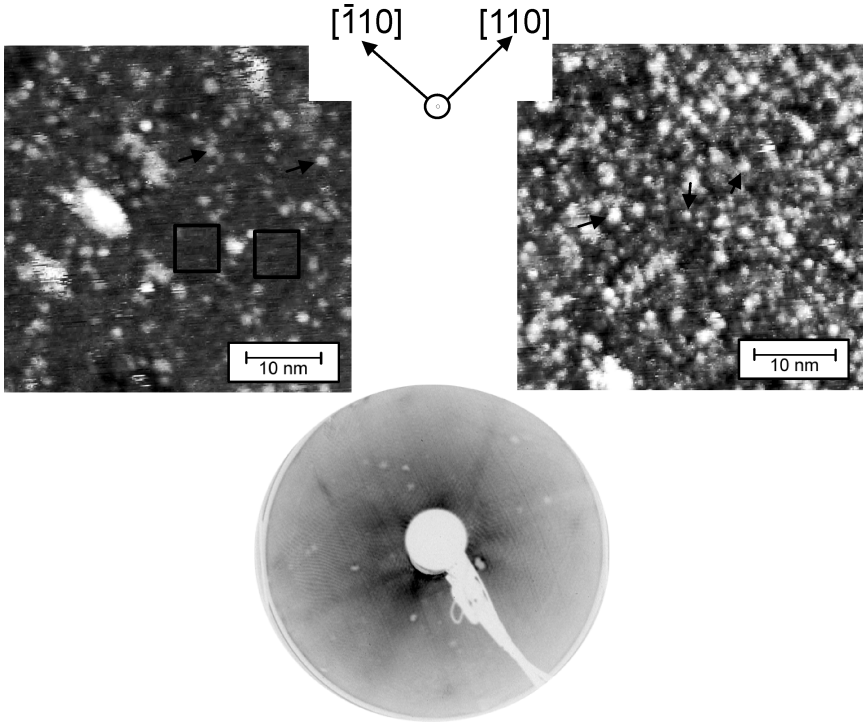


**Figure 7.9:** Filled-state STM images of a partly covered (left) (measured at U=-3.3 V) and cyclopentene saturated (right) (measured at U=-2.8 V) GaAs$(001)(4 \times 2)$ surfaces. No kind of ordering is found after the deposition of cyclopentene. Beside the STM images the LEED pattern of the saturated surface is pedicted in the middle taken at 42 eV.

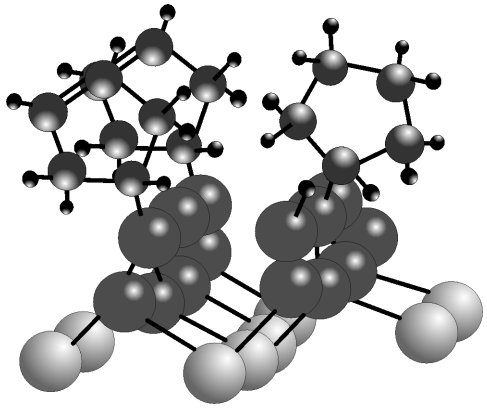

**Figure 7.10:** Favored bonding configuration for the adsorption of cyclopentene on the c$(4 \times 4)$ reconstructed surface. Three molecules per surface unit cell are possible due to the sterical interaction.

In the case of the c$(4 \times 4)$ reconstructed surface the $S_2$ feature is strongly reduced. This feature was assigned to the As dimers of the topmost layers and this strong change is an indication for an interaction with cyclopentene and the As dimer atoms [152]. In the valence band spectra a surface band bending was found which could be caused by a splitting of the

As dimer bond after the saturation of the surface. This is also the reason for the decrease of the $As_{dimer}$ related component in the As3d emission line while a new component $(As-C)$ emerges which is a direct proof for a chemical bond formation of the cyclopentene molecules to the surface. This component is shifted towards higher binding energies which indicate a relative charge depletion for example caused by a bonding to a more electronegative bonding partner like carbon.
The most likely adsorption sites of cyclopentene on the c$(4\times4)$ are presented in Fig. 7.10 with respect to the different intensities of the C1s components in detail of the $C-C$ compared to the $C-As$ and the $C=C$ components. Three molecules bond to a c$(4\times4)$ surface unit cell most likely by the dissociation of a hydrogen atom which is not bonded to a carbon atom involved in a double bond.

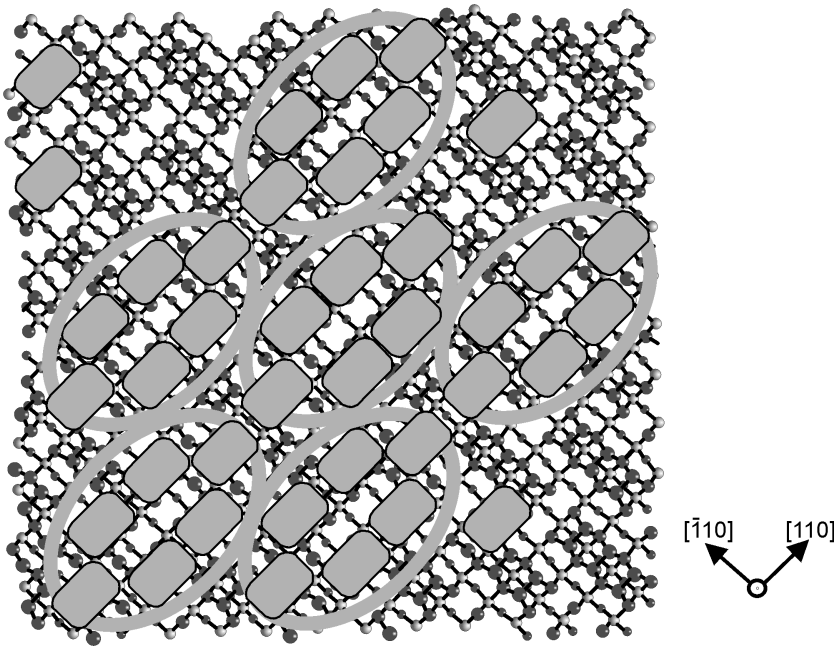


**Figure 7.11:** The resulting topview on the c$(4\times4)$ reconstructed surface saturated with cyclopentene. The ovals represent the ovals measured in the STM images and the gray rectangulars represent the single cyclopentene molecules.

More than three cyclopentene molecules per surface unit cell are very unlikely due to the sterical interaction of the cyclopentene molecules. Less than three cyclopentene molecules per surface unit cell is, of course, possible. In fact if cyclopentene bonds to one of the outer As dimers of the surface unit cell an adsorption of a second cyclopentene molecule at the other outer As dimer and at last an adsorption of cyclopentene at the third dimer is very likely. If cyclopentene bonds to a surface unit cell where not yet any other cyclopentene molecules are present it would most likely bond to the center As dimer because this dimer bond length is the smallest. The carbon atom which is involved in this bond formation could

be one of the carbon atoms which are participating in the double bond because the binding energy of the $\pi$ bond is lower than for a $\sigma$ bond. During this adsorption the dimer bond splits and hydrogen can adsorb on the other As dimer atom. In a second adsorption step additional cyclopentene molecules could bond to the As outer dimer atoms again by the splitting of the double bond or by the dissociation of a hydrogen atom. The latter one seem to be the most likely one due to the intensity comparison of the $C=C$ which has nearly half the hight of the $C-C$ components in the C1s core level. This results in the structure which is shown in Fig. 7.10.
This arrangement of the cyclopentene molecules results most likely in an oval consisting of six cyclopentene molecules. The corresponding topview for the c$(4\times4)$ is shown in Fig. 7.11 which reproduce the measured STM pictures very well. The oval like structures show the local ordering. The molecules (gray boxes) in these ovals can have small angles against each other and to the surface which are not considered in Fig. 7.11.

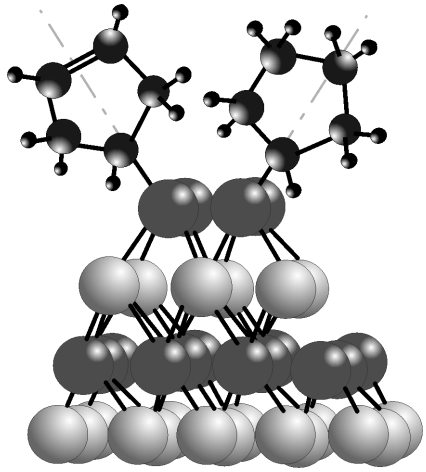

**Figure 7.12:** The favored bonding configuration for the adsorption of cyclopentene on the $(2\times4)$ reconstructed surface. The cyclopentene molecules can rotate around the light gray indicated axis to minimize the sterical interaction.

For the adsorption of cyclopentene on the GaAs$(001)(2\times4)$ reconstructed surface no change of surface related contributions in the RAS spectrum can be discussed because such contributions are not apparent. Thus the adsorption structure discussion has to focus on the SXPS and STM measurements.
In the SXPS measurements a new component related to a bond formation of carbon atoms to As atoms of the topmost layers was found in the As3d and the corresponding one in the C1s core level. Due to the fact that the $As_{dimer}$ component is less reduced than on the c$(4\times4)$ and that no surface band bending was observed it can be concluded that the dimer bond remains intact during the adsorption of cyclopentene.
The contributions in the C1s (Fig. 7.4) core level and their relative intensity are similar, to the ones of the C1s core level after the adsorption of cyclopentene on the c$(4\times4)$ beside the fact that the $C-As$ component is slightly smaller than the $C=C$ component. It has to

be pointed out that cyclopentene can not be adsorbed in the same way at the whole surface because of differences in the relative intensities of $C-C$, $C-As$ and $C=C$. Thus a preferred adsorption structure of cyclopentene on the $(2\times4)$ is shown in Fig. 7.12.

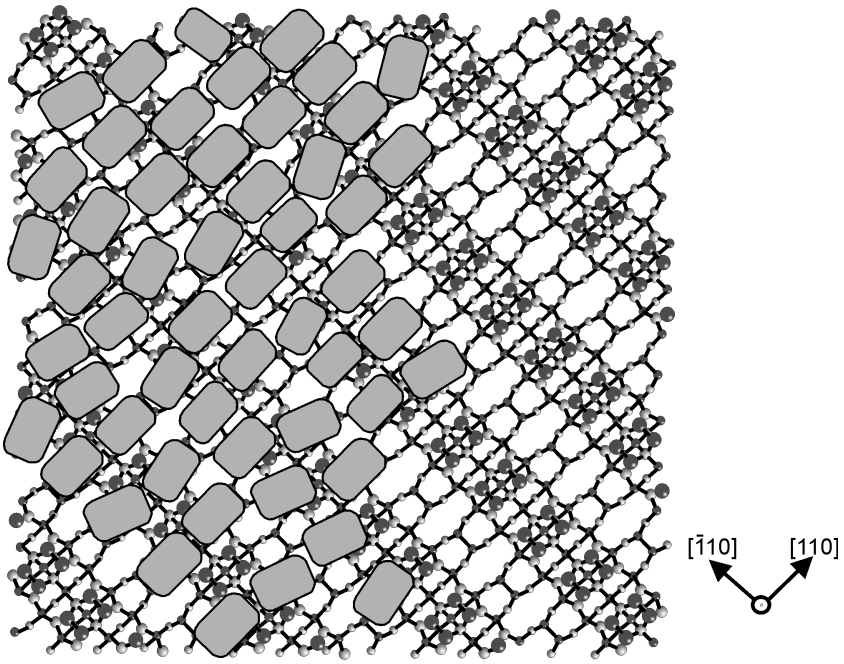


**Figure 7.13:** The resulting topview on the $(2\times4)$ reconstructed surface saturated with cyclopentene. The gray rectangulars represent the single cyclopentene molecules.

The STM images in Fig. 7.8 show a very regular structure similar to the one of the clean reconstructed surface but with lower resolution. No indication for a splitting of the As dimer is found. Due to the formation of only one bond the cyclopentene molecules have a degree of freedom. Thus they can arrange in that way that the sterical interaction between two cyclopentene molecules is minimized. A topview for the cyclopentene saturated $(2\times4)$ reconstructed surface is presented in Fig. 7.13. The gray rectangles represent the single cyclopentene molecules and they are not equally oriented to the rows along the $[\bar{1}10]$ direction of the surface.
Thereby a single electron remain at each As dimer atom which would lead to a double bond formation of these atoms. A charge transfer of the electron from the As atoms to the second layer Ga atoms could also occur which would result in an additional adsorption site for the cyclopentene molecules but no evidence for a new contribution in the Ga3d core level was found during measurements. However a new component which could be assigned to the double bond formation between the topmost As atoms was not found in the As3d core level, too.
An adsorption in a dimerized configuration of cyclopentene at the As dimer atoms is unlikely because of the relative intensities of the $C-As$ and the $C-C$ component. In the case of a dimerized adsorption this $C-As$ component would have to be more pronounced with respect

to the $C-C$ component. In addition this adsorption geometry would be symmetry forbidden by the Woodward-Hoffman selection rules.

In the case of the $(4\times2)$ reconstructed surface a quenching of the surface related contribution $S_1$ in the RAS spectrum is found after saturation with cyclopentene. This is a clear indication of an interaction of cyclopentene and the topmost atoms of the surface. This is confirmed by the analysis of the As3d and Ga3d core level because both core level emission lines exhibit a new component which is assigned to a covalent bond formation to an element with a higher electronegativity such as carbon. The bond formation to Ga atoms is reasonable due to the fact that the $(4\times2)$ reconstruction is a Ga-rich surface.
In the C1s core level emission line (see Fig. 7.4 right side) the relative intensities of the components can be compared. It is found that nearly the same amount of As bonds to the surface occur as single bonds between the carbon atoms of cyclopentene remain. The $Ga-C$ component as well as the $C=C$ are small. Besides this the $As_{sp2}$ and the $Ga_{dimer}$ components are reduced in intensities which is an indication for the adsorption of cyclopentene at these atoms. Thus the resulting adsorption sites of cyclopentene are depicted in Fig. 7.14.

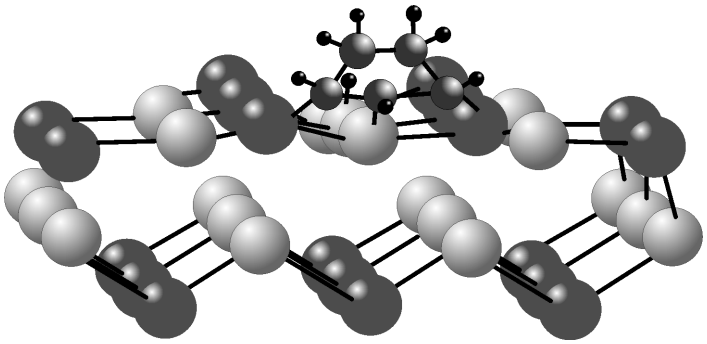

**Figure 7.14:** The resulting favored bonding configuration for the adsorption of cyclopentene on the $(4\times2)$ reconstructed surface.

An additional adsorption of hydrogen is reasonable because the dimer bond of the Ga dimer atom splits and an electron remains unbounded. This is energetically unfavorable so the dissociated hydrogen atom of the cyclopentene molecule can bond to this second Ga dimer atom. Considering that the STM image did not show any kind of ordering it has to be mentioned that this is one example for the possible adsorption sites of cyclopentene on the $(4\times2)$ reconstructed surface. As can be seen in Fig. 7.15 different possibilities exists for the adsorption of cyclopentene indicated by the different orientations of the gray rectangles in the picture which represent the cyclopentene molecules. The circles represent the brighter spots in the STM images and indicate cluster-like formations of cyclopentene on this surface reconstruction.

It has to be pointed out that the influence of the $(n\times6)$ to the intensities of the C1s core levels are neglected based on the fact that most parts of the surface are $(4\times2)$ reconstructed. Beside this it is also not known yet if these parts are $(1\times6)$ or $(2\times6)$ reconstructed and thus the suggestion of a structure model is difficult and was not the focus of this work.

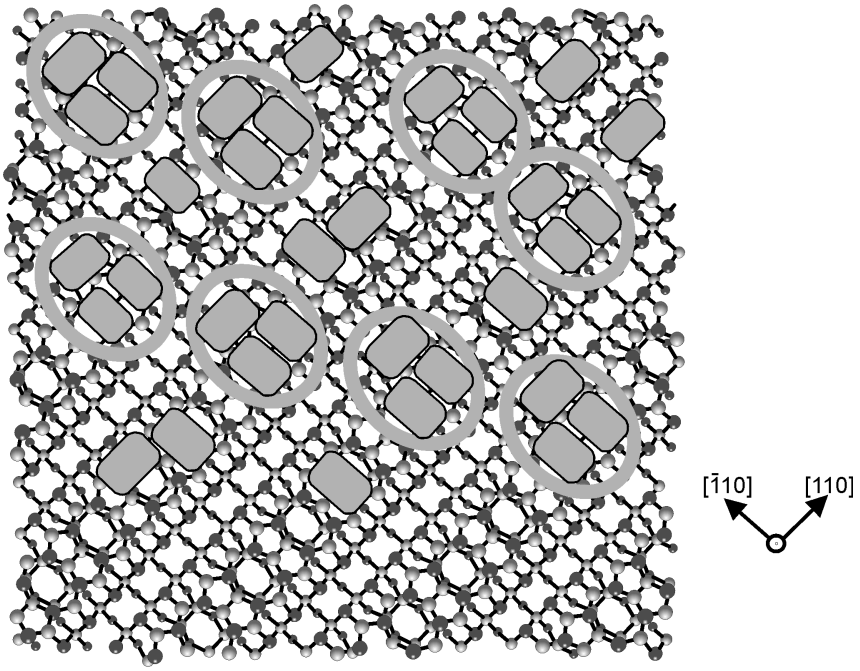


**Figure 7.15:** The topview of the $(4 \times 2)$ surface reconstructions with additional cyclopentene molecules adsorption (gray boxes) considering the adsorption sites found so far. Oval structures represent the ovals which were resolved with the STM images.

However, it is interesting that no long range order of the cyclopentene molecules seem to exist for the c$(4 \times 4)$ and the $(4 \times 2)$ but for the $(2 \times 4)$ and the parts of the GaAs(001) surface which are $(n \times 6)$ reconstructed. For these two surfaces a long range order along the $[\bar{1}10]$ is found, as can be seen in Fig. 7.16.

Since the $(n \times 6)$ surface reconstruction is more As-rich than the $(4 \times 2)$ it can be concluded that the cyclopentene molecules bond with a higher probability to the As atoms of the surface [139]. This is underlined by the higher increase of the $As_2$ component in the As3d core level emission line which was related to the $(n \times 6)$ reconstruction.

Finally the effective layer thickness of the cyclopentene saturated surface can be determined from the filled-state STM measurements. Therefore in Fig 7.17 the three saturated surfaces with cyclopentene are depicted and show in each case still features of the surface reconstruction like atomic steps which are marked with black arrows. If thick layers of cyclopentene would adsorb on the surface such steps would not be visible. Additional physisorption would lead to layers with a higher thickness but such surfaces have not been investigated here. Therefore it can be concluded that the effective layer thicknesses of cyclopentene on the three 'main' GaAs(001) surfaces are always in a magnitude of not more than a few monolayers.

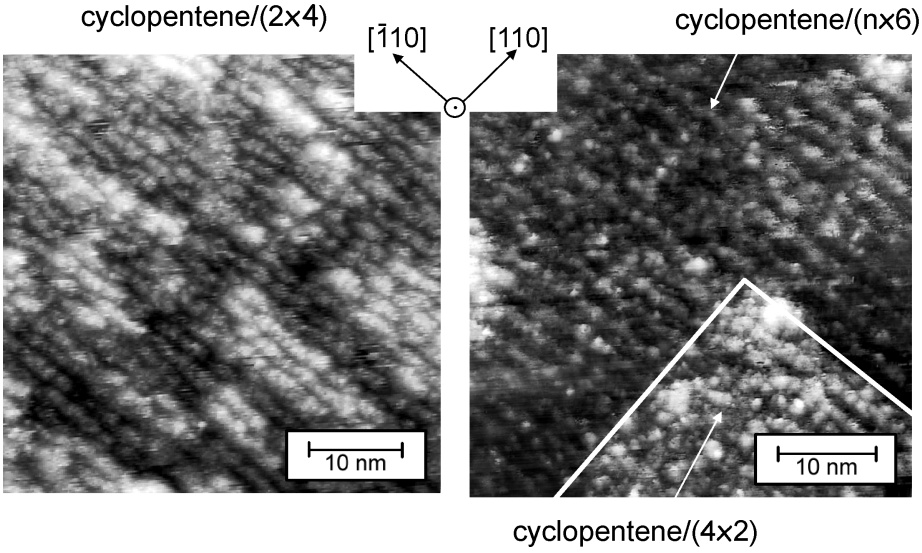


**Figure 7.16:** STM images of the cyclopentene saturated $(2 \times 4)$, $(n \times 6)$ and $(4 \times 2)$ reconstructed surfaces measured at U=-2.8 V. The $(4 \times 2)$ reconstructed part of the surface surface is indicated by white lines.

## 7.5. Summary for the Cyclopentene Adsorption on the GaAs(001) Surfaces

The effective layer thicknesses of cyclopentene on the three surface reconstructions is determined to a few monolayers from the STM images and additionally from the decrease of the intensity of the core level emission lines after the adsorption of the cyclopentene (after 4.8). More cyclopentene molecules deposited onto the surface could lead to an ongoing physisorption process for all three reconstructed surfaces.

It has to be pointed out that no $[2+2]$ cycloaddition reaction can occur for none of the GaAs(001) surface reconstructions because of the absence of asymmetry between the dimer atoms of each surface reconstruction.

In detail three main rules for the adsorption of cyclopentene on the c$(4 \times 4)$ reconstructed surface can be summarized as follows:

- Only one atom of the As dimer forms a bond to a cyclopentene molecule. The dangling bond which results after this reaction is saturated with a hydrogen atom or remains unbonded
- If the molecule can chose the bonding site at the As dimer triplet of the c$(4 \times 4)$ unit cell without limitation one As atom of the center dimer is chosen
- The molecules have small diffusion lengths and thus they bond nearly immediately where they have the first contact with the surface

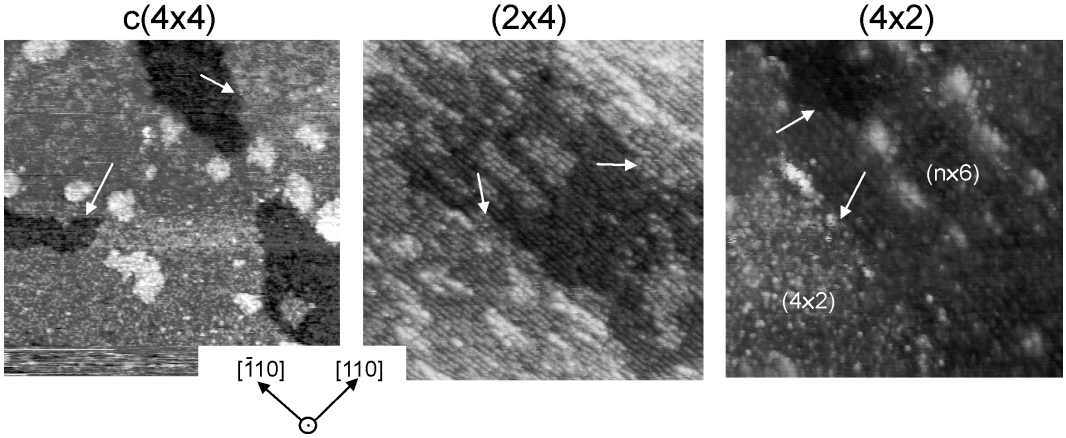


**Figure 7.17:** STM images of $100 \times 100\ nm^2$ of the cyclopentene saturated surfaces, the c$(4 \times 4)$, the $(2 \times 4)$ and the $(4 \times 2)$, respectively. Still visible are the underlying surface reconstructions thus it can be concluded that the effective layer thickness is not more than a few monolayers.

For the $(2 \times 4)$ it can be concluded:

- Only one atom of the As dimer forms a bond to a cyclopentene molecule. The dangling bond which results after this reaction is saturated with a hydrogen atom or remains unbonded
- One molecule can adsorb at one As dimer atom of the surface unit cell. Because of their dimensions the molecules arrange along the $[110]$-direction

For the $(4 \times 2)$ such a summary is not possible because compared to the adsorption structure of cyclopentene on the Si$(001)(2 \times 1)$ surface reconstruction (see chapter 2.5) a higher disorder was found. The surface unit cells are larger in the case of the GaAs$(001)$ surfaces and thus the adsorption of cyclopentene results in more complex adsorption structures. This is the reason for the higher degree of disorder found for the cyclopentene saturated GaAs$(001)$ surfaces. For the GaAs$(001)$ $(2 \times 4)$ reconstructed surface and the parts which have been $(n \times 6)$ reconstructed a long range ordering along the $[\bar{1}10]$ was found which is comparable to results found for the Si $(2 \times 1)$ surface. For the cyclopentene saturated c$(4 \times 4)$ reconstructed surface parts are found which show a kind of local ordering.
As a conclusion of the identification of the adsorption sites found for cyclopentene on the GaAs$(001)$ surfaces it was shown that preferred adsorption sites exsist. For the c$(4 \times 4)$ and the $(2 \times 4)$ surface reconstruction most likely an adsorption of cyclopentene with a single bond formation was found while for the adsorption on the $(4 \times 2)$ the formation of three bonds is possible. The As atoms of the top layer introduce a higher degree of order for the adsorption of the cyclopentene molecules, as it was found for the $(2 \times 4)$ and the $(n \times 6)$. Due to the absence of ordering several adsorption sites on the $(4 \times 2)$ surface are found.
It has to be pointed out that the adsorption structure of cyclopentene on the GaAs$(4 \times 2)$ is the one with the highest unclarity compared to the other two GaAs surface reconstruction investigated here.

In the next step it was investigated whether the resulting adsorption structures of organic molecules on the GaAs(001) surfaces depends on the amount of intra-molecular double bonds. Therefore the adsorption sites of 1,4-cyclohexadiene and benzene have been characterized in the following chapters.

# Chapter 8: Interaction of 1,4-Cyclohexadiene with the GaAs$(001)$ Surfaces

In the last chapter it was shown that cyclopentene adsorbs most likely on the GaAs$(001)$ surface reconstructions without an interaction of the double bond. This is in contrast to the bonding configuration of cyclopentene on the InP$(001)(2\times4)$ reconstructed surface.
In this chapter the bonding sites of 1,4-cyclohexadiene on the three 'main' GaAs$(001)$ surfaces are investigated. 1,4-cyclohexadiene has two double bonds and if the double bond exhibits an influence to the adsorption process the resulting preferred adsorption structures should be different as the ones of cyclopentene on these surface reconstructions.

## 8.1. Optical Anisotropy of the Interface

In comparison to the clean surface RAS spectra the spectra after the saturation with 1,4-cyclohexadiene are shown in Fig. 8.1.

The amplitudes in the RAS signal of the clean reconstructed c$(4\times4)$ surfaces are 1.3 times larger compared to the ones used for the adsorption of cyclopentene on the c$(4\times4)$ surface, see chapter 7. The reason for this could be a different doping level of $n = 1\cdot10^{18}\ cm^{-3}$ used for the saturation with 1,4-cyclohexadiene and $n = 5\cdot10^{17}\ cm^{-3}$ used for the saturation with cyclopentene. Nevertheless, it is obvious that $S_1$ and $S_2$ are quenched due to the adsorption of the 1,4-cyclohexadiene molecules (Fig. 8.1 left). Thus the dimer configuration on the c$(4\times4)$ reconstructed surface is changed during the adsorption because both surface related contributions are assigned to the As dimer.
The resulting amplitudes in the RAS signal results also after the adsorption of 1,4-cyclohexadiene compared to the ones after the saturation with cyclopentene are different. This could be either a result of a different doping level of the GaAs substrates or the difference between the adsorption of a $C6$ or a $C5$ ring molecule. The doping level could have an influence to the adsorption process but this influence is neglected in the present work. Hence, this strong change for the $S_2$ contribution is an effect of the adsorption of a $C6$ ring shaped molecule. This would lead in a higher strain induced by the splitting of the As dimer bond as it was the case after the adsorption of cyclopentene ($C5$ ring shaped molecule).

For the $(2\times4)$ (Fig. 8.1 middle) no definite surface related contributions are found but as mentioned in chapter 7.1 the shoulder around 2.5 eV could be caused by transitions located

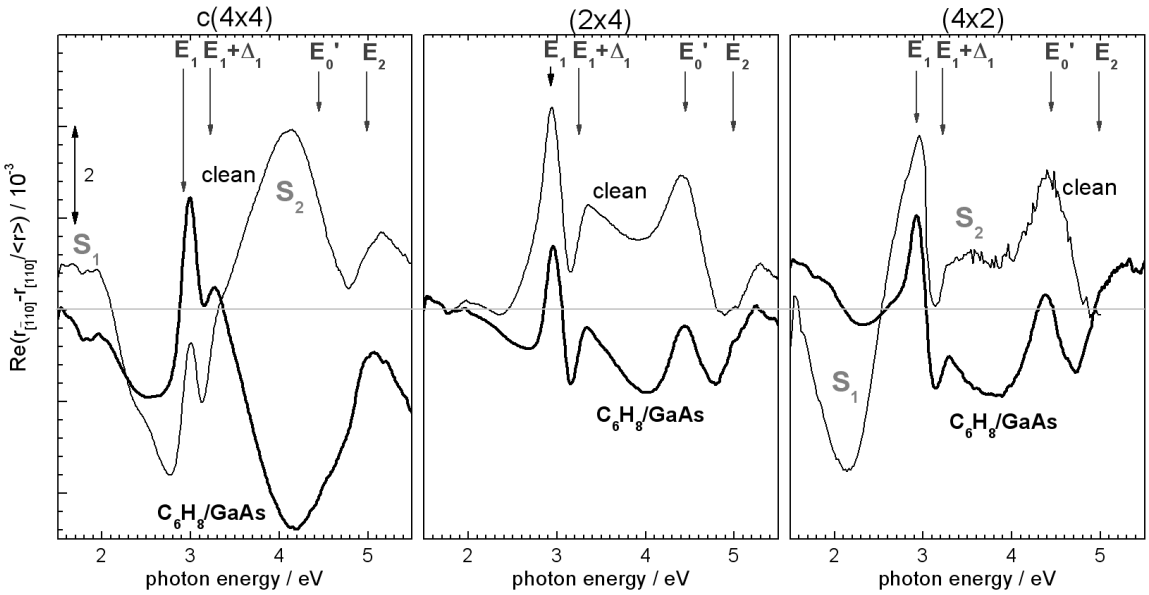


**Figure 8.1:** RAS spectra of the three 'main' GaAs(001) surfaces reconstructions (thin lines, $n = 1 \cdot 10^{18}\ cm^{-3}$) compared to the ones taken after the saturation with 1,4-cyclohexadiene (thick lines) on the c$(4 \times 4)$, the $(2 \times 4)$ and the $(4 \times 2)$, respectively.

at the topmost atoms of the surface. This would explain the fact that this shoulder shifts towards higher photon energies.

The RAS signal of the $(4 \times 2)$ surface (Fig. 8.1 right) exhibits a strong change of the surface related contribution $S_1$ compared to the RAS signal of the clean reconstructed surface. As this feature is not clearly assigned to surface transition of certain atoms no clear assignment of the adsorption site of 1,4-cyclohexadiene on the $(4 \times 2)$ can be done just by the analysis of the change in the RAS signature. It can be pointed out that the changes within the RAS line shape upon deposition of 1,4-cyclohexadiene on the GaAs(001) surfaces are similar to the changes upon cyclopentene deposition and indicate a covalent bond formation.

## 8.2. Surface Periodicity

In contrary to the adsorption of cyclopentene for the 1,4-cyclohexadiene saturated c$(4\times4)$ reconstructed surface a LEED pattern was obtained which is shown in Fig. 8.2 taken at 42 eV. This LEED pattern indicate a c$(2\times2)$-like symmetry on the surface after the saturation.

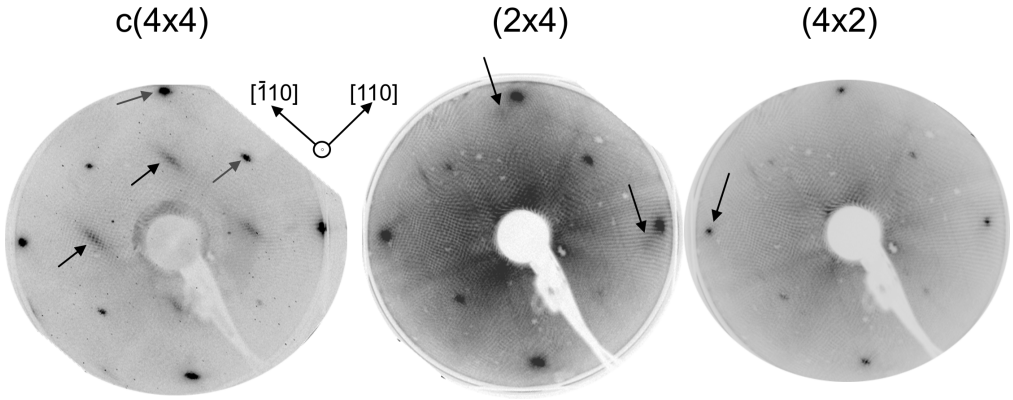


**Figure 8.2:** The LEED pattern obtained at the 1,4-cyclohexadiene saturated GaAs$(001)$c$(4\times4)$ (left), $(2\times4)$ (middle) and $(4\times2)$ (right). The c$(4\times4)$ LEED pattern after saturation with 1,4-cyclohexadiene results in a c$(2\times2)$-like symmetry, while the one of the $(2\times4)$ results in a $(1\times4)$ and for the $(4\times2)$ only $(1\times1)$ bulk spots remain.

For the $(2\times4)$ reconstructed surface the LEED spots along the $[110]$ direction of the crystal remain in the pattern which results in a $(1\times4)$ reconstructed surface. The LEED pattern of the $(4\times2)$ exhibits only bulk spots of the crystal without any indication for a different surface symmetry after saturation. For clarification of the bonding sites further SXPS measurements were performed as presented in the next section.

## 8.3. Core Level Spectroscopy at the Interface

After the saturation with 1,4-cyclohexadiene a new component is found in the As3d core level emission line for each surface reconstruction denoted with $As-C$ as it was the case for the cyclopentene saturated surfaces. For all three surface reconstructions this component is shifted towards higher binding energies with respect to the bulk component. Therefrom it can be concluded that a relative charge depletion occurs for the As atoms of the surface due to a bond formation to an atom with a higher electronegativity such as carbon.

Beside this the As3d core level emission line of the 1,4-cyclohexadiene saturated c$(4\times4)$ reconstructed surface is sharper compared to the As3d core level emission line taken after the adsorption of cyclopentene on the c$(4\times4)$ reconstructed surface shown in Fig. 7.2. This could be an result of an ordered arrangement of the 1,4-cyclohexadiene molecules on this surface reconstruction. In the As3d core level emission line of the c$(4\times4)$ the $As_{dimer}$

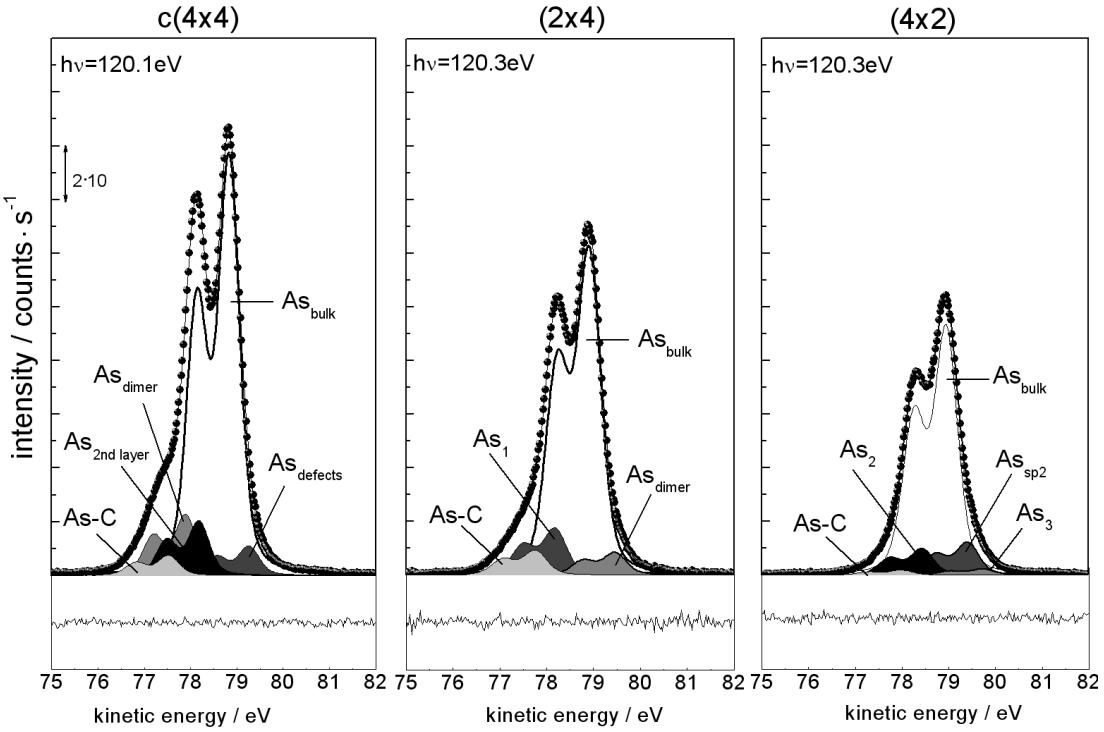


**Figure 8.3:** As3d core level emission lines taken after the saturation with 1,4-cyclohexadiene at an excitation energy of ∼120 eV for the c$(4\times4)$, the $(2\times4)$ and the $(4\times2)$, respectively. A new component $As-C$ is evident for all of the three surface reconstructions.

component is reduced to 60% of the initial value while the $As_{2ndlayer}$ component is reduced slightly to 70%. The shifts for the surface components of the As3d core level is increased by a factor of 1.35 except for the $As_{defect}$ contribution. The new $As-C$ component is shifted by +1.35 eV$\pm$0.05 eV to higher binding energies.

For the $(2\times4)$ the reduction of the $As_{dimer}$ component is strong which indicates an interaction of 1,4-cyclohexadiene with the As dimer atoms. The new $As-C$ component is shifted by +1.05eV$\pm$0.1eV towards higher binding energies but the shifts of the components ($As_1$ and $As_{dimer}$) which are present in the emission line before the deposition do not change within the resolution of the measurement.

In the core level emission line of the As3d core level of the $(4\times2)$ a forth component is revealed but this component is very weak and shifted by +1.0 eV$\pm$0.09 eV towards higher binding energies. After the deposition of 1,4-cyclohexadiene the $As_2$ contribution is more pronounced. This component is increased by a factor of 2 as it was also the case after the adsorption of cyclopentene (increase by a factor of 5) on the surface reconstruction, see chapter 7 while the $As_{sp2}$ component decreases. This behavior was found on this surface

reconstruction after the saturation with cyclopentene, too, which was discussed before. The increase of this component is assigned to a covalent bond formation of the topmost As atoms of the surface and the 1,4-cyclohexadiene molecules.

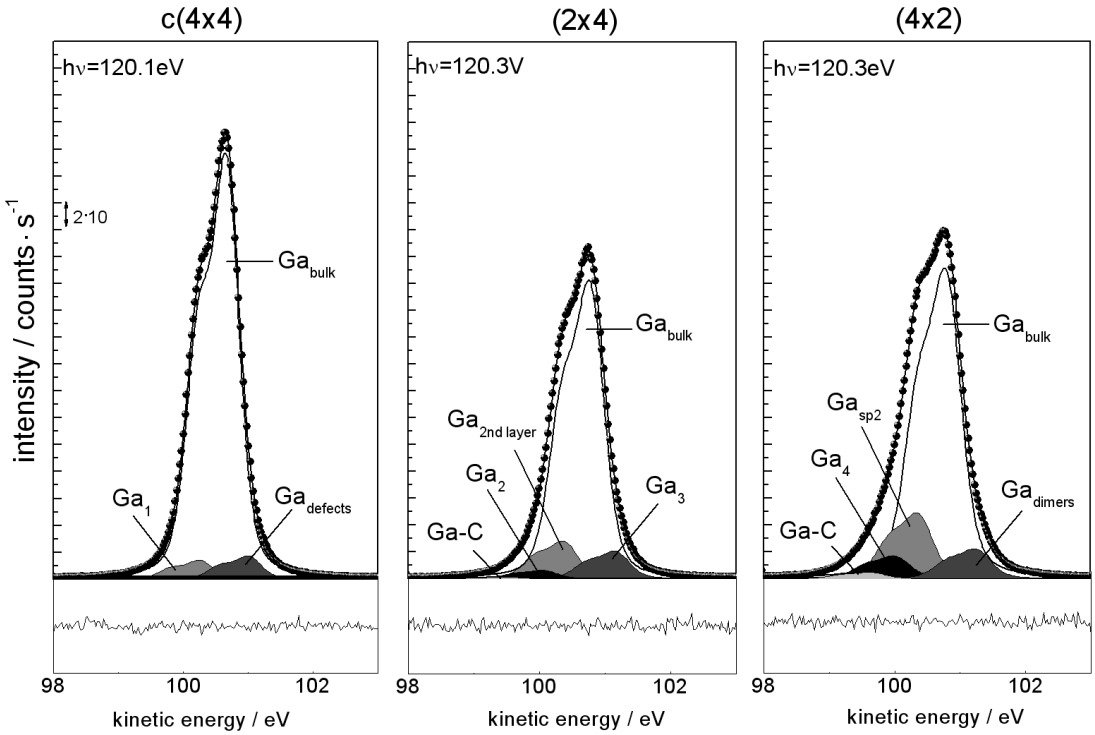


**Figure 8.4:** Ga3d core level emission lines taken after the saturation with 1,4-cyclohexadiene at an excitation energy of ∼120 eV for the c$(4\times4)$, the $(2\times4)$ and the $(4\times2)$, respectively. A new component $Ga-C$ is evident for the $(2\times4)$ and the $(4\times2)$.

In Fig. 8.4 the core level emission lines for the Ga3d core level taken at excitation energies of ∼120 eV are depicted. For the c$(4\times4)$ beside the fact that the $Ga_{defect}$ component is reduced by 60% no change for the surface related contributions within the resolution of the measurement is found. This is reasonable because the topmost layers of the surface consist only of As atoms.

The $(2\times4)$ reveals a new component $Ga-C$ shifted by +1.24 eV∼0.05 eV toward higher binding energies which is very weak. Comparative to this the new component in the $(4\times2)$ core level emission line is more pronounced and shifted by +1.08 eV∼0.08 eV. The shift of the $Ga_{dimer}$ component is slightly increased while the shifts of the other components do not change.

The C1s core level of each surface reconstruction have been taken at excitation energies around 345 eV, see Fig. 8.5, for the 1,4-cyclohexadiene saturated c$(4\times4)$, $(2\times4)$ and $(4\times2)$,

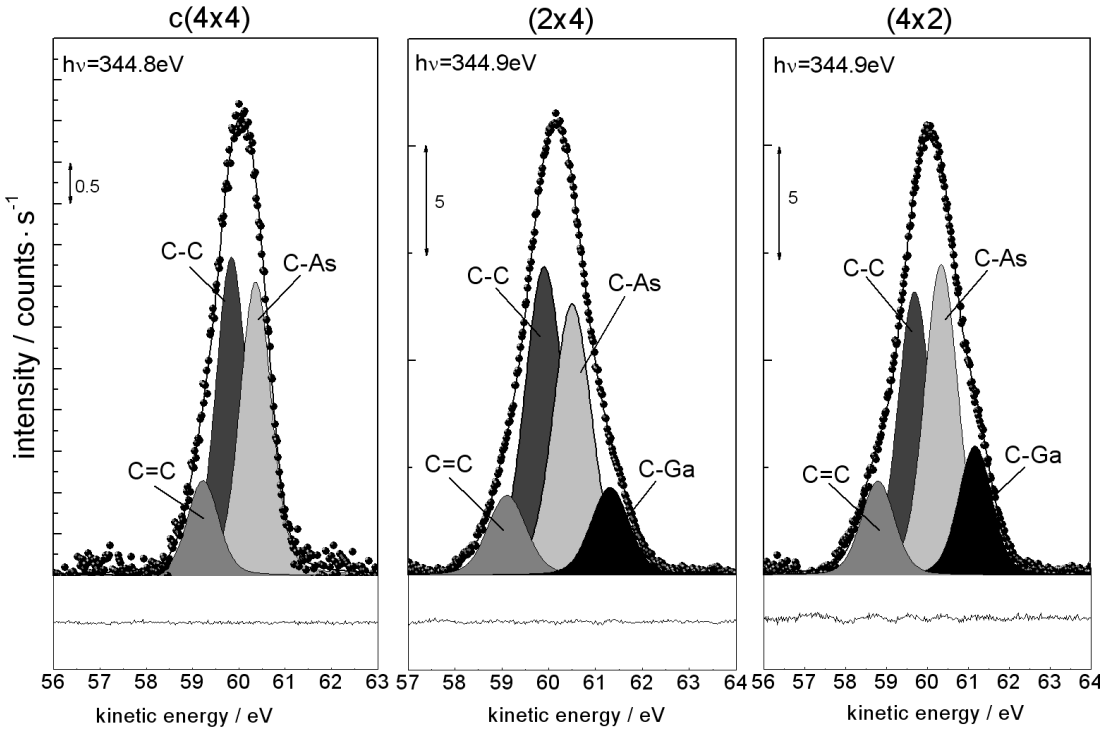


**Figure 8.5:** The C1s core level emission lines for the c$(4\times4)$ (left), $(2\times4)$ (middle) and the $(4\times2)$ (right) each taken after the saturation with 1,4-cyclohexadiene at an excitation energy of $\sim$345 eV.

respectively. Three components are revealed in the core level emission line of the c$(4\times4)$ reconstructed surface after saturation with 1,4-cyclohexadiene. The main component is assigned to electrons of C atoms which are involved in a $C-C$ bond. The shifts will be given with respect to this $C-C$ component because a bulk contribution is absent in the C1s core level. The assignment of these components is in agreement with results obtained after the adsorption of cyclopentene. The component which is shifted by +0.79 eV in binding energies can be assigned to electrons of C atoms which are involved in a $C=C$ double bond. Electrons which stem from C atoms which are involved in a $C-As$ bond contribute to the component which is shifted by -0.61 eV. This component is more pronounced after the saturation with 1,4-cyclohexadiene than it was the case for the cyclopentene saturated surface. The assignment is done considering that the electronegativities of atoms are different and the shifts are found to be equal to the ones for the adsorption of cyclopentene (see table 2.1).

The C1s core level taken at the 1,4-cyclohexadiene saturated $(2\times4)$ reconstructed surface exhibits a forth component beside the three which were resolved for the c$(4\times4)$ reconstructed surface, the $C-C$, the $C-As$ and the $C=C$. This additional component is shifted by -1.43 eV$\pm$0.05 eV toward lower binding energies and is related to electrons which stem

from C atoms involved in a $C-Ga$ bond formation. The corresponding $Ga-C$ component is very weak but present in the Ga3d core level (see Fig. 8.4). It has to be mentioned that also for this surface reconstruction the $C-As$ component is obviously more pronounced than it was the case after the adsorption of cyclopentene on this surface reconstruction.

For the $(4\times2)$ a forth component ($C-Ga$) is evaluated in the C1s core level spectrum, too, and the corresponding $Ga-C$ component was discussed before in the Ga3d core level emission line. Beside this, components assigned to electrons which stem from atoms involved in a $C-C$, a $C-As$ and a $C=C$ bond are present in the C1s spectrum.
For all three C1s core level a very pronounced $C-As$ component was found in the emission lines. This component indicates a high amount of bonds formed between the As atoms of the topmost layer of the surface and the C atoms of 1,4-cyclohexadiene. Remarkable is the fact that the component assigned to stem from C atoms involved in the $C=C$ bond are much smaller than for the adsorption of cyclopentene. This is a clear indication for an involvement of the double bond ($C=C$) in the bonding of the 1,4-cyclohexadiene molecules to the three GaAs(001) surface reconstructions, respectively.

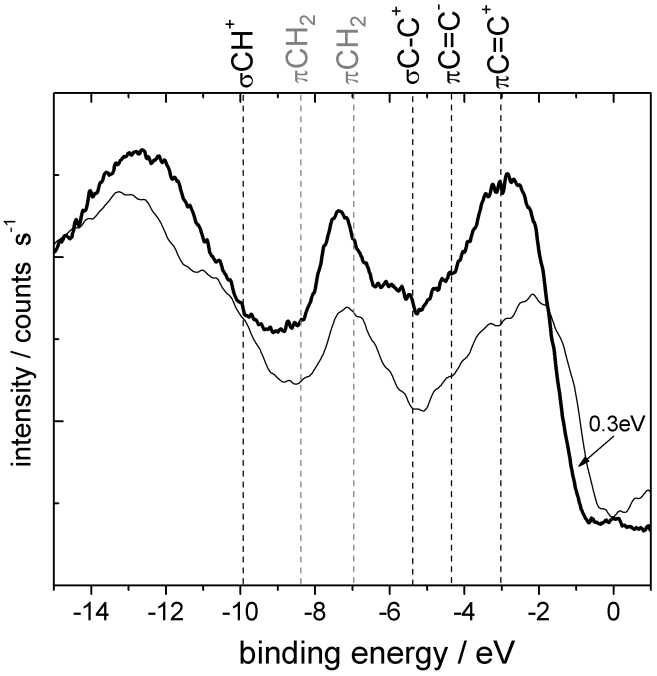


**Figure 8.6:** The valence band spectra of the clean reconstructed c$(4\times4)$ surface (thin line) depicted together with the corresponding 1,4-cyclohexadiene saturated surface (thick line). The different contributions of cyclohexene (gray) and 1,4-cyclohexadiene (black) are indicated in agreement with [28] in the figure. The valence band edge of the 1,4-cyclohexadiene saturated surface is shifted by 0.3 eV with respect to the valence band edge of the clean surface.

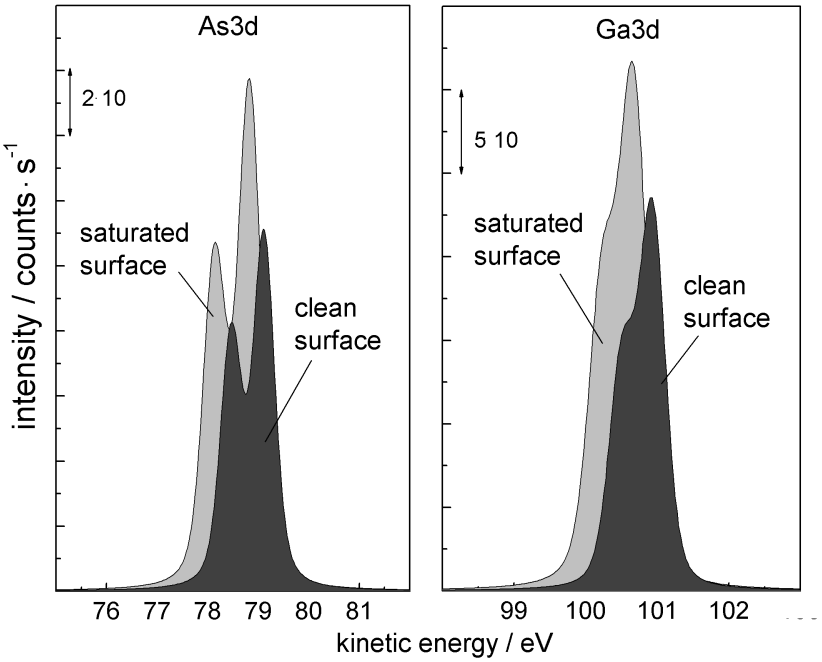


**Figure 8.7:** The bulk components of the Ga3d and As3d core level emission line for the c$(4 \times 4)$ reconstructed surface shown in comparison before (dark gray) and after the saturation with 1,4-cyclohexadiene (light gray). A shift of $\sim$350 meV is found for both bulk components. This is an indication for a surface band bending.

In Fig. 8.6 the valence band spectra of the clean reconstructed c$(4 \times 4)$ surface is depicted together with the valence band spectra taken after saturation with 1,4-cyclohexadiene. Again the valence band spectra were taken at high photon energies, in this case $\sim$95 eV. This is even higher than the excitation energy used for the measurements after the saturation with cyclopentene due to the different beamline properties. Nevertheless, possible positions of contributions of cyclohexene and 1,4-cyclohexadiene measured in gas phase [28] are indicated. The contributions of cyclohexene are indicated because if 1,4-cyclohexadiene bonds by an interaction of one double bond to the surface, another one remains intact. This molecule structure is similar to the one of cyclohexene.
For the clean reconstructed c$(4 \times 4)$ surface a band bending of $\sim$0.55 eV is found referred to the Fermi energy ($E_F$) [153]. After the saturation with 1,4-cyclohexadiene this shift is increased to $\sim$355 meV of the valence band edge with respect to $E_F$. Therefore a shift of

$\sim$300 meV between the valence band spectra taken before and after the deposition with 1,4-cyclohexadiene results. This is not the case for the valence band edges of the 1,4-cyclohexadiene saturated $(2\times4)$ and $(4\times2)$ surfaces (not shown here).
The shift of $\sim$350 meV is reproducibly found for the bulk components of the Ga3d and As3d core level which are depicted in Fig. 8.7. This is an indication for a surface bend bending due to the adsorption of 1,4-cyclohexadiene which was also the case after the saturation of the c$(4\times4)$ reconstructed surface with cyclopentene. A change of the charge density at the surface by the saturation with 1,4-cyclohexadiene could be a reason for this surface band bending. The compensation of this increased surface charges causes a shift in the surface states to higher binding energies in the space-charge-region. This has to be verified in further measurements but could be an indication of a splitting of the $As-As$ dimer bond.

## 8.4. Discussion: Adsorption Structures of 1,4-cyclohexadiene on the GaAs$(001)$ Surfaces

From the RAS measurements it can be derived that the surface related contributions are quenched and thus a proof for the interaction of the molecules and the topmost atoms is retrieved. Due to a different doping level of the samples used for the adsorption of 1,4-cyclohexadiene (doping level of $n=1\cdot10^{18}\ cm^{-3}$) the RAS amplitudes of the clean reconstructed c$(4\times4)$ surface are increased by a factor of 1.3 compared to the one used for the adsorption of cyclopentene (doping level of $n=5\cdot10^{17}\ cm^{-3}$). This difference in the doping level could have an effect to the adsorption process of the organic molecules. This influence of the doping level was not investigated in this work and thus the difference in the amplitudes will not be discussed in detail.
The results from the SXPS measurements will be interpreted with respect to the results obtained for the cyclopentene adsorption on the GaAs$(001)$ surfaces. Obvious for all three surface reconstructions is that 1,4-cyclohexadiene forms more bonds to the As atoms of the surface than cyclopentene because of the strong $C-As$ component in the C1s core level emission line. Furthermore, relative to the $C-C$ component the $C=C$ component does not increase, by the comparison of the adsorption of 1,4-cyclohexadiene and cyclopentene. Thus during the adsorption the double bonds of 1,4-cyclohexadiene seems to be involved in the bond formation to the surface.
For the c$(4\times4)$ it can be further concluded by the change in the RAS spectra that the molecules interact with the As dimer atoms because the two surface contributions vanish after the saturation and only bulk related contributions remain in the spectra, see Fig 8.1. This is also confirmed by the change in the As3d core level emission line because the $As_{dimer}$ component is clearly reduced. More confirmatory is the change in the surface band bending. Therefrom it can be concluded that the As dimer bond splits during the adsorption of 1,4-cyclohexadiene like it was the case during the adsorption of cyclopentene.
With the comparison to the adsorption structure and results obtained from the adsorption

of cyclopentene on the c$(4\times4)$ the following structure model for the adsorption of 1,4-cyclohexadiene is suggested:

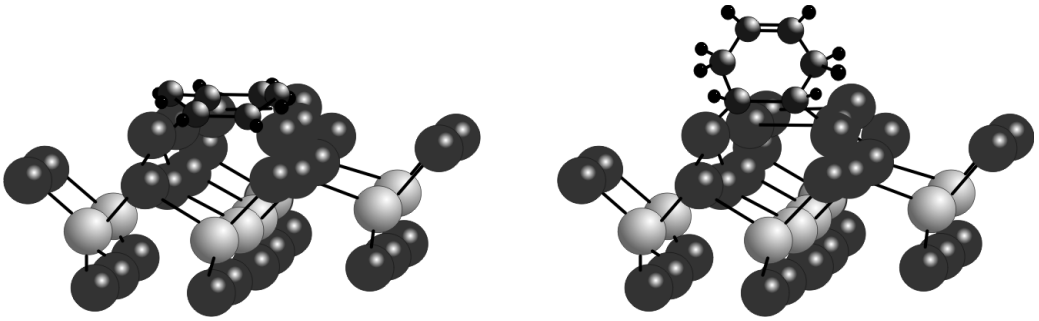

**Figure 8.8:** The possible adsorption sites which are suggested out of the experimental results for the adsorption of 1,4-cyclohexadiene on the c$(4\times4)$ reconstructed surface.

In the adsorption structure which is depicted in Fig. 8.8 the 1,4-cyclohexadiene molecules bond most likely in a bridge-like structure to the c$(4\times4)$ reconstructed surface. Additionally, because of the $C=C$ component and the intensity comparison of the three components in the C1s core level emission line, 1,4-cyclohexadiene molecules bonds in a di-$\sigma$ configuration, see Fig 2.9. Both components, the $C-C$ and the $C-As$ are very strong in the C1s core level of the 1,4-cyclohexadiene saturated surface. Thus the same amount of atoms which are involved in a $C-C$ and in a $C-As$ bond should occur which is the case for the suggested structure models in Fig. 8.8. The possibility of an additional physisorption can not be excluded. This was not clarified so far, just like the question if the adsorption configurations are in a cis- or a trans-type and if additional hydrogen interact with the surface.

The LEED pattern for the saturated surface shows a c$(2\times2)$-like symmetry after saturation which is depicted in Fig. 8.9 on the left. A topview of possible adsorption sites is presented beside the LEED pattern in Fig. 8.9 on the right. This topview shows that different adsorption sites exist for the 1,4-cyclohexadiene molecules on the c$(4\times4)$ reconstructed surface. The c$(2\times2)$-like symmetry which shows up in the LEED pattern can be explained by a possible overlap of different surface reconstructions which results after the saturation with 1,4-cyclohexadiene. An additional hydrogen adsorption can not be excluded.

In the case of the $(2\times4)$ reconstructed surface the C1s core level emission line is very similar to the one of the c$(4\times4)$ reconstructed surface beside the fact that an additional forth component appears which is due to an additional bonding of 1,4-cyclohexadiene to Ga atoms of the surface. In the suggested structure model this bonding is neglected, see Fig. 8.10.
In the LEED pattern in Fig. 8.11 on the left a $(1\times4)$ symmetry is found and the resulting topview for the adsorption of 1,4-cyclohexadiene on the $(2\times4)$ reconstructed surface is shown on the right. The image shows that the $(1\times4)$ symmetry is present after the adsorption.

In the RAS spectra of the $(4\times2)$ reconstructed surface the surface related transition $S_1$ is reduced and shifted toward higher photon energies as well as the surface related contribution

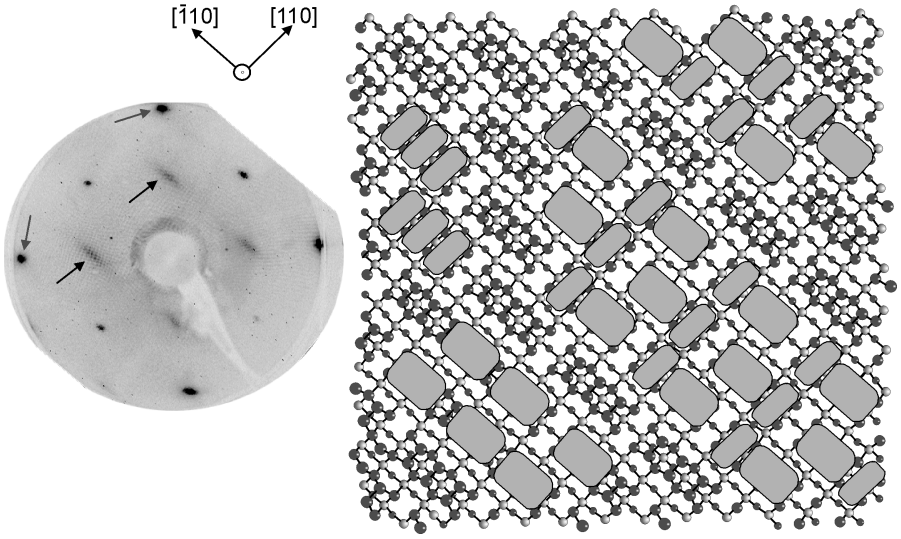


**Figure 8.9:** The LEED pattern of the 1,4-cyclohexadiene saturated c$(4 \times 4)$ surface on the left. Beside the bulk spots indicated with a black arrows the LEED pattern exhibits c$(2 \times 2)$-like pattern at the saturated state. Only stripes are indicating a c$(2 \times 2)$-like symmetry. A corresponding topview of possible adsorption sites on the c$(4 \times 4)$ is shown on the right. The gray boxes represent 1,4-cyclohexadiene molecules. Big boxes are flat lying and small ones are upright standing molecules.

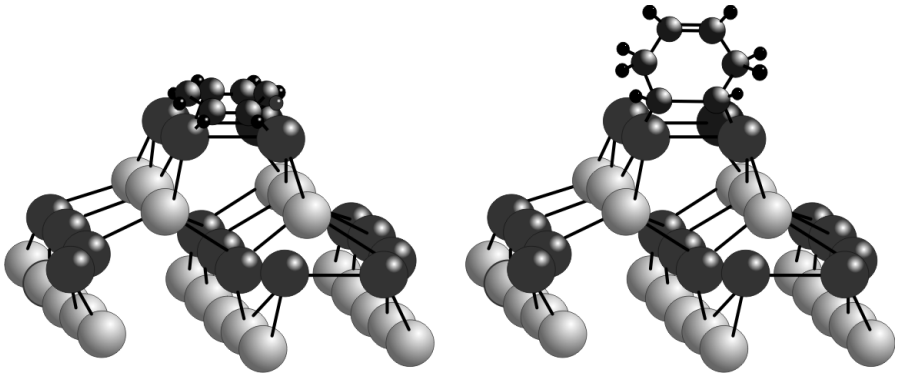

**Figure 8.10:** The possible adsorption structures which are suggested by the experimental results for the adsorption of 1,4-cyclohexadiene on the $(2 \times 4)$ reconstructed surface. Bond formations to the Ga atoms are not shown.

$S_2$ is reduced. Both changes are related to the adsorption of 1,4-cyclohexadiene molecules to the topmost atoms of the surface but a clear assignment can not be done because of the absent assignment of those contributions.
By the core level analysis a similar structure configuration as in the case of the adsorption of cyclopentene on the $(4 \times 2)$ reconstructed surface is suggested. As it is indicated in Fig. 8.12 an adsorption at the Ga dimer atoms and the neighboring As atoms with an additional ad-

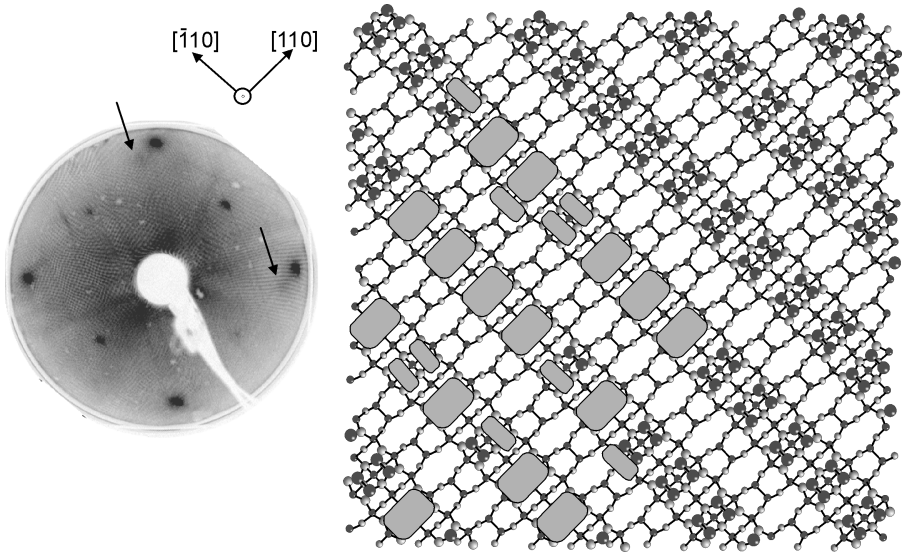


**Figure 8.11:** On the left: the LEED pattern of the 1,4-cyclohexadiene saturated $(2\times4)$ surface which show a weak $(1\times4)$ reconstruction. A resulting topview of possible adsorption sites on the $(2\times4)$ reconstructed surface is shown on the right. The gray boxes represent 1,4-cyclohexadiene molecule. Big boxes are flat lying and small ones are upright standing molecules.

sorption of hydrogen is possible. A resulting topview of such an adsorption configuration is depicted in Fig. 8.13.

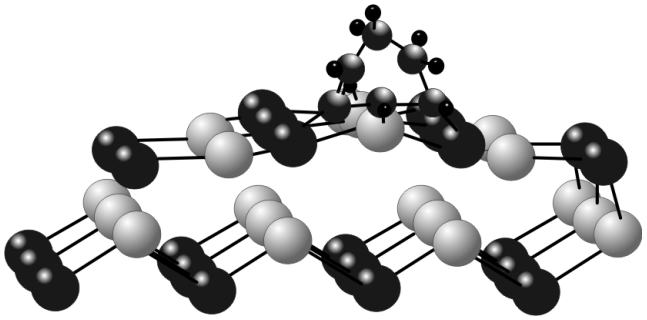

**Figure 8.12:** The scheme of the adsorption structure which is suggested by the experimental results for the adsorption of 1,4-cyclohexadiene on the $(4\times2)$ reconstructed surface.

The strong $As_2$ component in the As3d core level emission line is related to the parts of the surface which are $(n\times6)$ reconstructed. Therefrom a high amount of bondings of the 1,4-cyclohexadiene molecules to the As atoms of the surface parts which are $(n\times6)$ reconstructed is found as well as bondings to the As atoms of the $(4\times2)$ reconstructed parts.

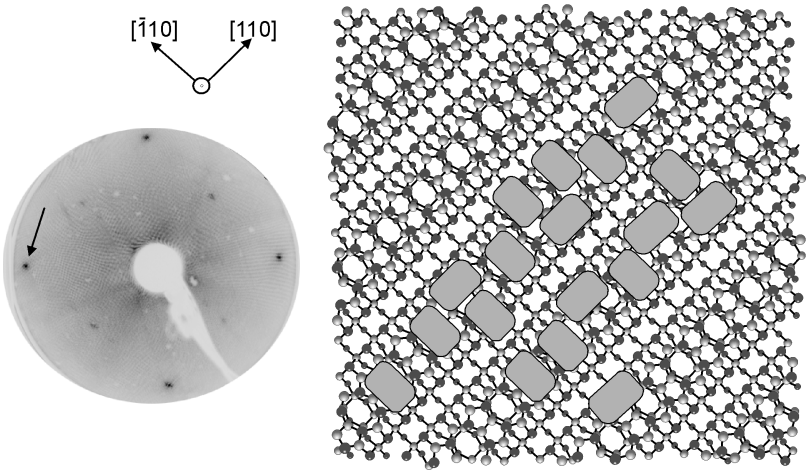


**Figure 8.13:** On the left: in the LEED pattern of the 1,4-cyclohexadiene saturated $(4 \times 2)$ surface only bulk spots remain. A resulting topview of possible adsorption sites on the $(4 \times 2)$ reconstructed surface is shown on the right. The gray boxes represent 1,4-cyclohexadiene molecules. The surface exhibits different adsorption sites.

## 8.5. Summary for 1,4-Cyclohexadiene Adsorption on the GaAs(001) Surfaces

In comparison to the adsorption structures of cyclopentene on the three 'main' GaAs(001) surface reconstructions and by the experimental results obtained at these modified surfaces, structure models were suggested for the adsorption of 1,4-cyclohexadiene.

It was found that more bonds of C atoms to As atoms of the topmost layers were formed compared to the adsorption of cyclopentene and it was concluded that for the c$(4 \times 4)$ and the $(2 \times 4)$ a bridge-like adsorption structure is the most likely one with additional upright standing 1,4-cyclohexadiene molecules. This is a clear indication that the number of $C = C$ double bonds plays a role during the adsorption process. Thus more bonds to the surface are formed.
The adsorption in a bridge-like structure is a different one compared to the adsorption structure which most likely appear on the Si$(001)(2 \times 1)$ reconstructed surface. On this surface a di-$\sigma$ bond formation was found. Additional for the $(2 \times 4)$ reconstructed surface a charge transfer from the As atoms to the Ga atoms of the topmost layer have to be taken into account and thus an adsorption of 1,4-cyclohexadiene would be possible at those Ga atoms, too. This could result in a single bond formation or a di-$\sigma$ structure. However, none of the adsorption structures can be interpreted as cycloaddition reaction.

The suggested adsorption structure configurations explain the available experimental results. For the $(4 \times 2)$ reconstructed surface the fact that the molecules additionally adsorb on the $(n \times 6)$ reconstructed parts of the surface complicate the analysis. The contributions resulting from the different adsorption structures overlap in the core level emission lines, but

it can be concluded that the adsorption on the As topmost atoms is preferred. This was also the case for the adsorption of cyclopentene. Therefore this result can be confirmed by the adsorption structures found for 1,4-cyclohexadiene.
Remarkable for the experimental results for the adsorption of 1,4-cyclohexadiene on the GaAs(001) surfaces is the periodic arrangement of 1,4-cyclohexadiene on the c$(4 \times 4)$ reconstructed surface which was not found for the adsorption of cyclopentene on this surface reconstruction.

# Chapter 9: Interaction of Benzene with the GaAs$(001)$ Surfaces

In the last two chapters it was shown that cyclopentene adsorbs most likely on the GaAs$(001)$ surface reconstructions without an interaction of the double bond while 1,4-cyclohexadiene bonds most likely with an interaction of the double bonds to the surface.
In this chapter the bonding sites of benzene on the three 'main' GaAs$(001)$ surfaces are investigated. Benzene contains of three double bonds and thus the influence of three double bonds can be clarified.
It has to be mentioned that these are results which have not yet been verified as often as the results for the adsorption of cyclopentene and 1,4-cyclohexadiene. So these findings are more preliminary.

## 9.1. Change in the Optical Anisotropy after the Adsorption of Benzene

The RAS spectra taken after the adsorption of benzene on the three GaAs$(001)$ surfaces are depicted in Fig. 9.1.

For the c$(4\times4)$ and the $(4\times2)$ the surface related features $S_1$ and $S_2$ exhibit a strong change. This is reasonable because if the benzene molecules bond to the topmost layers of the surface the surface transitions should be modified due to the interaction of the molecules with the surface. As discussed in chapter 8.1 the changes are more pronounced as it was the case for the adsorption of cyclopentene which could be either an effect of the doping level or the difference between the adsorption of a $C6$ or a $C5$ ring molecule.
The change in the RAS spectra of the c$(4\times4)$ is similar to the change observed after the adsorption of 1,4-cyclohexadiene. The reason could be an increase of the strain induced by the adsorption of a hydrocarbon ring shaped molecule which consists of six C atoms. Nevertheless, the quenching of the surface related contributions is obvious and can be related to the bonding of benzene molecules to As atoms of the surface.
In the case of the $(2\times4)$ the shoulder around 2.5 eV is reduced and shifts towards higher photon energies and the bulk related features are reduced in intensities.
In the spectrum after the adsorption of benzene on the $(4\times2)$ the contribution assigned to the surface $S_1$ is nearly totally quenched. This provides an interaction between benzene and the topmost surface atoms.

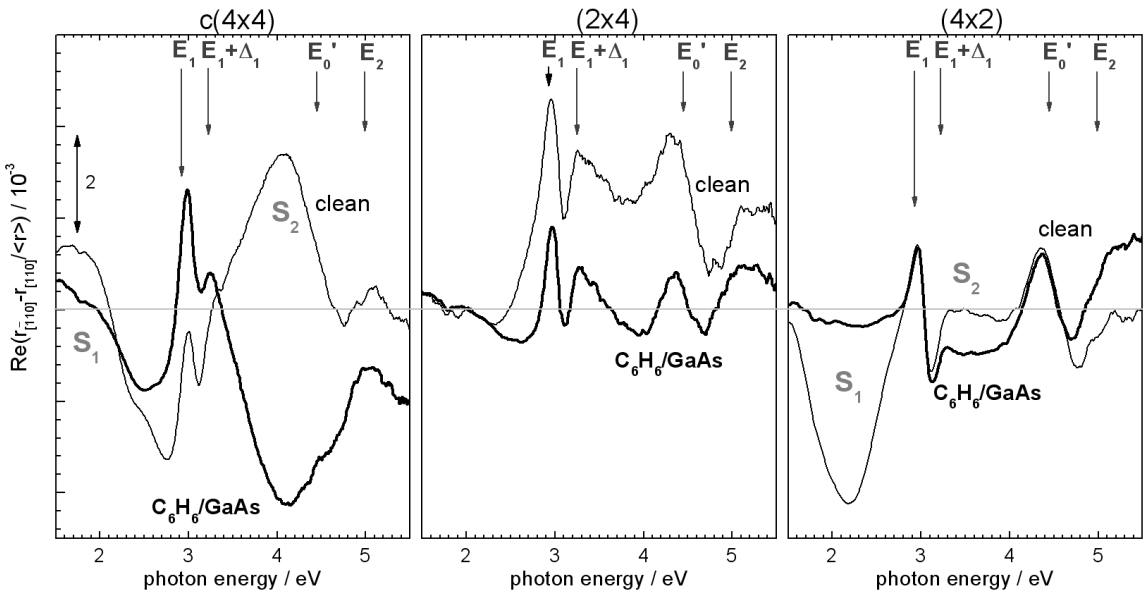


**Figure 9.1:** The RAS spectra of the corresponding clean reconstructed (thin lines, $n = 1 \cdot 10^{18}\ cm^{-3}$) and the benzene saturated surfaces (thick lines), of the c$(4 \times 4)$, the $(2 \times 4)$ and the $(4 \times 2)$, respectively.

## 9.2. Surface Periodicity

LEED pattern after the saturation of the surfaces with benzene are depicted in Fig. 9.2 taken at 42 eV. The LEED pattern of the initial c$(4 \times 4)$ reconstructed surface indicate a weak c$(4 \times 4)$ symmetry after the saturation with benzene.

For the $(2 \times 4)$ reconstructed surface the LEED pattern have not been taken but spots along the $[110]$ direction of the crystal indicating a $(1 \times 4)$ reconstructed surface have been observed. The LEED pattern of the $(4 \times 2)$ exhibits only bulk spots of the crystal without any indication for a different surface symmetry. For clarification of the bonding sites further SXPS measurements were performed as presented in the next section.

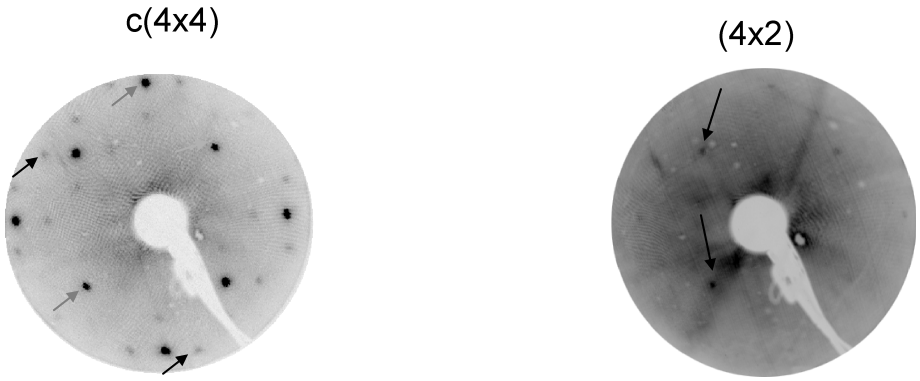


**Figure 9.2:** The LEED pattern obtained at the benzene saturated GaAs(001)c$(4\times4)$ (left taken at 42 eV) and $(4\times2)$ (right taken at 54 eV).

## 9.3. Core Level Spectroscopy at the Interface

The As3d core level taken after the adsorption of benzene at excitation energies of ∼120 eV are shown in Fig. 9.3. In the residuum of each core level compared to the ones which have been presented before a difference is apparent. The core level emission lines depicted in this chapter were taken at the DELTA where asymmetries caused by the analyzer were a problem during the measurements. Due to this problem the residua for the Ga3d and As3d core level are plotted in a different scale than it is the case for all other core level shown in this work.

In Fig. 9.3 for all three surface reconstructions a new $As-C$ component can be seen in the core level emission line. For the c$(4\times4)$ reconstructed surface the $As_{dimer}$ component is reduced by 65% and the $As_{2ndlayer}$ component to 80% of the initial value. The $As_{defects}$ contribution is nearly constant.
In the $(2\times4)$ core level line shape the $As_{dimer}$ and the $As_2$ components remain unchanged within the sensitivity of the measurements.
For the $(4\times2)$ not only the new component appears, but additionally the $As_2$ component increases again as it was also the case after the adsorption of cyclopentene and 1,4-cyclohexadiene.

As shown in Fig. 9.4 the Ga3d core level line shape reveals for the $(2\times4)$ and $(4\times2)$ an additional $(Ga-C)$ component. This component is in both cases shifted toward higher binding energies by +1.0 eV±0.09 eV. For the c$(4\times4)$ no change at the two surface related contributions is found.
In the C1s core level which are depicted in Fig. 9.5 taken at excitation energies of ∼356 eV two main components can be seen, the $C-C$ and the $C-As$ component which are shifted by 0.66 eV±0.05 eV. This shift is in agreement with the other measurements performed for the adsorption of cyclopentene and 1,4-cyclohexadiene on the corresponding surface reconstructions. No $C=C$ component was revealed in the best fit as it was found for the adsorption of cyclopentene and 1,4-cyclohexadiene on the corresponding surface reconstruction.

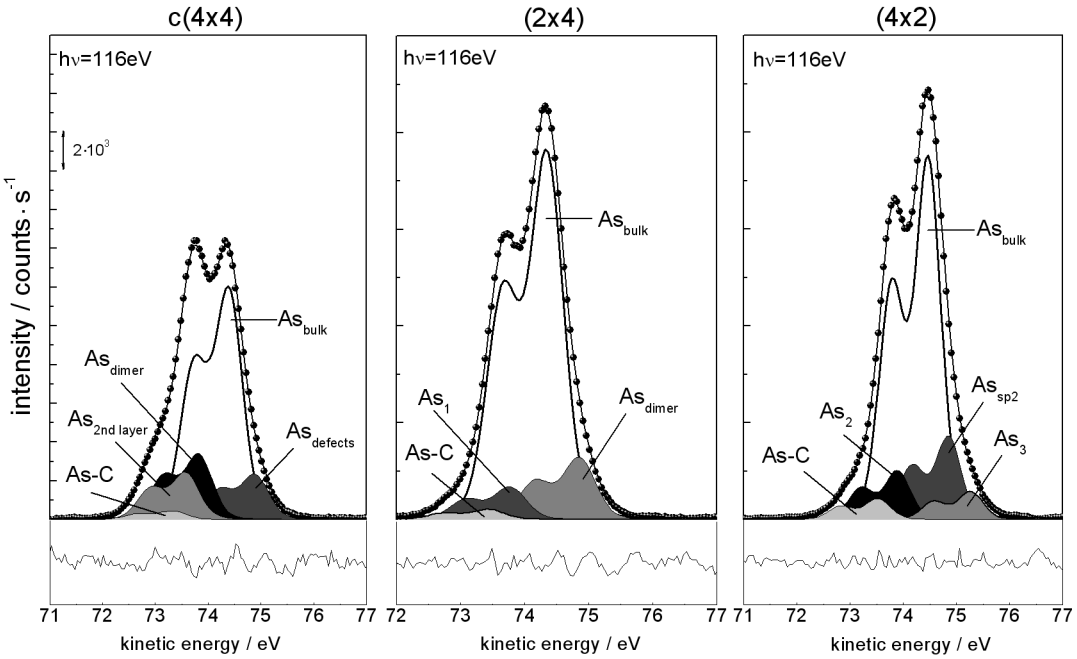


**Figure 9.3:** The As3d core level emission lines taken at an excitation energy of ∼120 eV after the adsorption of benzene on the c$(4\times4)$, the $(2\times4)$ and the $(4\times2)$, respectively. A new $As-C$ component can be revealed within the numerical analysis for all three surface.

The C1s core level emission line exhibits three components for the $(2\times4)$ reconstructed surface saturated with benzene. These components are assigned to C atoms which are involved in a $C-C$, a $C-As$ and a $C-Ga$ bond. The $C-As$ and the $C-Ga$ contributions are shifted by 0.67 eV$\pm$0.03 eV while the $C-As$ and the $C-C$ components are shifted by 0.62 eV$\pm$0.05 eV. No $C=C$ contribution was revealed in line shape analysis.
In the case of the benzene saturated $(4\times2)$ surface the C1s core level emission line contains four components as it was the case after the saturation with cyclopentene and 1,4-cyclohexadiene. The shifts of the components are related to the $C-C$ component. The $C-As$ component is shifted by -0.62 eV$\pm$0.03 eV and the $C-Ga$ by -1.31 eV$\pm$0.02 eV towards lower binding energies. Corresponding to this the $C=C$ contribution is shifted by +0.69 eV$\pm$0.03 eV towards higher binding energies. Within the resolution of the measurement the shifts are in agreement with the shifts which were observed for the adsorption of cyclopentene and 1,4-cyclohexadiene.
Due to the experimental setup it was not possible to determine the exact binding energies of the core level components. Therefore the binding energies can not be compared to the ones obtained for the adsorption of cyclopentene or 1,4-cyclohexadiene.

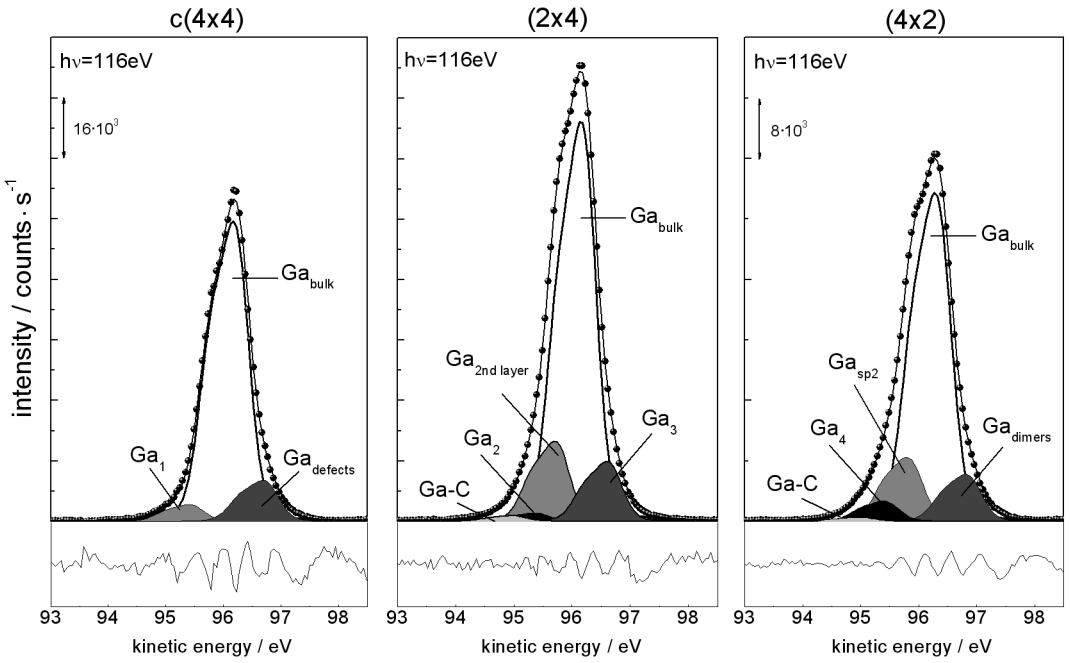


**Figure 9.4:** Ga3d core level emission lines taken after the saturation with benzene at an excitation energy of ∼120 eV of the c$(4\times4)$, the $(2\times4)$ and the $(4\times2)$, respectively. A new component $Ga-C$ is evident for the $(2\times4)$ and the $(4\times2)$.

## 9.4. Adsorption Structure of Benzene on GaAs$(001)$

The RAS spectra taken after the saturation with benzene of the c$(4\times4)$ show changes for the surface related features $S_1$ and $S_2$. These contributions are assigned to the As dimer atoms of the surface thus the surface dimer is modified during the adsorption with benzene. It can be concluded furthermore that the surface strain is increased because of the strong change in the feature $S_2$.

The As3d core level emission line exhibits an additional component which was shown in Fig. 9.3. This component was assigned to the $As-C$ bond formation and the corresponding component was found in the C1s core level.

It is reasonable that only two contributions are found in the C1s core level emission line because in the resulting adsorption structure only two different kinds of bonding configurations for the C atoms were found, the bond formation to As atoms ($C-As$) and the remaining single bonded C atoms ($C-C$ contribution). The contributions are in an adequate ratio for the suggested structure model. No $C=C$ contribution was evaluated which results in the adsorption structures of benzene on the c$(4\times4)$ reconstructed surface shown in Fig. 9.6. Dangling bonds remain at the two upwards buckled C atoms.

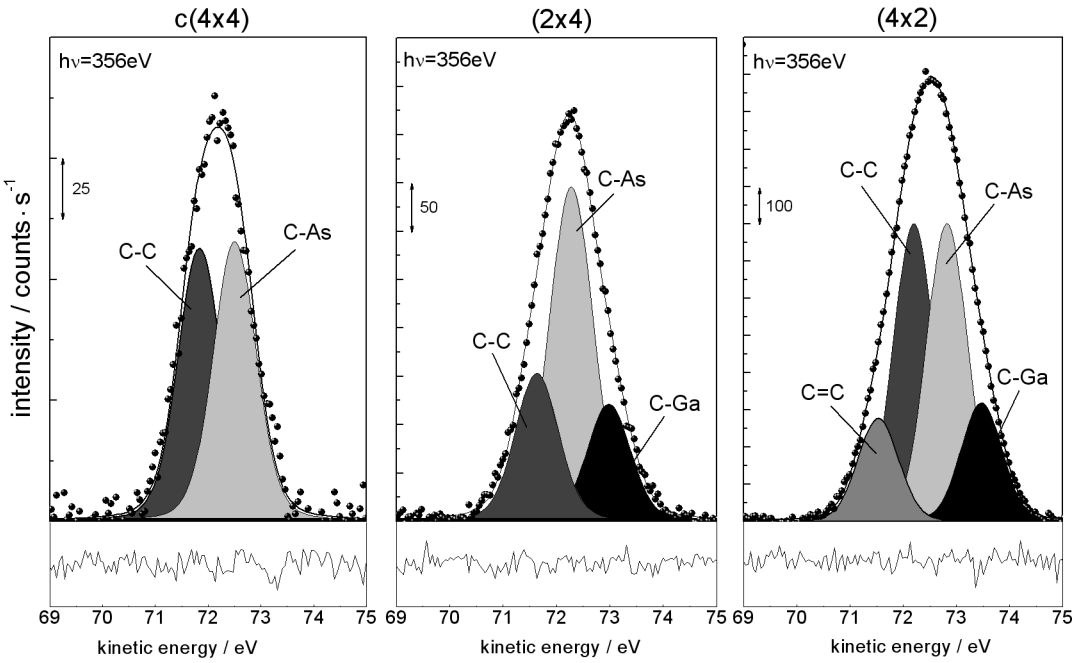


**Figure 9.5:** C1s core level emission lines taken after the saturation with benzene at an excitation energy of ∼355 eV of the c$(4\times4)$, the $(2\times4)$ and the $(4\times2)$, respectively.

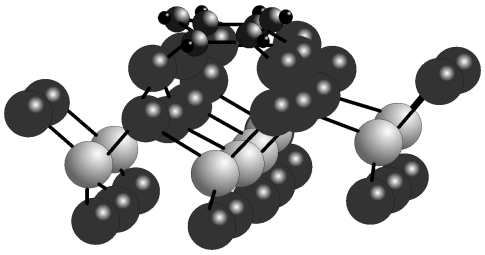

**Figure 9.6:** Possible adsorption structure which is suggested by the experimental results for the adsorption of benzene on the c$(4\times4)$ reconstructed surface.

Such a configuration with dangling bonds at the C atoms which are not bonded to the surface was also suggested for the adsorption of benzene on the Si$(001)(2\times1)$ reconstructed surface [35]. The topview of possible adsorption sites with the corresponding LEED pattern is shown in Fig. 9.7. It is obvious that the c$(4\times4)$ symmetry is kept after the adsorption of the benzene molecules.

For the $(2\times4)$ a change for the shoulder in the corresponding RAS signal after the adsorption of benzene was found (see Fig. 9.1). This shoulder is shifted further towards higher photon energies. The bulk related contributions were reduced in intensities.

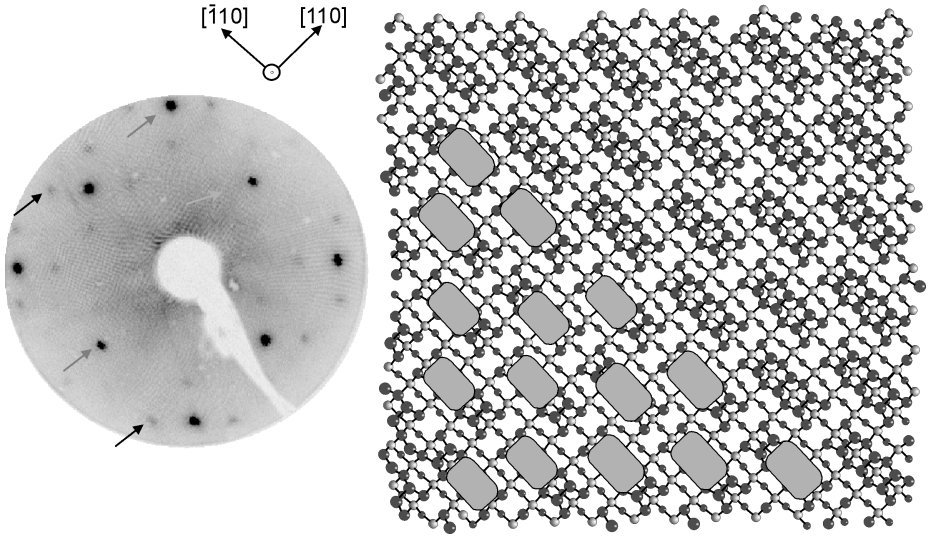


**Figure 9.7:** On the left: in the LEED pattern of the benzene saturated c$(4\times4)$ surface beside the bulk spots (gray arrows) a weak pattern of the c$(4\times4)$ remains in the picture (black arrows). A resulting topview of possible adsorption sites on the c$(4\times4)$ reconstructed surface is shown on the right. Each of gray boxes represents a benzene molecule.

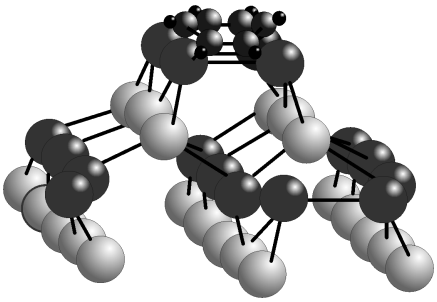

**Figure 9.8:** The resulting adsorption structure for the adsorption of benzene on the $(2\times4)$ reconstructed surface. A bond formation to Ga atoms is not shown.

In the core level line shape analysis of the As3d as well as of the Ga3d core level a new component could be evaluated, which is shifted towards higher binding energies, respectively. These components were assigned to a bond formation of C atoms to As and Ga atoms of the topmost layers. The resulting adsorption structure for benzene on the top As dimer is shown in Fig. 9.8. It can be suggested that a charge transfer of the As atoms to the Ga atoms could occur and this could be a reason for the bond formation of the Ga atoms to an additional benzene molecule, which is not shown in Fig. 9.8. The resulting possible adsorption sites of benzene on the $(2\times4)$ reconstruction are shown in Fig. 9.9 in a topview. Big gray boxes represent flat lying molecules while the small gray boxes indicate an adsorbed of upright standing molecules in the topview.

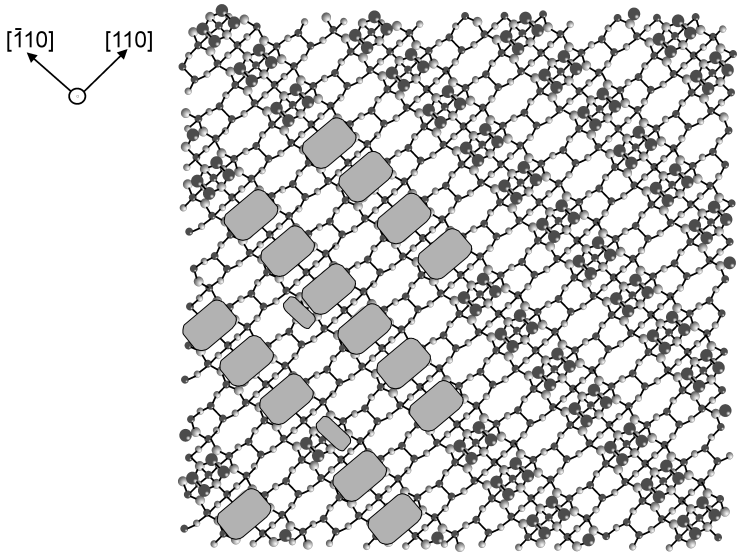


**Figure 9.9:** A resulting topview of possible adsorption sites on the $(2 \times 4)$ reconstructed surface is shown. The gray boxes represent a benzene molecule. Big boxes are flat lying and small ones are upright standing molecules.

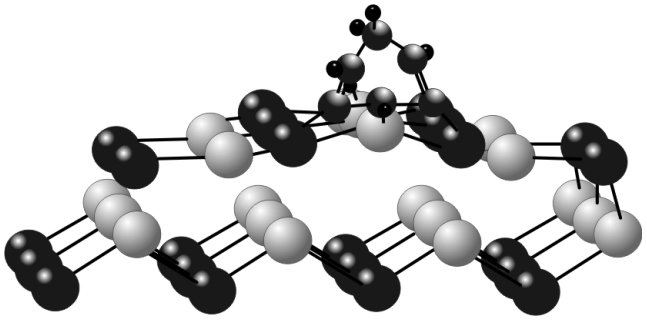

**Figure 9.10:** The resulting adsorption structure for the adsorption of benzene on the $(4 \times 2)$ reconstructed surface. Three bonds between benzene and the surface atoms are formed.

The $(4 \times 2)$ exhibits the additional reconstruction, the $(n \times 6)$, which is more As rich. The increase of the $As_2$ component after the adsorption of benzene in the As3d core level emission line again is an indication that the benzene molecules interact with the As atoms of the surface with a high probability. Corresponding to the additional component in the As3d core level emission line the benzene molecules bond to the $(4 \times 2)$ reconstructed parts of the surface. Due to the overlap of the corresponding contributions in the C1s core level emission line a direct assignment is not possible. As it was observed in the LEED pattern the $(4 \times 2)$ reconstruction dominates the surface and a structure model is given in Fig. 9.10. The resulting topview of the suggested adsorption structure of benzene adsorbed on the $(4 \times 2)$ reconstruction is shown in Fig. 9.11. The $(n \times 6)$ parts will not be discussed in terms of the

interface formation because the reconstruction itself is still under discussion and the $(4 \times 2)$ reconstruction is dominant.

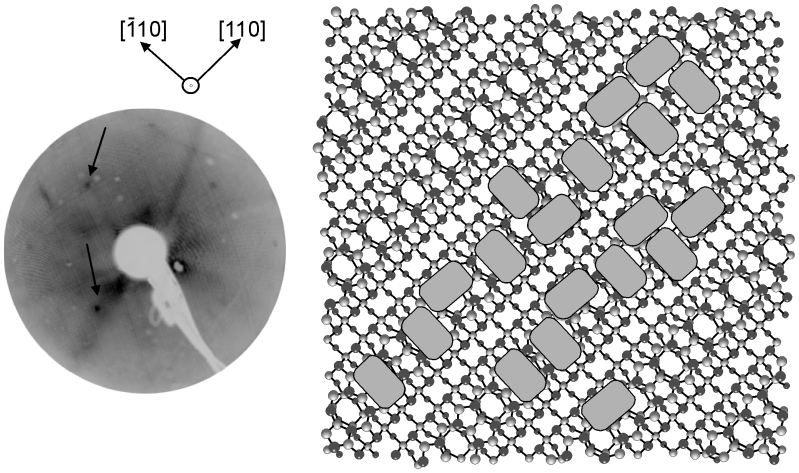


**Figure 9.11:** On the left: in the LEED pattern taken at 53 eV of the benzene saturated $(4 \times 2)$ surface only bulk spots remain. A resulting topview of possible adsorption sites on the $(4 \times 2)$ reconstructed surface is shown on the right. The gray boxes represent a benzene molecule and black arrows point at the remaining bulk sports.

As mentioned before it was not possible to measure the Fermi edge during these measurements. Due to this it was not possible to determine the exact binding energies of each atom species and thus they can not be compared to the results obtained for the adsorption of cyclopentene and 1,4-cyclohexadiene. Nevertheless, enough evidences for the suggestion of resulting adsorption structures in comparison to the adsorption of cyclopentene and 1,4-cyclohexadiene have been found for the presentation in this work.

## 9.5. Summary for Benzene Adsorption on the GaAs$(001)$ Surfaces

Due to the comparison to the experimental results obtained in each case for the adsorption of cyclopentene and 1,4-cyclohexadiene on the three 'main' GaAs$(001)$ surface reconstructions, structure models were suggested for the adsorption of benzene on these surfaces.

In comparison to the Si$(001)(2 \times 1)$ reconstructed surface a tight-bridge [39] adsorption configuration was found for the c$(4 \times 4)$ and the $(2 \times 4)$. Additional a similar charge transfer as it was the case for the adsorption of 1,4-cyclohexadiene on the $(2 \times 4)$ could occur and thus an adsorption of benzene at the Ga atoms of the topmost layer would be reasonable. This would explain the additional component in the Ga3d core level emission line.

For the $(4 \times 2)$ reconstructed surface a direct identification of the different components in the core level emission lines is more difficult because of the present $(n \times 6)$ reconstruction.

Although, a suggestion for the resulting structure model was made which is similar to the ones for the adsorption of cyclopentene and 1,4-cyclohexadiene on the $(4 \times 2)$ reconstruction, respectively.

# Chapter 10: Influence of the Intra-Molecular Double Bonds

In order to clarify whether the amount of intra-molecular double bonds has an influence on the adsorption process, different hydrocarbon ring shaped molecules have been used for the characterization of the first adsorption sites. Cyclopentene includes one double bond, while 1,4-cyclohexadiene and benzene contain of two and three, respectively.
The main difference between the adsorption of cyclopentene, 1,4-cyclohexadiene and benzene is the amount of bonds formed with the As atoms of the topmost layers. In contrast to the adsorption of cyclopentene on the $Si(001)(2\times1)$ reconstructed surface, cyclopentene molecules bond most likely without an interaction of the double bond to the $GaAs(001)$ surfaces. For the adsorption of 1,4-cyclohexadiene and benzene a different conclusion can be drawn for the adsorption on the $c(4\times4)$ and $(2\times4)$ due to a higher amount of bonds formed between the As and C atoms. The resulting adsorption structures are comparable to those which were in discussion for the adsorption of both molecules on the $Si(001)(2\times1)$. Due to a band bending found after the saturation of the $c(4\times4)$ reconstruction with cyclopentene (1,4-cyclohexadiene) a splitting of the dimer bond can be suggested.
Similar as for the $c(4\times4)$ are the results for the adsorption of cyclopentene, 1,4-cyclohexadiene and benzene on the $(2\times4)$ reconstructed surface, but no indication of a splitting of the dimer bond was found. Here again the main difference is found for the amount of C bonds formed to the As atoms of the surface. The corresponding $C-As$ component in the C1s core level is more pronounced after the saturation with 1,4-cyclohexadiene and benzene, respectively. After the adsorption of benzene no $C=C$ contribution can be found in the C1s core level of the $c(4\times4)$ and $(2\times4)$. If the molecules would not bond with an interaction of the double bond this component should increase successively with the increasing amount of double bond within the molecules. In the contrast to this a decrease in comparison to the $C-C$ component of each corresponding core level is found.

Only for the $(4\times2)$ this conclusion is not as clear as for the $c(4\times4)$ and the $(2\times4)$ due to the fact that a $(n\times6)$ surface reconstruction occurs beside the $(4\times2)$. Nevertheless for the $(4\times2)$ surface an interaction most likely with one double bond of the molecules can be found.
From this systematical study of the interface formation between small hydrocarbon ring shaped molecules it can be concluded that cyclopentene adsorbs in a single bond formation while 1,4-cyclohexadiene and benzene form more bonds to the $GaAs(001)$ surfaces investigated here.
Beside this an surface stoichiometry influence is present. An adsorption results more likely

in a bond formation to the As atoms of the surface than to the Ga atoms. This dependency on the surface geometry and stoichiometry will be discussed furthermore in the following chapter in comparison to the adsorption structure found for cyclopentene on the InP$(001)(2 \times 4)$ reconstructed surface.

# Chapter 11: Surface Structure and Stoichiometry Influence on the Adsorption Structure Formation

The adsorption of cyclopentene on the InP$(001)(2\times4)$ reconstructed surface was discussed as well as the one of cyclopentene on the different GaAs$(001)$ surface reconstructions. An important difference for the adsorption of cyclopentene between the InP$(001)(2\times4)$ and the GaAs$(001)$ surface reconstructions is the dimer configuration. The InP surface consists of an asymmetric 'hetero'-dimer while the GaAs$(001)$ surface reconstructions exhibit a symmetric 'homo'-dimer configuration. Thus for a discussion of the influence of the surface stoichiometry and dimer configuration to the adsorption process, the adsorption structures of cyclopentene on the InP$(001)(2\times4)$ reconstructed surface will be compared to the one of cyclopentene on the GaAs$(2\times4)$ reconstructed surface with respect to the results found in previous work for the adsorption of cyclopentene on the Si$(001)(2\times1)$ reconstructed surface.

On the Si$(001)(2\times1)$ reconstruction a regular arrangement due to a $[2+2]$-cycloaddition reaction was found for the adsorption of cyclopentene. This surface is characterized by an asymmetric dimer in the topmost layer with half filled dangling bonds. The influence of the dimer configuration to the the adsorption structure of the organic molecules is interesting and not yet clarified. Thus the adsorption structure of cyclopentene on the InP$(001)(2\times4)$ and the GaAs$(001)(2\times4)$ reconstructed surface are compared. It is important to remember that the GaAs$(2\times4)$ surface consists of a symmetric 'homo'-dimer while the InP$(2\times4)$ reconstruction exhibits an asymmetric 'hetero'-dimer.

In Fig. 11.1 the C1s core level emission lines of the cyclopentene saturated GaAs$(2\times4)$ (left) and the cyclopentene saturated InP$(2\times4)$ (right) reconstructed surfaces are depicted. Due to the electronegativities (C:2.6, P:2.2, As:2.2, Ga:1.8 and In:1.8) the shifts in the C1s core level emission lines are similar for the $C-As$ and the $C-P$ components with 0.59 and 0.50 eV towards lower binding energies, respectively. The shift for the $C-In$ component is higher caused by the different electronegativity (similar to the shift of $C-Ga$). The value for electronegativity of Si (electronegativity of 1.9) is higher than for In and smaller than for P and As. Thus the shift of the $Si-C$ component has to be smaller than the one measured for the $C-In$ and higher than measured for the $C-P$/$C-As$. This is in agreement compared to the measurements in [47] where a shift of the $Si-C$ component of 0.8 eV towards lower binding energies is given.

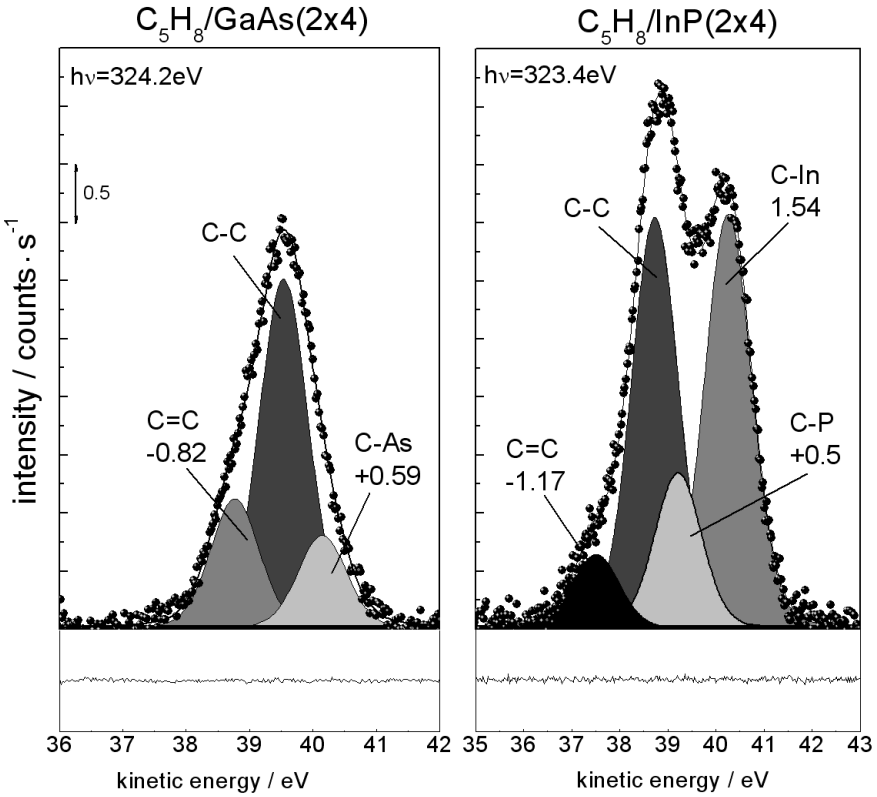


**Figure 11.1:** The C1s core level of the saturated cyclopentene GaAs$(2\times4)$ (left) and the saturated InP$(001)(2\times4)$ (right) reconstructed surfaces. Due to the electronegativities of the certain elements the shifts of the $C-As$, $C-P$ and $C-In$ components are different.

The resulting adsorption structures for both surface reconstructions after saturation with cyclopentene are depicted together in Fig. 11.2. The adsorption structure of cyclopentene on the GaAs$(001)(2\times4)$ surface is shown on the left and the one for cyclopentene on the InP$(001)(2\times4)$ reconstructed surface on the right. In the case of the GaAs surface cyclopentene is bonded with a single bond to the surface while on the InP surface a cycloaddition-like reaction occurs. This is possible due to the buckling of the 'hetero'-dimer. Additional, on this surface, a second adsorption site of cyclopentene was found. After the saturation of all dimer adsorption sites cyclopentene adsorbs at the second layer In atoms, despite the fact that the $In-In$ buckling is only weak. After the adsorption of cyclopentene this buckling is increased to 0.43 Å which is still less than the decreased buckling of the $In-P$ (0.53 Å ) bond after the adsorption. An adsorption of cyclopentene in a single bond formation with an additional adsorption of hydrogen to the InP$(2\times4)$ reconstructed surface is found to be very unlikely in the DFT calculations [150].

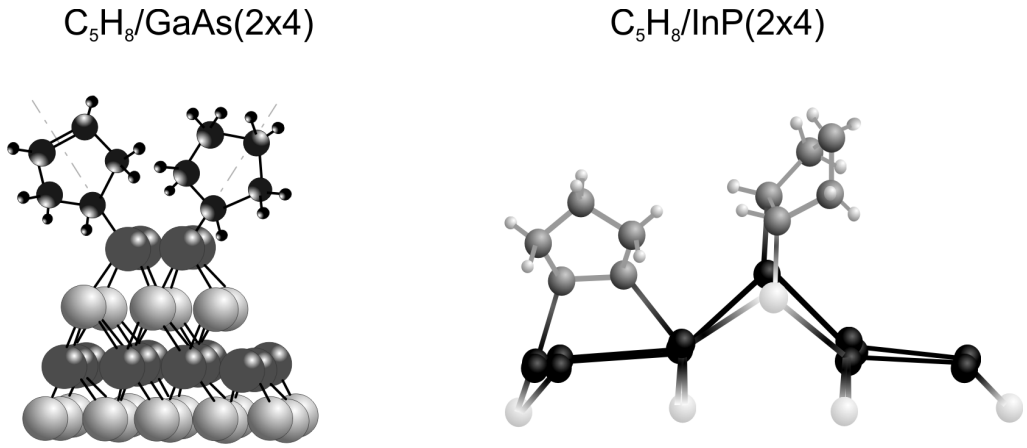


**Figure 11.2:** The resulting adsorption structures of cyclopentene on GaAs$(2\times4)$ (left) and InP$(001)(2\times4)$ (right). Obvious is that these adsorption structures does not result in an regular arrangement. This is in contrast to the adsorption structure of cyclopentene on the Si$(2\times1)$ reconstructed surface shown in Fig. 2.5.

On the GaAs surface only symmetric 'homo'-dimer exists and thus no cycloaddition-like reaction is possible.

Due to these experimental results it could be concluded that a symmetric 'homo'-dimer structure would lead to a single bond formation and no analogy to a $[2+2]$-cycloaddition reaction can be found while an adsorption of cyclopentene on an asymmetric 'hetero'-dimer would result in a $[2+2]$-cycloaddition like reaction. Compared to the Si$(001)(2\times1)$ surface reconstruction, where cyclopentene bonds in a $[2+2]$-cycloaddition reaction on the asymmetric $Si-Si$ dimer, the asymmetry of the dimer bond would be the important factor for the adsorption in a $[2+2]$-cycloaddition like adsorption structure.

However, for the adsorption of 1,4-cyclohexadiene and benzene on the GaAs$(001)(2\times4)$ reconstructed surface it was found that the molecules form more than one bond to the topmost atoms. This is in principle in agreement with the 'Woodward-Hoffman-rule' which was discussed in 2.5 because here a $[4+2]$-cycloaddition like reaction occur. Anyhow, the results indicate that these molecules bond to the surface in a structure where more than one atom of the surface and the molecule is involved.

The difference in the surface structure and stoichiometry within the different GaAs$(001)$ surface reconstructions was found to be not as dominant as for the difference compared to the InP$(001)(2\times4)$ reconstructed surface. On the c$(4\times4)$ and the $(2\times4)$, the two As-rich surface reconstructions, the adsorption structure and the first adsorption sites, have been the As atoms of the topmost dimer via a single bond formation. For the $(4\times2)$ reconstructed surface the first adsorption sites have been the same in that way that the molecules still seem to adsorb most likely on the As atoms at the topmost layer but because of the surface structure to Ga atoms, too, while more than one bond to the surface is formed.

# Chapter 12: Thermal Desorption of Organic Molecules

In this chapter the desorption of cyclopentene, 1,4-cyclohexadiene and benzene on the three 'main' GaAs$(001)$ surfaces will be characterized and discussed, respectively. Thus a conclusion about the desorption behavior of the three molecules on the GaAs$(001)$ surfaces can be drawn and the results obtained by the measurements can be compared to the one which are found for the desorption of the respective molecule on the Si$(001)(2 \times 1)$ and to the one found for cyclopentene on the InP$(001)(2 \times 4)$ reconstructed surface. It was not possible to determine exact desorption temperatures or desorption energies but the possibility of restoring of the clean reconstructed surfaces was investigated.

## Desorption Behavior of the Organic Molecules on the GaAs$(001)c(4 \times 4)$

In a first investigation the saturated (with cyclopentene, 1,4-cyclohexadiene or benzene, respectively) GaAs$(001)$c$(4 \times 4)$ reconstructed surface was heated stepwise to 350°C for $\sim$10 min. 350°C is the preparation temperature where in the end the increase of the temperature had to be stopped. With further heating the c$(4 \times 4)$ surface reconstruction would be destroyed due to the desorption of the topmost As layers.

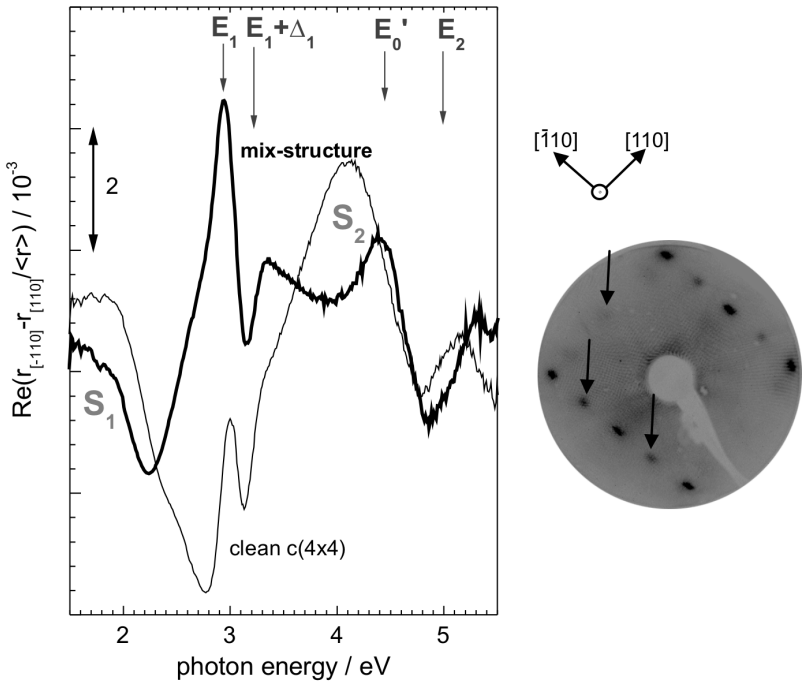


**Figure 12.1:** The RAS spectra of the clean reconstructed c$(4\times4)$ (thin line) after the decapping procedure to prepare the initial surface and the spectrum yielded after the thermal desorption of 1,4-cyclohexadiene by heating of the saturated c$(4\times4)$ surface to 350°C. The spectra are depicted together with the LEED pattern received after the desorption of the 1,4-cyclohexadiene molecules at 350°C for ∼10 min. Beside the obvious bulk spots, weak spots are visible which are indicated by the black arrows. These spots indicate the presence of a mix-structure between the c$(4\times4)$ and the $(2\times4)$.

It was found in the measurements so far that a desorption of the organic molecules did not take place below the preparation temperature for GaAs$(001)$c$(4\times4)$ reconstructed surface. In Fig. 12.1 the RAS spectrum of the clean reconstructed c$(4\times4)$ is presented together with the spectrum after the thermal treatment. Obvious is that the RAS line shape of the clean reconstructed surface can not be restored. This fact was not only found for the desorption of 1,4-cyclohexadiene, it was found for cyclopentene and benzene, too.

The presence of a mix-structure between the c$(4\times4)$ and the $(2\times4)$ is also verified in the Ga3d and the As3d core level taken after the heating to 350°C for ∼10 min, which are shown in Fig. 12.2. The As3d core level emission line shows a reduction of the $As_{dimer}$ which is a trend towards a $(2\times4)$ reconstructed surface. The same trend for the $Ga_{2ndlayer}$ can be found in the Ga3d core level emission line. This effect could be explained by a

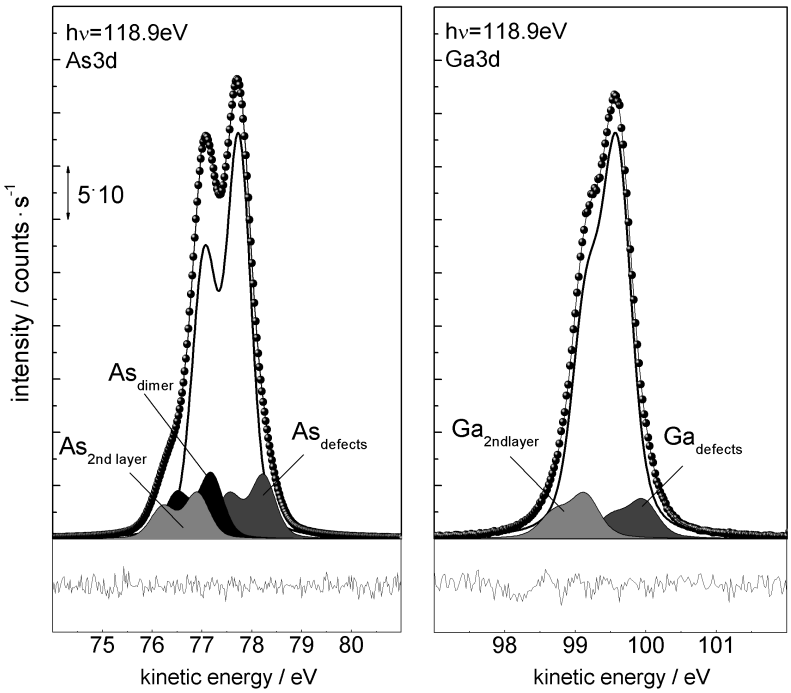


**Figure 12.2:** The As3d and Ga3d core level emission lines of the c$(4\times4)$ taken after the annealing to 350°C for ∼10 min for the desorption of the organic molecules at excitation energies of ∼120 eV. The As3d core level shows a reduction of a $As_{dimer}$ component compared to the As3d core level emission line of the clean reconstructed c$(4\times4)$. An increase of the component in the Ga3d core level shifted toward higher binding energies is found which tends to result in a $(2\times4)$ reconstructed surface.

strong bond formation between the organic molecules and the As atoms of the topmost layers. The annealing leads to a desorption of the first layer As atoms with the organic molecules. Therefore a mix-structure of the c$(4\times4)$ and the $(2\times4)$ is obtained.

In each case (cyclopentene, 1,4-cyclohexadiene and benzene) a further heating to 420°C for ∼10 min leads to the formation of the $(2\times4)$ reconstructed surface without contaminations of the molecules.

## Desorption Behavior of the Organic Molecules on the GaAs$(001)(2\times4)$

In the case of the saturated $(2\times4)$ reconstructed surface with the hydrocarbon molecules used in this work it was evaluated that the clean reconstructed surface (see Fig. 12.3) was restored after heating to 420°C for ∼10 min.

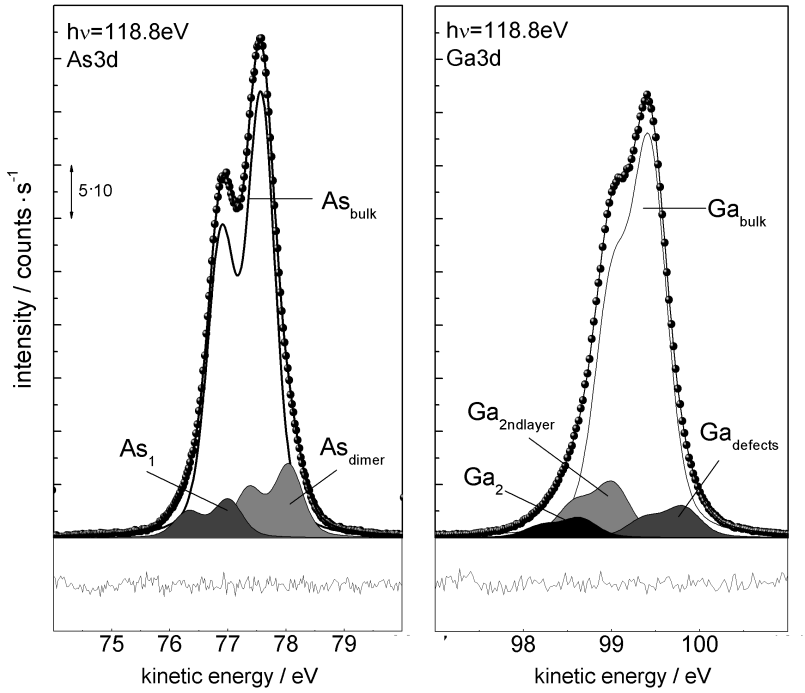


**Figure 12.3:** The As3d and Ga3d core level emission line taken after the heating of the saturated surface to 420°C for ∼10 min at excitation energies of ∼120 eV. These core level emission lines show no change compared to the initial As3d and Ga3d core level line shape of the clean reconstructed surface, which was shown in Fig. 5.9.

No evidence for a desorption at lower temperatures or a mix-structure was found, neither in the RAS spectra (not shown), nor in the As3d and Ga3d core level emission lines.

## Desorption Behavior of the Organic Molecules on the GaAs$(001)(4\times2)$

By heating up to 530°C for ∼10 min a desorption of all of the three molecules, cyclopentene, 1,4-cyclohexadiene and benzene was found, see Fig. 12.4 for the thermal desorption of cyclopentene as an example.

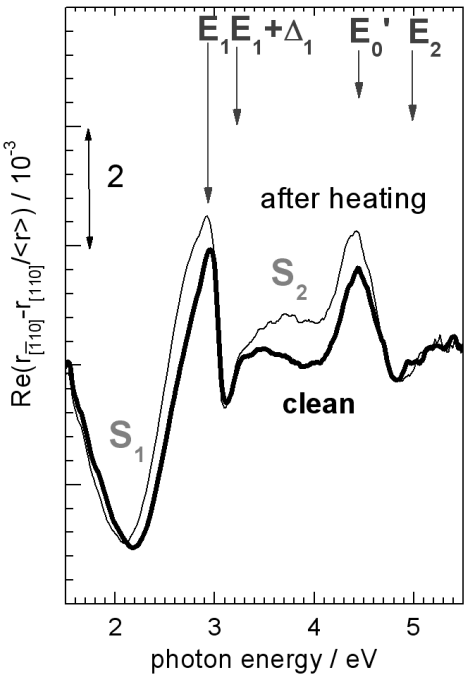


**Figure 12.4:** The RAS spectra taken at the initial reconstructed surface and after the desorption of cyclopentene molecules.

The desorption was verified by SXPS measurements taken after the heating procedure. It was found that no contaminations of the molecules remain on the surface as can be seen in Fig. 12.5.
It can be pointed out the all of the three GaAs$(001)$ surface were heated to the preparation temperatures for the desorption of the organic molecules cyclopentene, 1,4-cyclohexadiene and benzene, respectively.
In the case of the GaAs$(001)$c$(4\times4)$ it was found that the clean surface reconstruction can not be restored thus a mix-structure between the c$(4\times4)$ and the $(2\times4)$ was obtained after heating to 350°C for $\sim$10 min. Further annealing leads to a formation of the clean reconstructed $(2\times4)$. This surface reconstruction was in each case restorable after the desorption of the organic molecules at 420°C for $\sim$10 min.
In the case of the $(4\times2)$ reconstructed surface a desorption of all molecules was found after heating the saturated surface to the preparation temperature of 530°C $\sim$10 min.

Therefore the resulting desorption temperatures are lower than the desorption temperatures of cyclopentene, 1,4-cyclohexadiene or benzene on the Si$(001)(2\times1)$ reconstructed surface (T$\sim$900°C) [3,51]. Thus the bonding energy of the molecules on the GaAs$(001)$ surface is lower than the bonding energy of these molecules on the Si$(001)(2\times1)$ reconstructed surface. This is also the case for the desorption of cyclopentene of InP$(001)(2\times4)$ surface which was confirmed by DFT calculations.

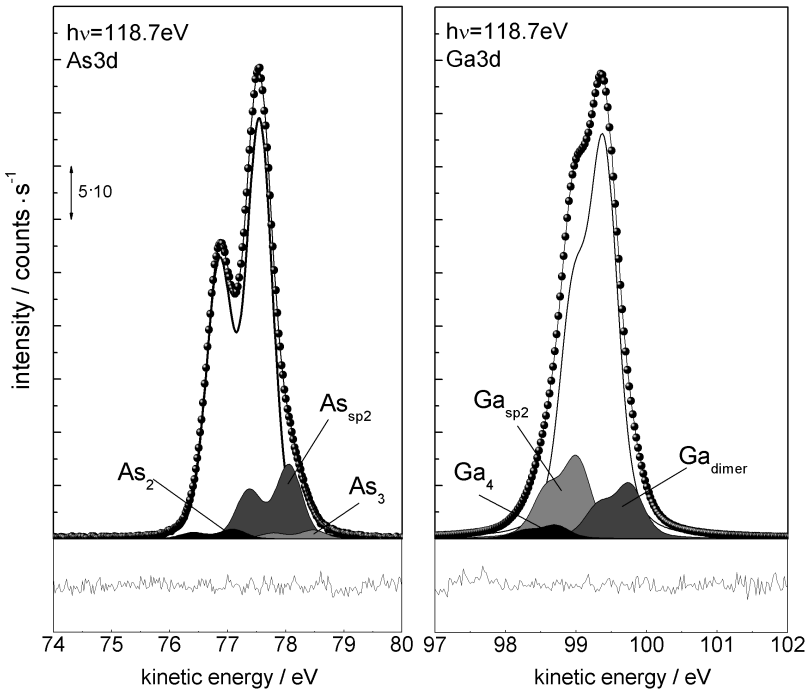


**Figure 12.5:** The As3d and Ga3d core level emission lines taken after the desorption of cyclopentene. No changes for the core level line shape appear and they are comparable to the ones for the initial clean surface reconstruction.

Finally it can be concluded that the binding energies of cyclopentene, 1,4-cyclohexadiene and benzene on the III-V surface investigated in this work are lower than it is the case for these molecules adsorbed on the $\mathrm{Si}(001)(2 \times 1)$ reconstructed surface, respectively.

# Chapter 13: Summary and Outlook

In the past the main focus of the investigations of hybrid systems was the characterization of the interface formation between organic molecules and Silicon surfaces. In this work a first systematical study of the interface formation between small hydrocarbon ring molecules and III-V surfaces was performed. Thereby the bonding sites of hydrocarbon ring molecules on III-V surfaces were characterized. Accordingly, the investigation was divided into two main parts: the investigation of the influence of the amount of intra-molecular double bonds to the adsorption process and the characterization of the influence of the surface structure and surface stoichiometry to the adsorption process. For the determination of the effect of the surface structure and stoichiometry to the adsorption process the measurements were performed on the three 'main' GaAs$(001)$ surfaces and the InP$(001)(2 \times 4)$ reconstructed surfaces. For the identification of the influence of the number of intra-molecular double bonds cyclopentene, 1,4-cyclohexadiene and benzene were used. The different adsorption structures were investigated with RAS, SXPS, STM and LEED. For the interpretation of the experimental results, the identification of the bonding sites and the development of structure models the comparison to theoretical calculations are necessary. Only in the case of the adsorption of cyclopentene on the InP$(001)(2 \times 4)$ reconstructed surface this comparison was possible because of missing calculations. The calculation for this surface based on DFT were performed by W. G. Schmidt and P. Favero. The structure models for the adsorption of the molecules on the three main 'main' GaAs$(001)$ surface reconstructions are extracted on the comparison of the possible bonding site on the Si$(001)(2 \times 1)$ and the results for the InP$(001)(2 \times 4)$ reconstructed surface.

## Determination of the Influence of Intra-Molecular Double Bonds to the Adsorption process

It was already known in what kind of preferred adsorption structures cyclopentene, 1,4-cyclohexadiene and benzene bond to the Si$(001)(2 \times 1)$ reconstructed surface but until now there was no aim to identify the influence of the intra-molecular double bond to the adsorption process on III-V semiconductors in a systematical study.

Here a discussion was given for these three molecules adsorbed on the three 'main' GaAs$(001)$ surface reconstructions, the c$(4 \times 4)$, the $(2 \times 4)$ and the $(4 \times 2)$. It was found for the adsorption of cyclopentene, 1,4-cyclohexadiene and benzene that the first adsorption sites are the topmost As atoms. Similar adsorption structures of these molecules on the

c$(4\times4)$ and the $(2\times4)$ were found on the Si$(001)(2\times1)$ reconstructed surface. In the case of the Ga-rich $(4\times2)$ reconstructed surface the molecules bond not only to the Ga atoms of the surface in the contrast to this it seems that the molecules bond most likely to the As atoms and additionally due to the surface stoichiometry to the Ga atoms.

In the case of the discussion of the different amount of double bonds and their influence on the adsorption sites and the resulting adsorption structure it can be concluded that more bonds to the surface were formed with a higher amount of intra-molecular double bonds on the c$(4\times4)$ and on the $(2\times4)$. For the adsorption of cyclopentene only a single bond formation to the surface was found while 1,4-cyclohexadiene and benzene formed four bonds. For the $(4\times2)$ reconstructed surface the adsorption structures seem to be similar for all three molecules but the results of the measurement are not as clear as for the As-rich surface reconstructions.

## Discussion of the Influence of the Surface Structure and Surface Stoichiometry on the Adsorption Process

The surface structure and surface stoichiometry was found to have an influence on the interface formation. In the case of the adsorption of the molecules on the GaAs$(001)$ surface reconstructions the conclusion can be drawn that the molecules bond more likely to the As atoms than to the Ga atoms. For cyclopentene, where the most experiments were realized with, it was found that only one bond was formed to the c$(4\times4)$ and the $(2\times4)$ surfaces. This is in contrast to the adsorption configuration of the molecule on the Si$(001)(2\times1)$ reconstructed surface where a $[2+2]$-cycloaddition like reaction occurred.

In the case of the InP$(001)(2\times4)$ reconstructed surface a similar reaction was found for the adsorption of cyclopentene on the asymmetric dimer of the surface. This asymmetry is similar to the one found on the Si$(001)(2\times1)$ surface. Thus it can be concluded that the asymmetric dimer configuration supports a $[2+2]$-cycloaddition like reaction.

# Outlook

Further valence band measurements at smaller excitation energies have to be performed for the adsorption of all three molecules on each surface reconstruction. Thereby a better identification of additional new contributions in the valence bands caused by the molecule adsorption would be possible. First indications have been found during this work for new contributions which have been assigned to the respective molecules. An additional band bending was found after the adsorption of cyclopentene and 1,4-cyclohexadiene on the c$(4 \times 4)$, respectively. For the corresponding core level emission lines of the As3d and Ga3d core levels a shift occurred but this has to be verified in more measurements.

In further measurements it would be interesting to continue these investigations with small molecules where one carbon atom is substituted by other atom species like nitrogen or oxygen which have a higher electronegativity. The surface core level shifts would be more pronounced by a higher difference in the electronegativities. Such molecules with functional groups could be interesting for the development of applications.
Another interesting fact for the development of application could be the passivation of a certain surface by organic molecules. A passivation would prevent the surface to be contaminated during an exposure to air. For the cyclopentene saturated $(4 \times 2)$ reconstructed GaAs$(001)$ surface a passivation was found. After an exposure to air of the cyclopentene saturated sample a clean reconstructed surface was obtained again. Such a passivation cycle is depicted in Fig 13.1.

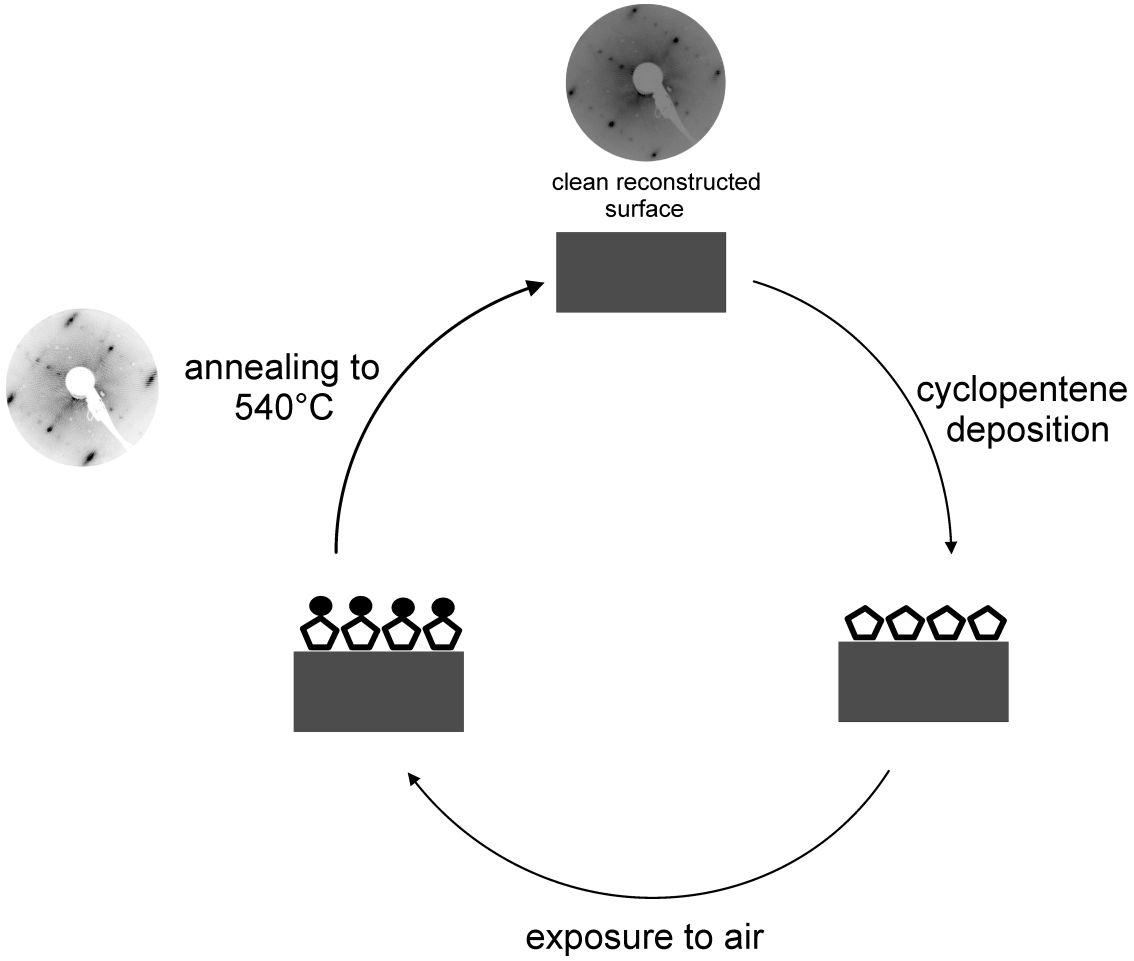


**Figure 13.1:** The passivation cycle for the $(4 \times 2)$ reconstructed surface. After the deposition of cyclopentene molecules until saturation the sample was exposed to air. By heating the sample to the preparation temperature the clean reconstructed surface was restored.

This cycle did work for the cyclopentene saturated GaAs$(001)(4 \times 2)$ reconstructed surface but has to be verified in further measurements and for further different organic molecules to find out the parameters which are essential for this process.

# List of Figures

# List of Tables

# Bibliography


[1] Stutzmann, M., Garrido, J. A., Eickhoff, M., and Brandt, M. S. *phys. stat. sol. (a)* **203**, 3424 (2006).

[2] Hamers, R. *Nature* **412**, 489 (2001).

[3] Bent, S. F. *Surf. Sci.* **500**, 879 (2002).

[4] Liu, Z., Yasseri, A. A., Lindsey, J. S., and Bocian, D. F. *Science* **302**, 1543 (2003).

[5] Vilan, A. and Cahen, D. *Trends in Biotechn.* **20**, 22 (2002).

[6] Hovis, J. S., Liu, H., and Hamers, R. J. *Surf. Sci.* , 1 (1998).

[7] Schmidt, W. G., Fuchs, F., Hermann, A., Seino, K., Bechstedt, F., Passmann, R., Wahl, M., Gensch, M., Hinrichs, K., Esser, N., Wang, S., Lu, W., and Bernholc, J. *J. Phys.: Condens. Matter* **16**, S4323 (2004).

[8] Kim, J. W., Carbone, M., Tallarida, M., Dil, J. H., Horn, K., Casaletto, M. P., Flammini, R., and Piancastelli, M. N. *Surf. Sci.* **559**, 179 (2004).

[9] Hacker, C. A. and Hamers, R. J. *J. Phys. Chem. B* **107**, 7689 (2003).

[10] Hermann, A., Schmidt, W. G., and Bechstedt, F. *Phys. Rev. B* **71**, 153311 (2005).

[11] Yang, H. Q., Zhu, C. X., Xue, Z. Q., and Pang, S. J. *Surf. Sci.* **448**, 225 (2000).

[12] Schmidt, W. G., Bechstedt, F., and Bernholc, J. *Phys. Rev. B* **63**, 045322 (2001).

[13] Palummo, M., Onida, G., Sole, R. D., and Mendoza, B. S. *Phys. Rev. B* **60**, 2522 (1999).

[14] Silaghi, S. D. and Zahn, D. R. *Appl. surf. sci.* **252**, 5462 (2006).

[15] Kampen, T. U., Rossow, U., Schumann, M., Park, S., and Zahn, D. R. T. *J. Vac. Sci. Technol. B* **18**, 2077 (2000).

[16] Chen, Y., Schmidt, J., Siller, L., Bernard, J. C., and Palmer, R. E. *Phys. Rev. B* **58**, 1177 (1998).

[17] Angot, T., Salomon, E., Papageorgiou, N., and Leyet, J. M. *Surf. Sci.* **572**, 59 (2004).

[18] Passmann, R., Kropp, M., Bruhn, T., Fimland, B. O., Bloom, F. L., Gossard, A. C., Richter, W., Esser, N., and Vogt, P. *Appl. Phys. A* **87**, 469 (2007).

[19] Pashley, M. D. *Phys. Rev. B* **40**, 10481 (1989).

[20] Mortimer, C. E. *Chemie, Das Basiswissen der Chemie*. Georg Thieme Verlag, Stuttgart New York, 1996, ISBN 3-13-484306-4.

[21] Koch, N. *J. Phys.: Condens. Matter* **20**, 184008 (2008).

[22] Wassermann, A. *Diels-Alder Reactions: Organic Background and Physio-Chemical Aspects*. Elsevier, New York, 1965.

[23] Gill, G. B. and Willis, M. R. *Pericyclic Reactions*. Chapman and Hall, London, 1974.

[24] Curruthers, W. *Cycloaddition Reactions in Organic Synthesis*. Pergamon Press, New York, 1990.

[25] Woodward, R. B. and Hoffmann, R. **21**, 797 (1969).

[26] Garcia, M. A., Losurdo, M., Wolter, S. D., Kim, T.-H., Lampert, W. V., Bonaventura, J., Bruno, G., Giangregorio, M., and Brown, A. *J. Vac. Sci. Technol. B* **25**, 1504 (2007).

[27] Goringe, C. M., Clark, L. J., Lee, M. H., Pyne, M. C., Stich, I., White, J. A., Gillan, M. J., and Sutton, A. P. *J. Phys. Chem. B* **101**, 1498 (1997).

[28] Hamaguchi, K., Machida, S., Yamashita, Y., and Yoshinobu, J. *Phys. Rev. B* **62**, 7576 (2000).

[29] Chao, Y., Svensson, K., Radosavkić, D., Dhanak, V. R., Ŝiller, L., and Hunt, M. R. C. *Phys. Rev. B* **64**, 235331 (2001).

[30] Northrup, J. E. *Phys. Rev. B* **44**, 1419 (1991).

[31] Chen, D. and Boland, J. J. *Phys. Rev. B* **65**, 165336 (2002).

[32] Chadi, D. J. *Phys. Rev. Lett.* **43**, 43 (1979).

[33] Staufer, M., Birkenhauer, U., Belling, T., Nörtemann, F., Rösch, N., Widdra, W., Kostov, K. L., Moritz, T., and Menzel, D. *J. Chem. Phys.* **112**, 2498 (2000).

[34] Witkowski, N., Pluchery, O., and Borensztein, Y. *Phys. Rev. B* **72**, 075354–1 (2005).

[35] Witkowski, N., Hennies, F., Pietzsch, A., Mattsson, S., Fröhlisch, A., Wurth, W., Nagasono, N., and Piancastelli, M. N. *Phys. Rev. B* **68**, 115408 (2003).

[36] Gokhale, S., Trischberger, P., Menzel, D., Widdra, W., Dröge, H., Steinrück, H.-P., Birkenhauer, U., Gutdeutsch, U., and Rösch, N. *J. Chem. Phys.* **112**, 2498 (2000).

[37] Lopinski, G. P., Fortier, T. M., Moffatt, D. J., and Wolkow, R. A. *J. Vac. Sci. Technol. A* **16**, 1037 (1998).

[38] Jeong, H. D., Ryu, S., Lee, Y. S., and Kim, S. *Surf. Sci.* **344**, L1226 (1995).

[39] Hofer, W. A., Fischer, A. J., Lopinski, G. P., and Wolkow, R. A. *Phys. Rev. B* **63**, 085314 (2001).

[40] Craig, B. I. *Surf. Sci. Lett.* **280**, L279 (1993).

[41] Taguchi, Y., Fujisawa, M., Takaoka, T., Okada, T., and Nishijima, M. *J. Chem. Phys.* **95**, 6870 (1991).

[42] Kim, Y. K., Lee, M. H., and Yeom, H. W. *Phys. Rev. B* **71**, 115311 (2005).

[43] Hamaguchi, K., Machida, S., Nagao, M., F.Yasui, Mukai, K., Yamashita, Y., Yoshinobu, J., Kato, H. S., Okuyama, H., Kawai, M., Sato, T., and Iwatsuki, M. *J. Phys. Chem. B* **105**, 3718 (2001).

[44] Kato, H. S., Wakatsuchi, M., Kawai, M., and Yoshinobu, J. *J. Phys. Chem. C* **111**, 2557 (2007).

[45] D'Amico, F., Gunnella, R., Shimomura, M., Abukawa, T., and Kono, S. *Phys. Rev. B* **76**, 165315 (2007).

[46] Cho, J.-H., Oh, D.-H., Kim, K. S., and Kleinman, L. *Phys. Rev. B* **116**, 3800 (2002).

[47] Lui, H. and Hamers, R. J. *Surf. Sci.* **416**, 354 (1998).

[48] Machida, S., Hamaguchi, K., Nagao, M., Yasui, F., Mukai, K., Yamashita, Y., and Yoshinobu, J. *J. Phys. Chem. B* **106**, 1691 (2002).

[49] Yamashita, Y., Hamaguchi, K., Machida, S., Mukai, K., Yoshinobu, J., Tanaka, S., and Kamada, M. *Appl. surf. sci.* **169**, 172 (2001).

[50] Schmidt, W. G. and Bernholc, J. *Phys. Rev. B* **68**, 115327 (2003).

[51] Cho, J.-H. and Kleinman, L. *Phys. Rev. B* **64**, 235420 (2001).

[52] Silvestrelli, P. L., Pulci, O., Palummo, M., Sole, R. D., and Ancilotto, F. *Phys. Rev. B* **68**, 235306 (2003).

[53] Howard, A., McIver, J., and Collins, J. *HyperChem, Release 8*. Hypercube, Inc., Gainesville, 2007.

[54] Allinger, N. L., Cava, M. P., de Jongh, D. C., Johnson, C. R., Lebel, N. A., and Stevens, C. L. *Organische Chemie*. Walter de Gryter Verlag, Berlin New York, 1980, ISBN: 3-11-004594-X.

[55] Linde, D. R. *Handbook of Chemistry and Physics*. Chemical Rubber Company, Roca Raton, 1995.

[56] Binning, G. and Rohrer, H. *Helvetica Physica Acta* **55**, 726 (1982).

[57] Binning, G. and Rohrer, H. *Phys. Rev. Lett.* **49**, 57 (1982).

[58] Binning, G. and Rohrer, H. *Surf. Sci.* **126**, 236 (1983).

[59] Bardeen, J. *Phys. Rev. Lett.* **6**, 57 (1961).

[60] Tersoff, J. and Hamann, D. R. *Phys. Rev. Lett.* **50**, 1998 (1983).

[61] Tersoff, J. and Hamann, D. R. *Phys. Rev. B* **31**, 805 (1985).

[62] Wiesendranger, R. and Güntherodt, H.-J. *Scanning Tunnelling Microscopy*. volume I-III, Springer-Verlag, Berlin Heidelberg New York, $2^{nd}$ edition, 1996, ISBN: 3-540-60824-2.

[63] Bonnell, D. A. *Scanning Tunnelling Microscopy and Spectroscopy*. VCH Publishers, Inc., 1993, ISBN: 0-89573-768-X.

[64] Sakurai, T. and Watanabe, Y. *Advances in Scanning Probe Microscopy*. Springer-Verlag, Berlin Heidelberg New York, 2000, ISBN: 3-540-66718-0.

[65] Feenstra, R. M., Thompson, W., and Fein, A. *Phys. Rev. Lett.* **56**, 608 (1986).

[66] Schneider, W. D. *Journal of Electron Spectroscopy and Related Phenomena* **109**, 1 (2000).

[67] Hertz, H. *Ann. Phys.* **31**, 983 (1887).

[68] Thompson, J. J. *Phil. Mag* **44**, 293 (1897).

[69] Einstein, A. *Ann. Phys.* **17**, 132 (1905).

[70] Hüfner, S. *Photoelectron Spectroscopy, Principles and Applications*. Springer Verlag, Berlin Heidelberg New York, 2nd edition, 1996, ISBN: 3-540-60875-3.

[71] Cardona, M. and Ley, L. *Photoemission in Solids I*. Springer Verlag, Berlin Heidelberg New York, 2nd edition, 1978, ISBN: 3-540-08685-4.

[72] Seah, M. P. and Dench, W. A. *Surf. Interf. Anal.* **1**, 2 (1979).

[73] Bertness, K. A., Yeh, J.-J., Friedmann, D. J., Mahowald, P. H., Wahi, A. K., Kendelewicz, T., and Lindau, I. *Phys. Rev. B* **38**, 5406 (1988).

[74] Carlisle, J. A., Sieger, M. T., Miller, T., and Chiang, T.-C. *Phys. Rev. Lett.* **71**, 2955 (1993).

[75] Chassé, A., Nowak, C., Rennert, P., Braun, W., Richter, W., and Zahn, D. R. T. *Surf. Sci.* , 389 (1995).

[76] Sieger, M. T., Miller, T., and Chiang, T. C. *Phys. Rev. Lett.* **75**, 2043 (1995).

[77] Esser, N., Frisch, A., Richter, W., Vogt, P., Braun, W., Follath, R., and Jung, C. *Solid State Commun.* **113**, 443 (2000).

[78] Margaritondo, S. B. C. G. and Rowe, J. E. *Phys. Rev. B* **19**, 2850 (1979).

[79] Yu, P. and Cardona, M. *Fundamentals of Semiconductors*. Springer Verlag, Berlin Heidelberg New York, 1996, ISBN: 3-540-58307-6.

[80] Marquardt, D. W. *J. Soc. Ind. Appl. Math.* **11**, 431 (1963).

[81] Stephens, C. *Temperature Effects in Metal-InP(110) Interface Formation, PhD thesis University Dublin*. 1990.

[82] Richter, W. *Phil. Trans. R. Soc. A* **344**, 453 (1993).

[83] Weightman, P., Martin, D. S., Cole, R. J., and Farrell, T. *Rep. Prog. Phys.* **68**, 1251 (2005).

[84] Martin, D., Blanchard, N., and Weightman, P. *Surf. Sci.* , 1 (2003).

[85] Haberland, K. *Optical in-situ Studies during Metal-organic Vapor Phase Epitaxy with Respect to III-V Device Production, PhD thesis Technische Universität Berlin*. Mensch and Buch Verlag, 2002, ISBN: 3-89820-395-6.

[86] Azzam, R. M. A. *Opt. Commun.* **76**, 122 (1976).

[87] Berkowitz. *JETP Lett.* **41**, 551 (1985).

[88] Aspnes, D. E. and Studna, A. A. *Phys. Rev. Lett.* **54**, 1956 (1985).

[89] Aspnes, D. E., Harbinson, J. P., Studna, A. A., and Florez, L. T. *J. Vac. Sci. Technol. A* **6**, 1327 (1988).

[90] Reinhardt, F., Jonsson, J., Zorn, M., Richter, W., Ploska, K., Rumberg, J., and Kurpas, P. *J. Vac. Sci. Technol. B* **12**, 2541 (1994).

[91] Zorn, M., Jonsson, J., Krost, A., Richter, W., Zettler, J.-T., Ploska, K., and Reinhardt, F. *J. Cryst. Growth* **145**, 53 (1994).

[92] Hofmann, P., Rose, K. C., Fernandez, V., and Bradshaw, A. M. *Phys. Rev. Lett.* **75**, 2039 (1995).

[93] Richter, W. and Zettler, J.-T. *Appl. surf. sci.* , 465 (1996).

[94] Paget, D., Bonnet, J., Berkovits, V., Chiaradia, P., and Avila, J. *Phys. Rev. B* **53**, 4604 (1996).

[95] Fernandez, V., Pahlke, D., Esser, N., Stahrenberg, K., Hunderi, O., Bradshaw, A., and Richter, W. *Surf. Sci.* , 328 (1997).

[96] Stahrenberg, K., Hermann, T., Esser, N., Sahm, J., Richter, W., Hoffmann, S. V., and Hofmann, P. *Phys. Rev. B* **58**, R10207 (1998).

[97] Aspnes, D. E. *Phys. Rev. B* **41**, 10334 (1990).

[98] Aspnes, D. *J. Vac. Sci. Technol. B* **3**, 1498 (1985).

[99] Martin, D. S., Blanchard, N. P., Weightman, P., Roseburgh, D. S., Cole, R. J., Hansen, J.-K., Bremer, J., and Hunderi, O. *Phys. Rev. B* **76**, 115403 (2007).

[100] Sheridan, B., Martin, D., Power, J., Barrett, S., Smith, C., Lucas, C., Nichols, R., and Weightman, P. *Phys. Rev. Lett.* **85**, 4618 (2000).

[101] Martin, D. and P.Weightman. *Surface Review and Letters* **7**, 389 (2000).

[102] Cardona, M., Pollack, F., and Shaklee, K. *J. Phys. Soc. Jpn. Suppl.* **21**, 89 (1966).

[103] Berkovits, V. L., Ivantsov, L. F., Kiselev, V. A., Makarenko, I. V., Minashvili, T. A., and Safarov, V. I. *JETP Lett.* **41**, 551 (1985).

[104] Aspnes, D. E., Harbison, J. P., Studna, A. A., and Florez, L. T. *J. Vac. Sci. Technol. A* **6**, 1327 (1988).

[105] Azzam, R. *J. Optics (Paris)* **12**, 317 (1981).

[106] Aspnes, D. *Proc. SPIE* **2**, 1037 (1988).

[107] Carr, E. P. and Stücklen, H. *J. Chem. Phys.* **6**, 55 (1938).

[108] Dreizler, R. M. and Gross, E. K. *Density Functional Theory*. Springer Verlag, Berlin Heidelberg New York, 1990, ISBN: 0-306-44905-6.

[109] Hohenberg, P. and Kohn, W. *Phys. Rev.* **136**, B846 (1964).

[110] Kohn, W. and Sham, L. J. *Phys. Rev.* **140**, A1133 (1976).

[111] Tran, F., Laskowski, R., Blaha, P., and Schwarz, K. *Phys. Rev. B* **75**, 115131 (2007).

[112] Knorr, K., Pristovsek, M., Resch-Esser, U., Zorn, M., and Richter, W. *J. Cryst. Growth* **170**, 230 (1997).

[113] Resch-Esser, U., Esser, N., Wang, D. T., Kuball, M., Zegenhagen, J., Fimland, B. O., and Richter, W. *Surf. Sci.* , 71 (1996).

[114] Hovis, J. S., Lee, S. L., Liu, H., and Hamers, R. J. *J. Vac. Sci. Technol. B* **15**, 1153 (1997).

[115] Schmidt, W. G., Bechstedt, F., Esser, N., Pristovsek, M., Schultz, C., and Richter, W. *Phys. Rev. B* **57**, 14596 (1998).

[116] Schmidt, W. G., Esser, N., Frisch, A. M., Vogt, P., Bernholc, J., Bechstedt, F., Zorn, M., Hannappel, T., Visbeck, S., Willig, F., and Richter, W. *Phys. Rev. B* **61**, R16335 (2000).

[117] Vogt, P. *Atomic Structure of the (001) Surface of InP, GaP and InGaP*. PhD thesis, Technische Universität Berlin, 2002, ISBN: 3-89685-202-7.

[118] Frisch, A. *Untersuchungen der electronischen und atomaren Structur von InP(001) und GaP(001)-Oberflächen mittels Photoemissionsspektroskopie und Reflexions-Anisotropie-Spektroskopie*. PhD thesis, Technische Universität Berlin, 2000, ISBN: 3-89820-150-3.

[119] Schmidt, W. G., Bechstedt, F., Esser, N., Pristovsek, M., Schultz, C., and Richter, W. *Phys. Rev. B* **57**, 596 (1998).

[120] Pulci, O., Lüdge, K., Vogt, P., Esser, N., Schmidt, W. G., Richter, W., and Bechstedt, F. *Comp. Mat. Sci.* **22**, 32 (2001).

[121] Schultz, C., Frisch, A. M., Hinrichs, K., Kinsky, J., Hermann, T., Rossow, U., Esser, N., and Richter, W. *J. Vac. Sci. Technol. B* **15**, 1260 (1997).

[122] Esser, N., Schmidt, W. G., Bernholc, J., Frisch, A. M., Vogt, P., Zorn, M., Pristovsek, M., Richter, W., Bechstedt, F., Hannappel, T., and Visbeck, S. *J. Vac. Sci. Technol. B* **17**, 1691 (1999).

[123] Chao, Y., Svensson, K., Radosavkić, D., Dhanak, V. R., Ŝiller, and Hunt, M. R. C. *Surf. Sci.* **236**, 15 (1990).

[124] Schmidt, W. G. *Appl. Phys. A* **75**, 89 (2002).

[125] Xue, Q.-K., Hashizume, T., and Sakurai, T. *Appl. surf. sci.* **141**, 244 (1999).

[126] LaBella, P., Yang, H., Bullock, D. W., Thibado, P. M., Kratzer, P., and Scheffler, M. *Phys. Rev. Lett.* **83**, 2989 (2000).

[127] Lee, S.-H., Moritz, W., and Scheffler, M. *Phys. Rev. Lett.* **85**, 3890 (2000).

[128] Lüdge, K. *Interface Formation During Epitaxial Growth of Cobalt Layers on III-V Semiconductor* (001) *surfaces*. PhD thesis, Technische Universität Berlin, 2003, ISBN: 3-89685-201-9.

[129] Schmidt, W. G., Mirbit, S., and Bechstedt, F. *Phys. Rev. B* **62**, 8087 (2000).

[130] Schmidt, W. G., Bechstedt, F., and Bernholc, J. *Appl. surf. sci.* **190**, 264 (2002).

[131] Avery, A. R., Holmes, D. M., Sudijono, J., Jones, T. S., and Joyce, B. A. *Surf. Sci.* **323**, 91 (1995).

[132] Nagashima, A., Tazima, M., Nishimura, A., Takagi, Y., and Yoshino, J. *Surf. Sci.* , 71 (2001).

[133] Northrup, J. E. and Froyen, S. *Phys. Rev. B* **50**, 2015 (1994).

[134] Schmidt, W. G. and Bechstedt, F. *Phys. Rev. B* **54**, 742 (1996).

[135] Moll, N., Kley, A., Pehlke, E., and Scheffler, M. *Phys. Rev. B* **54**, 8844 (1996).

[136] Garreau, Y., Sauvage-Simkin, M., Jedrecy, N., Pinchaux, R., and Veron, M. B. *Phys. Rev. B* **54**, 17638 (1996).

[137] McCoy, J. M., Korte, U., and Maksym, P. A. *Surf. Sci.* **418**, 273 (1998).

[138] private communication with P. Vogt.

[139] Biegelsen, D. K., Bringans, R. D., Northrup, J. E., and Swartz, L.-E. *Phys. Rev. B* **41**, 5701 (1990).

[140] Xue, Q.-K., Hashizume, T., Zhou, J. M., Sakata, T., Ohno, T., and Sakurai, T. *Phys. Rev. Lett.* **74**, 3177 (1995).

[141] Seino, K., Schmidt, W. G., Bechstedt, F., and Bernholc, J. *Surf. Sci.* , 406 (2002).

[142] Kumpf, C., Marks, L. D., Ellis, D., Smilgies, D., Landemark, E., and Nielsen, M. *Phys. Rev. Lett.* **86**, 3586 (2001).

[143] Esser, N., Schmidt, W. G., Cobet, C., Fleischer, K., A. I. Shkrebtii, B. O. F., and Richter, W. *J. Vac. Sci. Technol. B* **19**, 1756 (2001).

[144] Schmidt, W. G., Bechstedt, F., Fleischer, K., Cobet, C., Esser, N., Richter, W., Bernholc, J., and Onida, G. *phys. stat. sol. (a)* **188**, 1401 (2001).

[145] Lautenschlager, P., Garriga, M., Logothetidis, S., and Cardona, M. *Phys. Rev. B* **35**, 9174 (1987).

[146] Ono, K., Mano, T., Nakamura, K., Mizuguchi, M., Nakazono, S., Horiba, K., Kihara, T., Kiwata, H., Waki, I., Oshima, M., Koguchi, N., and Kakizaki, A. *Proc. 25th Int. Conf. Phys. Semicond* , 293 (2000).

[147] Lay, G. L., Mao, D., Kahn, A., Hwu, Y., and Margaritondo, G. *Phys. Rev. B* **43**, 14301 (1991).

[148] Spindt, C. J., Yamada, M., Meissner, P. L., Miyano, K. E., Kendelewicz, T., Herrera-Gomez, A., Spicer, W. E., and Arko, A. J. *Phys. Rev. B* **45**, 11108 (1992).

[149] Ohtake, A., Tsukamoto, S., Pristovsek, M., Koguchi, N., and Ozeki, M. *Phys. Rev. B* **65**, 233311 (2002).

[150] Passmann, R., Favero, P., Schmidt, W. G., Braun, W., Richter, W., Kneissl, M., Esser, N., and Vogt, P. *Phys. Rev. B* , submitted (2008).

[151] Cho, J.-H. and Kleinman, L. *Phys. Rev. B* **67**, 115314 (2003).

[152] Pahlke, D., Arens, M., Esser, N., Wang, D. T., and Richter, W. *Surf. Sci.* , 66 (1996).

[153] Mönch, W. *Semiconductor Surfaces and Interfaces*. Springer Verlag, New York, 1993, ISBN 978-3-540-67902-8.

# Appendix A: Fit Parameters for the three GaAs$(001)$ Surface Reconstructions

In the following table the fit parameters used for the core level emission line shape analysis are shown.

For the c$(4\times4)$:

| | $\Delta E/eV$ | $\gamma/eV$ | $\sigma/eV$ | R | $SO/eV$ |
|---|---|---|---|---|---|
| $As_{dimer}$ | -0.74±0.05 | 0.09±0.01 | 0.47±0.03 | 1.47±0.03 | 0.68±0.02 |
| $As_{2ndlayer}$ | -0.45±0.05 | 0.09±0.01 | 0.47±0.03 | 1.47±0.03 | 0.68±0.02 |
| $As_{defects}$ | +0.44±0.06 | 0.09±0.01 | 0.47±0.03 | 1.47±0.03 | 0.68±0.02 |
| $Ga_{defects}$ | +0.43±0.03 | 0.09±0.01 | 0.36±0.03 | 1.68±0.08 | 0.44±0.01 |
| $Ga_1$ | -0.37±0.02 | 0.09±0.01 | 0.36±0.03 | 1.68±0.08 | 0.44±0.01 |

**Table A.1:** Fit parameters for the Ga3d and As3d core levels obtained on the clean reconstructed GaAs$(001)c(4\times4)$ surface. In the table the surface core level shifts (SCLS) in the kinetic energy with respect to the bulk component, and the values for lifetime broadening $\gamma$, experimental broadening $\sigma$, branching ratio R and spin orbit-splitting $\Delta_{SO}$ are shown.

For the $(2\times4)$:

| | $\Delta E/eV$ | $\gamma/eV$ | $\sigma/eV$ | R | $SO/eV$ |
|---|---|---|---|---|---|
| $As_{dimer}$ | +0.48±0.02 | 0.09±0.01 | 0.47±0.03 | 1.47±0.03 | 0.68±0.02 |
| $As_1$ | -0.61±0.05 | 0.09±0.01 | 0.47±0.03 | 1.47±0.03 | 0.68±0.02 |
| $Ga_{2ndlayer}$ | +0.38±0.02 | 0.09±0.01 | 0.36±0.02 | 1.64±0.04 | 0.44±0.01 |
| $Ga_2$ | -0.74±0.04 | 0.09±0.01 | 0.36±0.02 | 1.64±0.04 | 0.44±0.01 |
| $Ga_3$ | +0.34±0.04 | 0.09±0.01 | 0.36±0.02 | 1.64±0.04 | 0.44±0.01 |

**Table A.2:** Fit parameters for the Ga3d and As3d core levels obtained on the clean reconstructed GaAs$(001)(2\times4)$ surface. In the table the surface core level shifts (SCLS) in the kinetic energy with respect to the bulk component, and the values for lifetime broadening $\gamma$, experimental broadening $\sigma$, branching ratio R and spin orbit-splitting $\Delta_{SO}$ are shown.

For the $(4\times2)$:

| | $\Delta E/eV$ | $\gamma/eV$ | $\sigma/eV$ | R | $SO/eV$ |
|---|---|---|---|---|---|
| $As_{sp^2}$ | +0.51±0.03 | 0.06±0.03 | 0.46±0.03 | 1.54±0.05 | 0.46±0.03 |
| $As_3$ | +0.8±1.0 | 0.06±0.03 | 0.46±0.03 | 1.54±0.05 | 0.46±0.03 |
| $As_2$ | -0.46±0.02 | 0.06±0.03 | 0.46±0.03 | 1.54±0.05 | 0.46±0.03 |
| $Ga_{sp2}$ | -0.39±0.02 | 0.06±0.03 | 0.37±0.03 | 1.66±0.05 | 0.44±0.01 |
| $Ga_{dimers}$ | +0.35±0.02 | 0.06±0.03 | 0.37±0.03 | 1.66±0.05 | 0.44±0.01 |
| $Ga_4$ | -0.77±0.02 | 0.06±0.03 | 0.37±0.03 | 1.66±0.05 | 0.44±0.01 |

**Table A.3:** Fit parameters for the Ga3d and As3d core levels obtained on the clean reconstructed GaAs$(001)(4\times2)$ surface. In the table the surface core level shifts (SCLS) in the kinetic energy with respect to the bulk component, and the values for lifetime broadening $\gamma$, experimental broadening $\sigma$, branching ratio R and spin orbit-splitting $\Delta_{SO}$ are shown.

# Appendix B: Fit Parameters for the three saturated GaAs$(001)$ Surface Reconstructions

In this section the fit parameters obtained at surfaces which were saturated with cyclopentene, 1,4-cyclohexadiene and benzene will be presented.
The resulting shifts after the saturation with cyclopentene and 1,4-cyclohexadiene on the three 'main' GaAs$(001)$ surfaces are similar while the ones after the saturation with benzene are slightly (0.1 eV) larger (will not be shown in detail here).

For the GaAs$(001)$c$(4\times4)$:

| | $\Delta E/eV$ | $\gamma/eV$ | $\sigma/eV$ | R | $SO/eV$ |
|---|---|---|---|---|---|
| $Ga_{defects}$ | +0.36±0.03 | 0.1±0.01 | 0.36±0.01 | 1.71±0.07 | 0.44±0.01 |
| $Ga_1$ | -0.43±0.05 | 0.1±0.01 | 0.36±0.01 | 1.71±0.07 | 0.44±0.01 |
| $As_{dimer}$ | -0.98±0.02 | 0.1±0.05 | 0.43±0.02 | 1.52±0.05 | 0.69±0.01 |
| $As_{defects}$ | +0.46±0.04 | 0.1±0.05 | 0.43±0.02 | 1.52±0.05 | 0.69±0.01 |
| $As-C$ | -1.35±0.05 | 0.1±0.05 | 0.43±0.02 | 1.52±0.05 | 0.69±0.01 |
| $C=C$ | -0.79±0.03 | 0.1±0 | 0.85±0.05 | - | - |
| $C-As$ | +0.61±0.09 | 0.1±0 | 0.85±0.05 | - | - |
| $C-Ga$ | -1.43±0.05 | 0.1±0 | 0.85±0.05 | - | - |

**Table B.1:** For comparison to Tab. A.1 the fit parameters for the Ga3d and As3d core levels obtained after the adsorption of cyclopentene (1,4-cyclohexadiene) on the GaAs$(001)c(4\times4)$. The shifts for the C1s components are given with respect to the C-C component. This shifts shifts in the kinetic energy, the values for lifetime broadening $\gamma$, experimental broadening $\sigma$, branching ratio R and spin orbit-splitting $\Delta_{SO}$ are shown.

For the GaAs$(001)(2\times4)$:

| | $\Delta E/eV$ | $\gamma/eV$ | $\sigma/eV$ | R | $SO/eV$ |
|---|---|---|---|---|---|
| $Ga_{2ndlayer}$ | -0.42±0.03 | 0.8±0.03 | 0.39±0.05 | 1.65±0.05 | 0.43±0.01 |
| $Ga_3$ | -0.75±0.04 | 0.8±0.03 | 0.39±0.05 | 1.65±0.05 | 0.43±0.01 |
| $Ga_2$ | +0.41±0.05 | 0.8±0.03 | 0.39±0.05 | 1.65±0.05 | 0.43±0.01 |
| $Ga-C$ | -1.24±0.05 | 0.8±0.03 | 0.39±0.05 | 1.65±0.05 | 0.43±0.01 |
| $As_{dimer}$ | +0.50±0.03 | 0.1±0.05 | 0.50±0.04 | 1.505±0.054 | 0.69±0.01 |
| $As_1$ | -0.66±0.08 | 0.1±0.05 | 0.50±0.04 | 1.505±0.054 | 0.69±0.01 |
| $As-C$ | -1.05±0.1 | 0.1±0.05 | 0.50±0.04 | 1.505±0.054 | 0.69±0.01 |
| $C=C$ | -0.79±0.03 | 0.1±0 | 0.85±0.05 | - | - |
| $C-As$ | +0.61±0.09 | 0.1±0 | 0.85±0.05 | - | - |
| $C-Ga$ | -1.43±0.05 | 0.1±0 | 0.85±0.05 | - | - |

**Table B.2:** For comparison to Tab. A.2 the fit parameters for the Ga3d and As3d core levels obtained after the adsorption of cyclopentene (1,4-cyclohexadiene) on the GaAs$(001)(2\times4)$. The shifts for the C1s components are given with respect to the C-C component. This shifts shifts in the kinetic energy, the values for lifetime broadening $\gamma$, experimental broadening $\sigma$, branching ratio R and spin orbit-splitting $\Delta_{SO}$ are shown.

For the GaAs$(001)(4\times2)$:

| | $\Delta E/eV$ | $\gamma/eV$ | $\sigma/eV$ | R | $SO/eV$ |
|---|---|---|---|---|---|
| $Ga_{sp2}$ | -0.40±0.03 | 0.1±0.01 | 0.38±0.03 | 1.68±0.07 | 0.44±0.01 |
| $Ga_{dimers}$ | +0.43±0.03 | 0.1±0.01 | 0.38±0.03 | 1.68±0.07 | 0.44±0.02 |
| $Ga_4$ | -0.74±0.05 | 0.1±0.01 | 0.38±0.03 | 1.68±0.07 | 0.44±0.02 |
| $Ga-C$ | -1.08±0.08 | 0.1±0.01 | 0.38±0.03 | 1.68±0.07 | 0.44±0.02 |
| $As_{sp^2}$ | +0.46±0.1 | 0.1±0.02 | 0.45±0.03 | 1.55±0.04 | 0.69±0.01 |
| $As_2$ | -0.55±0.09 | 0.1±0.02 | 0.45±0.03 | 1.55±0.04 | 0.69±0.01 |
| $As-C$ | -1.0±0.09 | 0.1±0.02 | 0.45±0.03 | 1.55±0.04 | 0.69±0.01 |
| $C=C$ | -0.79±0.03 | 0.1±0 | 0.85±0.05 | - | - |
| $C-As$ | +0.61±0.09 | 0.1±0 | 0.85±0.05 | - | - |
| $C-Ga$ | -1.43±0.05 | 0.1±0 | 0.85±0.05 | - | - |

**Table B.3:** For comparison to Tab. A.3 the fit parameters for the Ga3d and As3d core levels obtained after the adsorption of cyclopentene (1,4-cyclohexadiene) on the GaAs$(001)(4\times2)$. The shifts for the C1s components are given with respect to the C-C component. This shifts shifts in the kinetic energy, the values for lifetime broadening $\gamma$, experimental broadening $\sigma$, branching ratio R and spin orbit-splitting $\Delta_{SO}$ are shown.

# Appendix C: Fit Parameters for the clean and cyclopentene saturated InP$(001)(2\times4)$ Surface Reconstructions

| | $\Delta E/eV$ | $\gamma/eV$ | $\sigma/eV$ | R | $SO/eV$ |
|---|---|---|---|---|---|
| $P1$ | +0.31±0.04 | 0.061±0.03 | 0.41±0.06 | 2.07±0.07 | 0.86±0.01 |
| $P2$ | -0.59±0.04 | 0.061±0.03 | 0.41±0.06 | 2.07±0.07 | 0.86±0.01 |
| $In1$ | +0.45±0.05 | 0.1±0 | 0.46±0.06 | 1.47±0.08 | 0.86±0.01 |
| $In2$ | -0.38±0.04 | 0.1±0 | 0.46±0.06 | 1.47±0.08 | 0.86±0.01 |
| $In3$ | -0.84±0.05 | 0.1±0 | 0.46±0.06 | 1.47±0.08 | 0.86±0.01 |
| $C-In$ | +1.535±0.015 | 0.1±0 | 1.032±0.01 | - | - |
| $C-P$ | +0.50±0.02 | 0.1±0 | 1.032±0.01 | - | - |
| $C=C$ | -1.17±0.04 | 0.1±0 | 1.032±0.01 | - | - |

**Table C.1:** Fit parameters for the In4d and P2p core levels obtained on the InP$(001)(2\times4)$ surface. The shifts are given for the kinetic energy with respect to the bulk component. For the C1s core level the shifts are given with respect to the C-C component. In the table the surface core level shifts (SCLS), and the values for lifetime broadening $\gamma$, experimental broadening $\sigma$, branching ratio R and spin orbit-splitting $\Delta_{SO}$ are shown.

# Thanks!

The development of this work would not have been possible with the help of many people. I hope that I always have been able to express my gratitude. Finally I want to thank everybody who contributed to this work either directly with physical aspects, or indirectly with any kind of assistance:

...Prof. Dr. N. Esser for supervising this work, for the discussions as well as for his advises and for the opportunity to work in the field of surface science.
...Prof. Dr. W. Richter and Prof. Dr. M. Kneissl for their support during this work and especially Prof. Dr. N. Esser and Prof. Dr. M. Kneissl for the opportunity to work in a close cooperation between the ISAS-Institute for Analytical Sciences and the TU Berlin.
...Dr. P. Vogt for his help during the whole time of preparing this work, for the discussions not only about physics and for his initiative of solving any kind of problems.
...Prof. Dr. W. G. Schmidt and MSc. P. Favero for the close collaboration and the DFT calculations concerning the adsorption of cyclopentene on the InP$(001)(2 \times 4)$ reconstruction.
...Dr. G. Gavrila for her help during all BESSY beamtimes and Dipl. Phys. D. Weier and all other BESSY/DELTA people for their help during the beamtimes. Dr. P. Vogt, Dipl. Phys. C. Friedrich, Dipl. Phys. T. Bruhn, and Dipl. Phys. M. Kropp for the nice BESSY and DELTA beamtimes, the pleasant atmosphere and the good work together. These beamtimes therefore became much more enjoyable.
...B. O. Fimland for the growth of the GaAs$(001)$ samples and Dr. S. Weeke as well as Dr. M. Pristovsek for the growth of the InP$(001)$ samples.
...My 'office-staff' Dipl. Phys. R. Kremzow and Dipl. Phys. C. Friedrich for making the time in the office and of course in the lab so enjoyable. This was something unique. Dipl. Phys. T. Bruhn for the nice discussions and the fun we had during the whole time and M. Ewald for the last year measuring together.
...Engelbert Eder, Christof Maerker, the workshop staff of the TU Berlin and the workshop staff of the ISAS-Institute for Analytical Sciences as well as the glassblower N. Zelinski of the TU Berlin for their support in all kind of problems.
...The former members of the Richter group and the current staff of the Kneissl group for the pleasant atmosphere
...For proof reading Dr. P. Vogt, Dr. S. Chandola, Dipl. Phys. T. Bruhn and D. Frömel.

I want to thank my parents Elisabeth and Hermann Paßmann for their continuous help and understanding. My sister Jutta who always was willing to listen to my problems and for all the fun we have and my sister Michaela with her nice family (Patrick, Lea and Tim) for some change in my life.

Finally I want to thank Dennis Frömel for all his patience and understanding during the last two years. His persistent motivation gave me the power to finalize this work.